INCORPORATION OF COMPLEX MOLECULES AND SUPRAMOLECULAR STRUCTURES INTO METAL-ORGANIC FRAMEWORKS

Mark Newman

JUNE 8, 2023

UNIVERSITY OF NOTTINGHAM

Contents

Acknowledgements

I would like to thank all the people who have made this work possible.

Firstly, I would like to thank Neil Champness and Ben Pilgrim for their help and guidance throughout this work, as well as all the past and present members of the Champness and Pilgrim groups that assisted me with this research.

Phillip Langer for his work in developing the TAR4 architecture; Connie Pfeiffer, Rosie Young and Eleanor Stemple for their work on the NDI-MOF nanotubes and Nic Pearce for his scientific expertise in all things interconnected.

I must also thank William Lewis and Stephen Argent for their help with crystallographic measurements and Graham Rance for the Raman measurements.

Finally, I would like to thank everyone I have met along this last four years and the four before that.

Abbreviations

°C – degrees Celsius

CV – cyclic voltammetry

DCM - dichloromethane

DDQ – 2,3-Dichloro-5,6-dicyano-1,4-benzoquinone

DMF – *N, N'*-dimethylformamide

DNA – deoxyribonucleic acid

DPMNDI - dipyridyl methyl naphthalene diimide

HMTA – hexamethylenetriamine

HOMO – highest occupied molecular orbital

LUMO – lowest unoccupied molecular orbital

MIM – Mechanically interlocked molecules

MOF-NT – metal-organic framework nanotubes

MOF – metal-organic framework

MORF – metal-organic rotaxane framework

MS-TOF – time of flight mass spectroscopy

NDA – naphthalene dianhydride

NDI – naphthalene diimide

NHCs – N-heterocyclic carbene

PDI – perylene diimide

RT – room temperature

SCXRD - single-crystal X-ray diffraction

SEM – scanning electron microscopy

SWCNTs - single-walled carbon nanotubes

UV - ultraviolet

Abstract

In this thesis, three different supramolecular frameworks will be described.

The first is a novel naphthalene diimide (NDI) metal-organic framework-based, flexible, nanotube structure. The crystal structure is reported and described. The structure was spectroscopically probed to investigate the formation of an NDI radical upon exposure to UV/Visible radiation and investigated by Raman spectroscopy to measure chemical changes upon mechanical bending of the nanotubes.

In the second section, two tetra-acid rotaxanes, TAR4 and TAR8 are synthesised and analysed by proton NMR and the single X-ray crystal of the former, is detailed. Once synthesised, attempts were made to incorporate these into metal-organic frameworks motifs through several methods. Two other diacid rotaxane syntheses were also started and the preliminary reactions to form them detailed.

The final chapter details the synthesis of a naphthalene diimide/porphyrin [2]handcuff rotaxane; which was planned and started, with these discussed.

1. Introduction

1.1 Supramolecular Chemistry

Supramolecular chemistry was famously defined by Jean-Marie Lehn, the recipient of the 1987 Nobel Prize, as "chemistry beyond the molecule."[1] Supramolecular chemistry, although first postulated as a concept in its own right in the early 1970s,[2,3] has been studied under different guises as far back as the 1890s, with Emil Fischer suggesting the idea of a 'lock and key'[4] relationship between enzymes and binding substrates in which interactions occur between the host and guest to create a system more ordered than the respective separate parts.

Of course, this supramolecular concept is not unique to purely enzymatic systems and complex architectures which are formed of smaller constituent parts are exhibited in many natural examples. Perhaps the most obvious example, is that of the double helical structure of DNA formed from nucleotide bases,[5] but both cell membranes[6,7] and micelles[8,9] are also examples of other supramolecular motifs.

Supramolecular chemistry focuses not on covalent bonding but instead concerns weaker interactions between entities (Figure 1.1). These weaker interactions such as hydrogen bonds, around 1-40 $kJmol^{-1}$, and electrostatic interactions, ~1 $kJmol^{-1}$, are less rigid in nature and therefore can accommodate many different architectures. The flexibility of these inter-molecular forces is key to molecular self-assembly, an area of chemistry that will now be discussed in more detail.

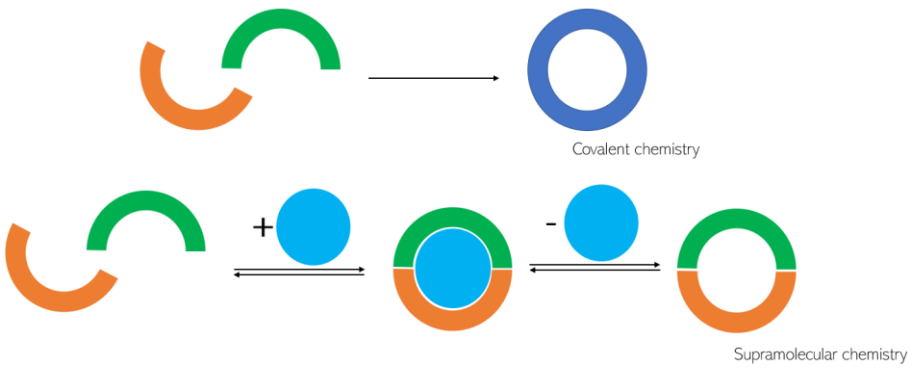

Figure 1.1 A comparison between traditional covalent chemistry (top) and supramolecular chemistry (bottom). Molecular guest shown in blue.

1.2 Molecular Self-Assembly

As previously mentioned, natural examples of self-assembly are abundant but a foray into inorganic self-assembling structures was not made successfully until the work by Charles Pedersen in 1970.[2,3] These structures, named crown ethers, consist of a series of ethyleneoxy groups that are joined at both ends to form a cyclic structure (Figure 1.2). These structures form by utilising cationic templating in the form of an alkali metal cation. The interactions between the guest cation and the crown ether structure are the deciding factor on the size of the final crown ether.

The influence that the guest ion has in the formation of crown ethers illustrates the symbiotic relationship that supramolecular components in a system have; with each separate part (or parts) of a system interacting with one another and affecting the final overall structure.

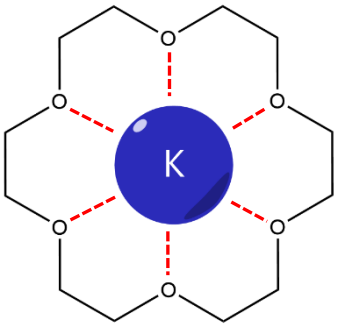

Figure 1.2. 18-Crown-6, an example of a crown ether, coordinating a potassium ion.

Following the synthesis of crown ethers, other three-dimensional structures based on the crown ether motif, were synthesised. Spherands; more complex crown ethers,[10,11] and cryptands;[10,12,13] three-dimensional multi-armed crown ethers, also similarly templated by metal cations, were synthesised. This was then followed by calixarenes,[14] hollow cone-shaped molecules able to trap molecules in the cavity present. Following this, more complex structures have been synthesised such as molecular knots, cation-

templated helices[15] and, maybe most famously, Stoddart's molecular Borromean Rings.[16] The latter of which is an example of a molecularly interlocked structure, and these will be discussed later with an emphasis on rotaxane architectures.

1.3 Metal-Organic Frameworks

Metal-organic frameworks (MOFs) are porous three-dimensional coordination polymers. They are formed through spontaneous assembly through interactions between metal centres, which can be single metal atoms or metal clusters, linked together by coordinate bonds to organic linkers (Figure 1.3).[17]

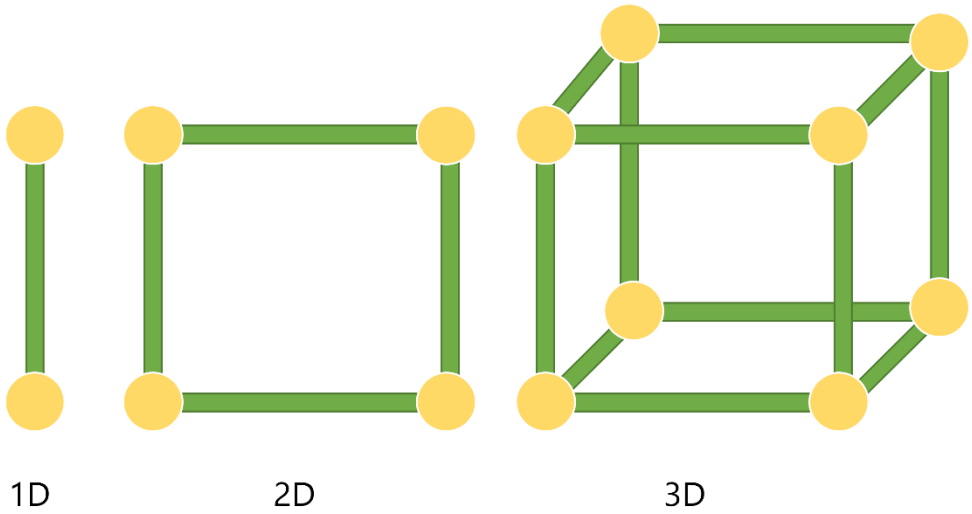

Figure 1.3. A simplified representation of 1D, 2D and 3D structures built from metal centres and structural ligands. Yellow: metal centres, Green: ligands

MOFs can be synthesised in several different ways. The most common of these is by solvothermal synthesis. Solvothermal synthesis consists of dissolving a metal salt and an organic linker in a suitable solvent, and then heating the solution in a sealed vessel to generate autogenous pressure.[18,19] This ideally forms single crystals or powders that can be analysed. Some MOF structures can be formed at ambient temperatures and conditions[20,21], and other methods such as microwave, electrochemical, sonochemical and mechanochemical.[22] These methods all have their relative positives and negatives. Ambient methods are simple to set up and easy to repeat but slow in most cases. Solvothermal synthesis methods utilise more extreme conditions to drive the reaction but can lead to the production of unwanted reactions and side products, reducing reaction efficiency. Microwave synthesis can solve some of these problems by being

highly adaptable, relatively fast and employing mild conditions, however, generally produce products as powders or crystalline materials on the nanometre scale,[23] meaning single-crystal analysis methods are not suitable to analyse these products, therefore making chemical and structural determination of novel structures difficult. Mechanochemical methods do not use solvents and therefore provide a greener alternative in some cases, without sacrificing yield and purity[24] but also produce amorphous products not suitable for single-crystal analysis methods. Electrochemical and sonochemical methods can eliminate some of the issues associated with other synthetic methods and can be used in conjunction with other techniques, most commonly solvothermal methods, to achieve efficient and fast synthesis of products[23] but are not suitable for all MOF formation reactions.

1.4 Metal-Organic Framework Nanotubes

Nanotubes are tubular structures, formed from a two-dimensional layer of material rolled into a cylindrical tube.[25] These structures, originally reported as being pure or partially doped carbon, have been extensively studied due to their ability to trap molecules internally or for reactions to happen on their surface.[26,27] Nanotubes are also relatively easy to functionalise, whether this be on the walls or at the terminal edges.[28] Nanotubes came to the fore when cylindrical multi-walled carbon nanotubes (c-MWNTs) were first synthesised in 1991 by Iijima by an arc-discharge evaporation[29–31] These multi-walled nanotubes were formed from rolled tubes of graphite and measured around 10-80 nm in diameter. Later, in 1993, Iijima and Ichihashi reported single-walled nanotubes with diameters as small as 1 nm.[31] Building on this work, helical-CNTs (HCNTs) were first theorised by Itoh *et al.* in 1993[32] and were then first observed by Zhang *et al.* in 1994.[33] These HCNTs have been shown to have strong ferromagnetic properties,[34] demonstrating that a change in the fundamental nanotube structure can induce different chemical properties.

Because nanotubes are open ended, it is not unreasonable to assume that host-guest chemistry is possible with CNTs, and this has been extensively studied in literature.[35–38] Surface modification is also possible with CNTs and has also been widely studied in a variety of different contexts.[39–46]

Reported nanotube structures are not exclusively carbon-based, and examples of nanotubes constructed from different materials have been reported. Such examples are boron nitride; which is arranged in a physical analogue to graphene with a hexagonal structure,[37,38,47] halloysite; a naturally occurring aluminosilicate[42,48] and more complex examples with multiple groups making up the tubular structure, such as metal-organic framework nanotubes.

Reported examples of MOF nanotubes are very limited but the first published example is work from Jenkins & Murdock reported in 2014.[49] These nanotubes were formed

from flexible ditriazole ligands bridging rigid metal chains capped by a suitable anion to form the tubular shape. These one-dimensional structures can be formed with different metals centres, Cu(I), Cu(II) and Ag(I), to give sized and shaped channels with the same ligands due to the differing metal centre geometry. These structures also behaved in a similar manner to conventional cubic or rectangular MOF, with respect to gas adsorption allowing for the uptake of both carbon dioxide and methane.

Another example was reported in 2018 by Zou *et al.*[50] Co-MOF nanotubes were synthesised by heating cobalt acetate tetrahydrate and 2,5-dihydroxyterephthalic acid in a methanol solution at room temperature to give amorphous MOF-74 nanoparticles, which were then recrystallized into single-crystal nanotubes. These were then further functionalised to create a hierarchical nanotube structure featuring CNT with a guest cobalt atom exhibiting electrochemical activity for oxygen reduction (Figure 1.4).

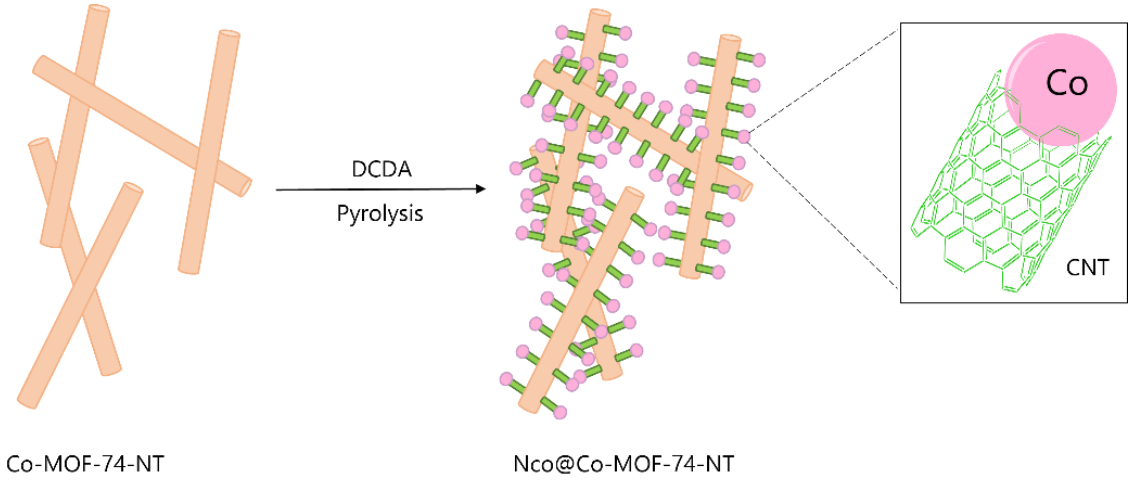

Figure 1.4. The reaction between the Co-MOF nanotubes and DCDA to form branched nanotube structures. Adapted from work by Zou *et al.*[50]

1.5 Mechanically Interlocked Molecules

Mechanically interlocked molecules (MIMs) are compounds that are linked together but not by way of covalent bonds. These interlocked structures cannot be unlinked without the breaking of covalent bonds in either one or multiple components. This interlocking of structures is known as the 'mechanical bond' and was first suggested in 1961.[51] It was in this work that MIMs were classified as single discrete molecules as opposed to molecular assemblies.

Catenanes were the first MIMs synthesised and are a class of molecules that consist of two mechanically interlocked rings. They were first reported in appreciable yields in 1964 by Lüttringhaus and Schill (Scheme 1.1).[52] To achieve this, two long chain ester moieties were added to 4,5-dimethoxyisophthalaldehyde (**1**) *via* a Wittig reaction and subsequent hydrogenation, this was then converted to a dinitrile *via* the diol. After cyclisation of the dinitrile, hydrolysis formed a cyclic ketone which was then reduced and demethylated to form the catechol (**2**). This was then reacted with 1,25-dichloropentacosan-13-one (**3**) to form a ketal which was then nitrated and reduced to give the amine (**4**), which was then cyclized to give 2,2,*N,N*-bisdodecamethylene-4,6-pentacosamethylene-5-amino-1,3-benzo[d]dioxole (**5**). The ketal linkage is cleaved and after dehydrogenation, a hydrolysis reaction is performed to break the C-N bond between the two rings forming the catenane structure (**6**). After acylation and alkaline hydrolysis of the tetraacetate formed, the final product (**7**) was formed. The final product was confirmed by elemental analysis and UV/Visible spectral analysis.

Catenanes allowed for the formation of more complex classes of materials, one of which is rotaxane. These will now be discussed in more detail.

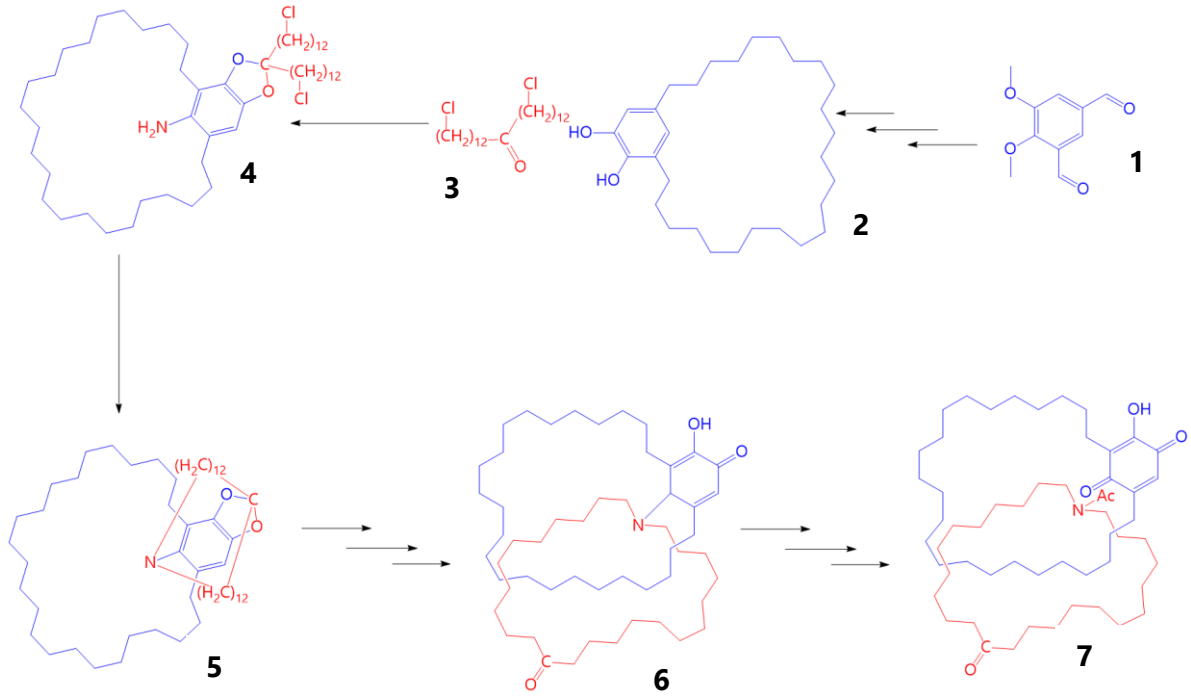

Scheme 1.1 A simplified reaction scheme for the synthesis of the first catenane by Lüttringhaus and Schill in 1964.[52]

1.5 Rotaxanes

Stable threaded structures were first suggested in 1961 by Frisch and Wasserman.[53] Six years later, the first rotaxane structure was synthesised in 1967 by Harrison and Harrison.[54] This structure consisted of an alkyl rod threaded through a large macrocycle and capped at both ends with bulky stopper groups (Scheme 1.2) This was achieved by forming a macrocycle around a hydrocarbon chain with triphenyl groups on either end. The reaction between 2-hydroxycyclotriacontanone and succinic anhydride was performed to give a hemi succinate ester that was then coupled using a peptide resin[55] to form the final interlocked rotaxane structure bound to the resin. The resin was then removed to give the final product. Initially yields were very low but after repeated syntheses, a yield of 6% was obtained. These initial reactions used a statistical threading approach with no real driving force promoting the threading of the rotaxane, hence the low yields. Targeted approaches were later developed, and these will be detailed later in this chapter.

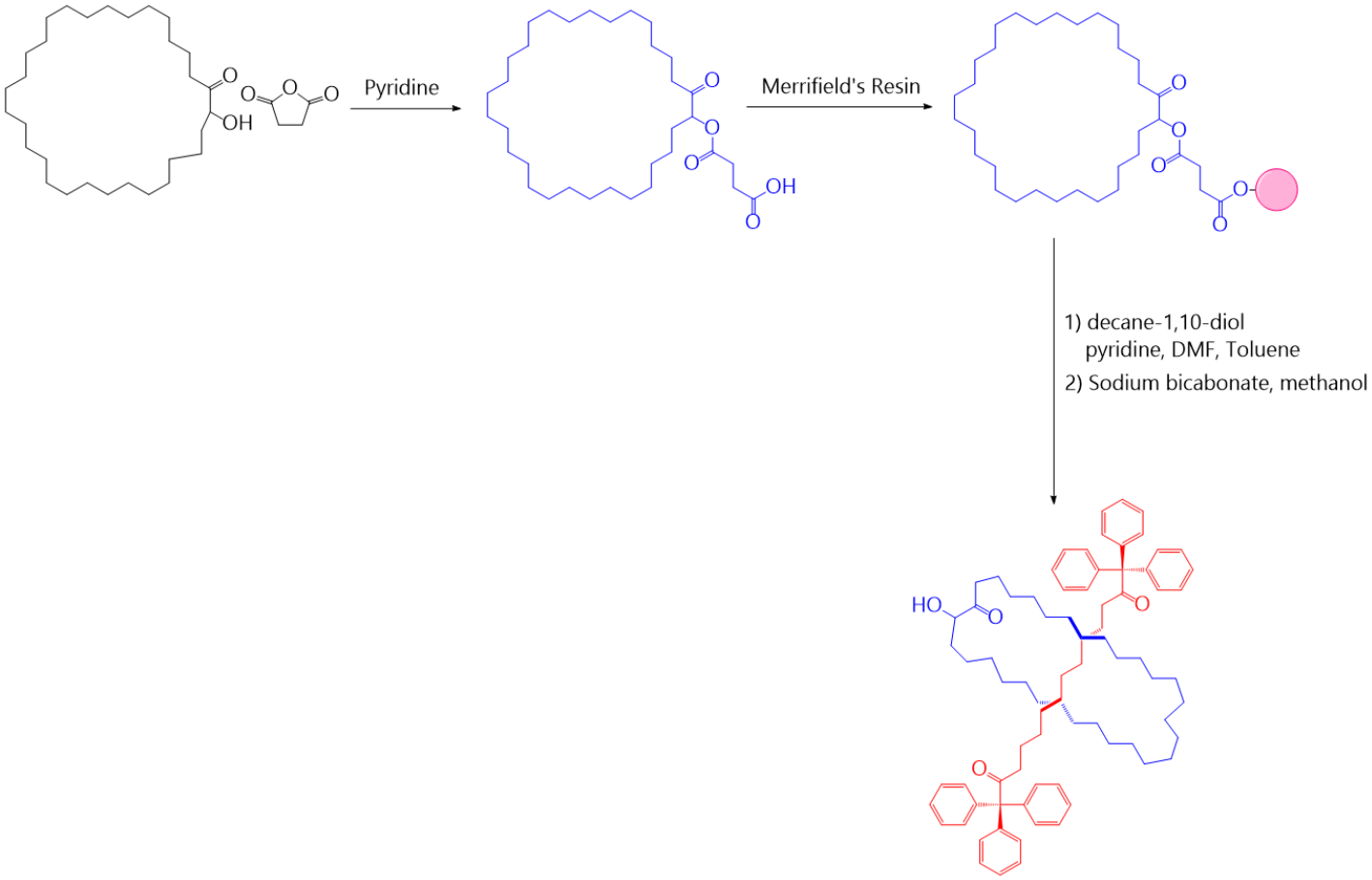

Scheme 1.2. The synthetic route for the first rotaxane reported by Harrison and Harrison in 1967. The macrocycle formed during the reaction is depicted in blue.[54]

This structure by Harrison and Harrison[54]became the template for the basic rotaxane structure consisting of a central rod, threaded through a macrocycle of some kind and then capped, either at one end or both, trapping the macrocycle onto the central rod. There is a wide myriad of different rotaxane structures reported due to flexibility of the rotaxane motif. At this point it is apt to detail the naming convention of rotaxane structures. Rotaxanes can be labelled as [n]rotaxanes where [n] denotes the number of individual interlocked components. For example, a [2]rotaxane (Figure 1.5) is formed from one rod threaded through one macrocyclic ring, whereas a [3]rotaxane is formed of one rod threaded through two rings.

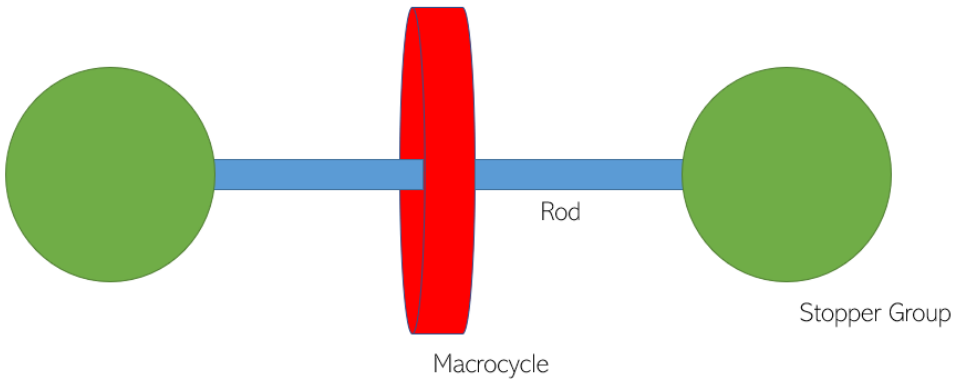

Figure 1.5. The basic structure of a [2]rotaxane

As previously stated, the first rotaxane was formed by a statistical synthesis resulting in low experimental yields. To increase the yield of these reactions, alternate methods were developed that utilise a driving force for the threading step of the reaction forming and forming the intermediate known as a pseudorotaxane, before stopper groups are added to prevent dethreading.[56–59] An example of this is the capping approach in the work published by Takata *et al.* in 1999,[59] in which a rod formed from a dibenzylammonium salt is combined with a crown ether to form a hydrogen bonded pseudorotaxane, and then reacted with an acyl chloride or an anhydride to cap the

rod, preventing dethreading (Scheme 1.3). This resulted in the final threaded rotaxane structure.

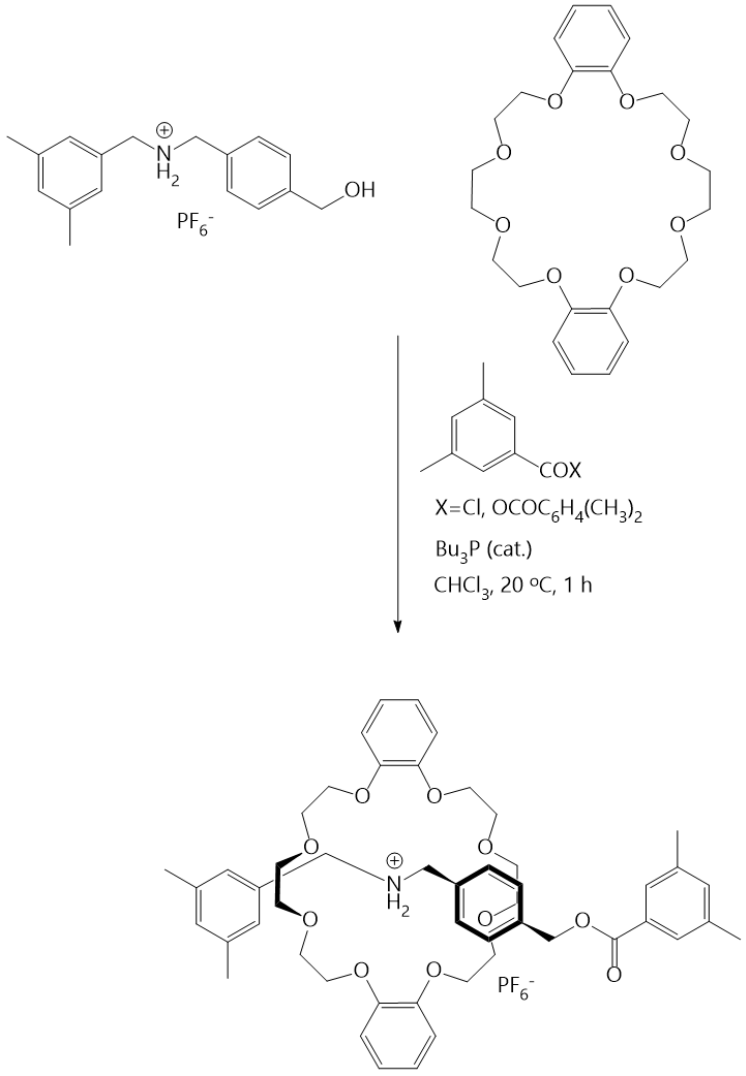

Scheme 1.3. The preparation of the rotaxane synthesised by Takata *et al*. published in 1999 using a directed capping approach to rotaxane synthesis.

Three other synthetic routes to rotaxanes have also been reported: slipping, clipping and active templating (Figure 1.6).

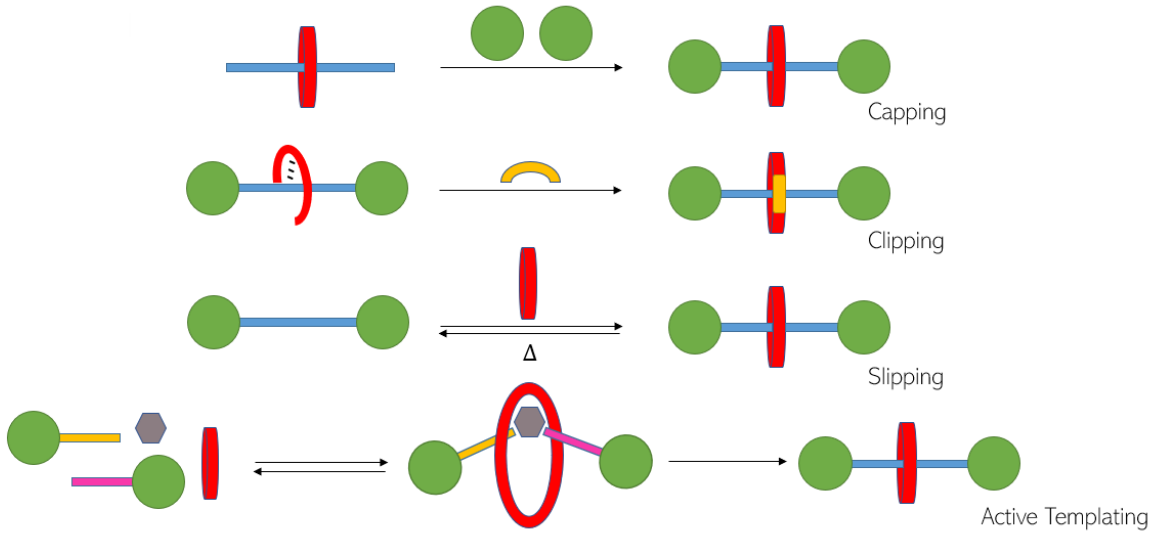

Figure 1.6. A simplified graphical representation for the four methods used for the synthesis of rotaxanes.

Slipping[60–63] uses thermal energy to make the stopper groups in a di-capped rod malleable enough to allow a macrocycle to thread onto the rod, forming a rotaxane. However, because of the increased propensity of the macrocycle to thread during heating, there is also the chance of dethreading to occur. This reversibility gives an equilibrium that can lead to low experimental yields if optimal conditions are not employed for reactions. This assembly method can produce [2], [3], [4] and even higher order rotaxanes as more than more one macrocycle can thread onto a rod, assuming it is of sufficient length to accommodate the macrocycles. Work published by Stoddart *et al.* in 1993[64] illustrates this principle with the initial construction of a bis-4-pyridylpyridinium rod with large, sterically bulky triphenyl groups at either end. This is then heated with a crown ether to form both a [2] and [3]rotaxane (Scheme 1.4)

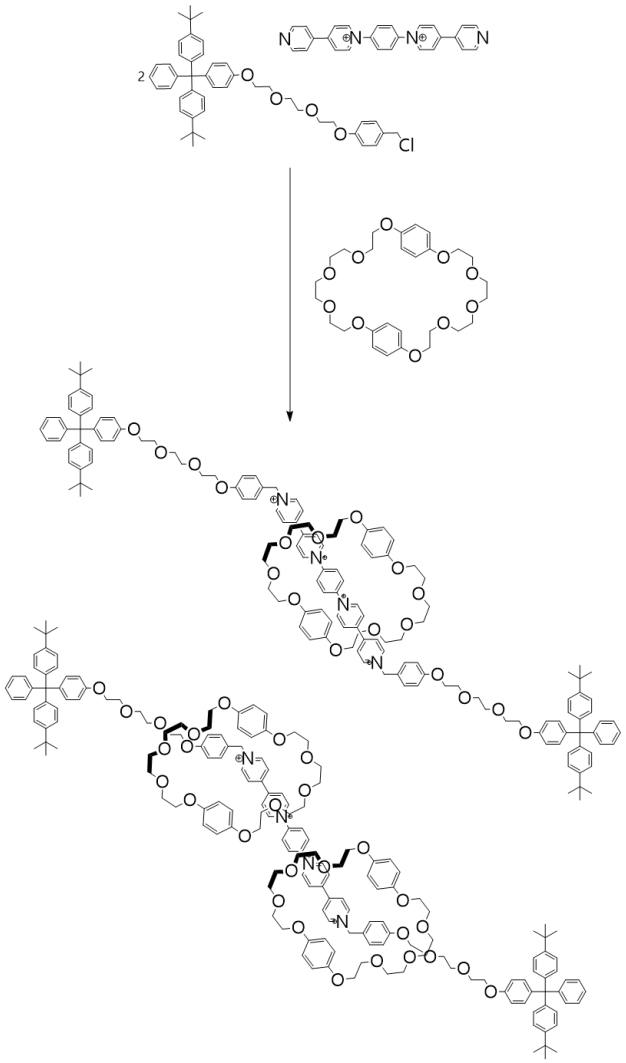

Scheme 1.4. The synthetic method to form [2] and [3]rotaxanes *via* the slipping method.[64]

Clipping[65–68] uses the formation of the macrocycle as the driving force for the formation of the rotaxane architecture. A macrocyclic fragment is positioned onto the rod, which has been previously capped at both ends, and held in position with the aid of molecular interactions, and then the ring closed by reaction with another fragment. This coupling reaction closes the macrocycle and creates the mechanical bond. The positioning of the macrocyclic fragment is reversible but the ring closing reaction is irreversible, resulting in a high yield of the final, desired rotaxane. This reaction can be templated using positive ions and electron rich macrocyclic fragments, holding the

fragments in place to allow a coupling reaction to occur. An example of this is the work from Chiu *et al.* in which a diamine and a dialdehyde are clipped together around an oligo(ethylene glycol) unit to form a rotaxane (Scheme 1.5).[67] This reaction also illustrates a draw-back of the clipping approach, the production of unwanted side products. In this case, that is a catenane formed from two macrocycles that couple simultaneously or a free macrocycle that is not threaded onto a rod.

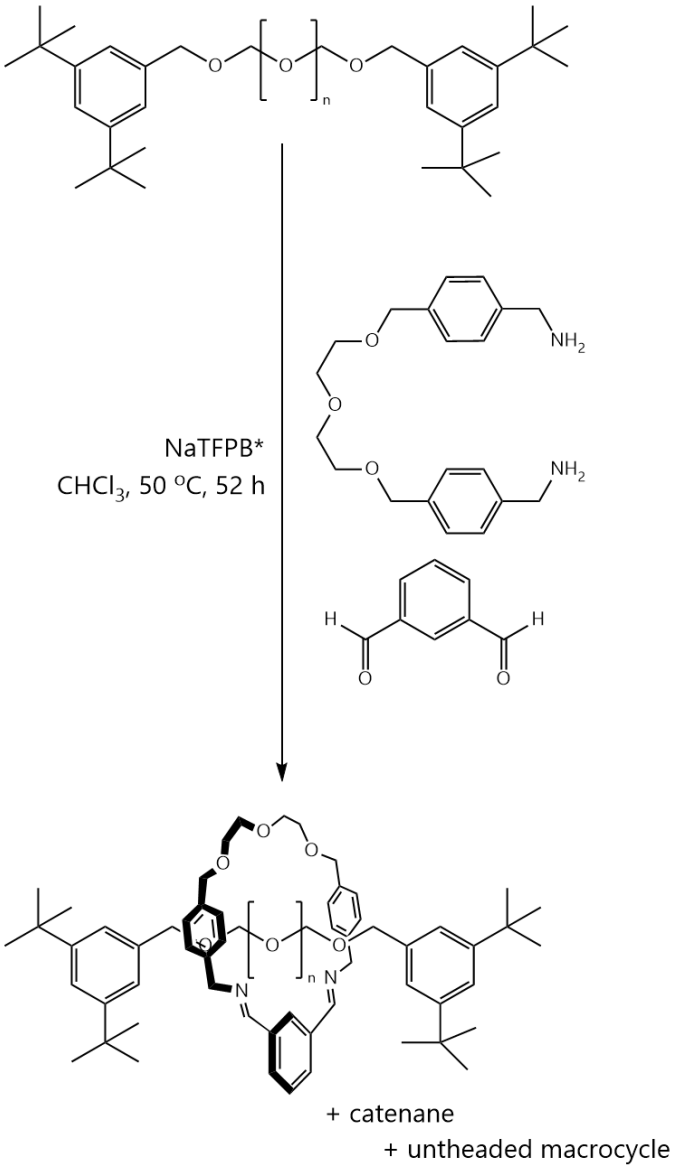

*Sodium tetrakis[3,5-bis(trifluoromethyl)phenyl]borate

Scheme 1.5. The formation of a rotaxane using a clipping method employed by Chiu *et al.*[67]

Active templating is, in effect, the opposite of the clipping method, in that, the rod is formed from two constituent parts inside the macrocycle. This is usually achieved by using a metal mediated coupling reaction,[69,70] the original being a Cu-mediated alkyne–azide cycloaddition (CuAAC) reaction, first reported by Aucagne *et al.,* in 2007.[71] In this reaction, both components of the rod are assembled using the copper centre coordinated to a pyridyl group in the macrocyclic ring. This brings the two halves the rod together and the CuAAC reaction can occur, forming the rotaxane. Some dumbbell molecules, which are rods without a macrocycle, are also formed as a side-product. One of the advantages of this active templating method is that a catalytic reaction regime that can be observed. The reaction path takes the form of a macrocycle interaction confining the metal atom or complex within its cavity which then mediates the coupling of both halves of the rod and then, once reaction is complete, the metal component can leave and initiate another rotaxane formation (Scheme 1.6). This results in a very high reaction yield, approaching 95% in some cases.[72]

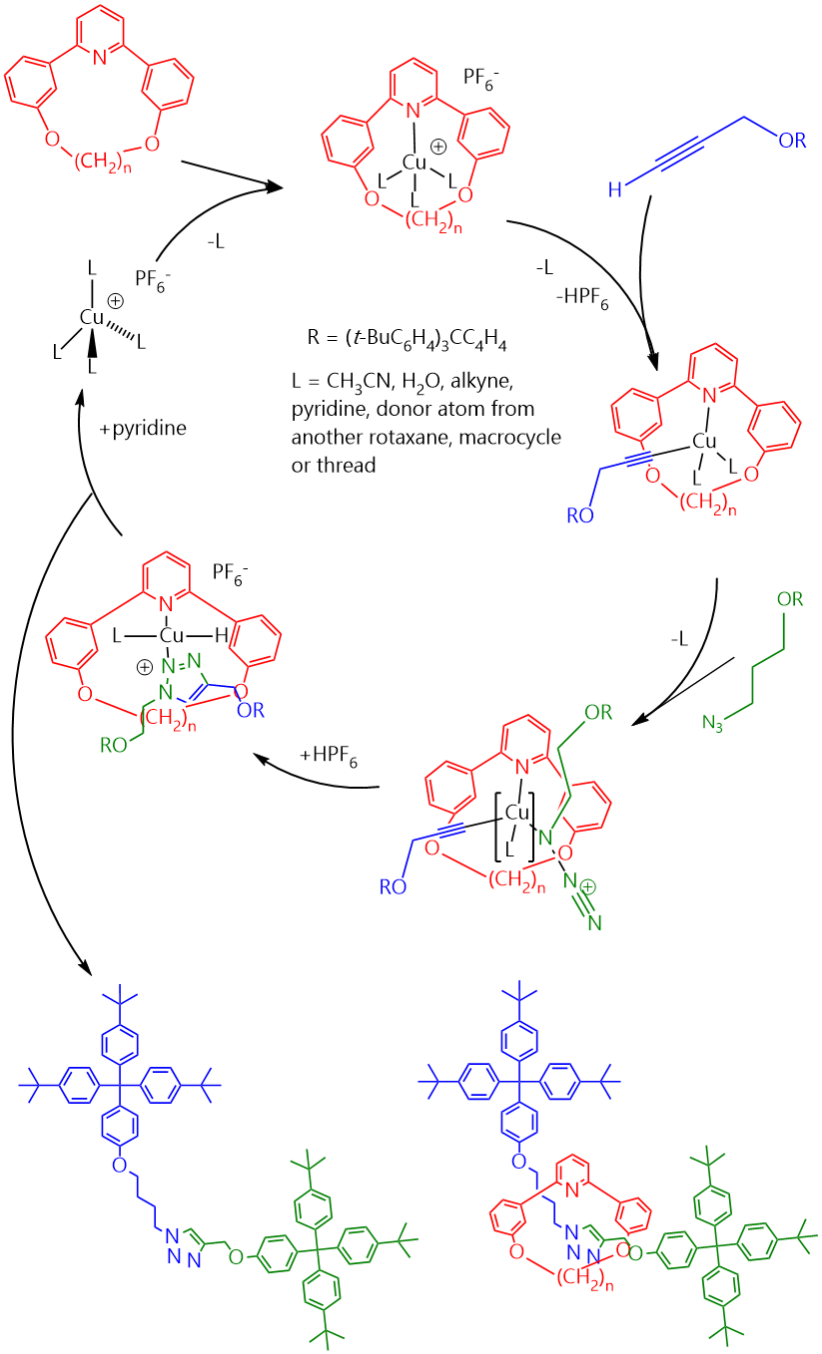

Scheme 1.6. The reaction scheme for the CuAAC addition reaction reported by Leigh *et al.* in 2007[71] which uses the active templating rotaxane formation approach.

1.6 Functionalised Rotaxanes

Rotaxanes can be functionalised in an almost infinite number of ways. This could be a single structural component; the stopper, rod or macrocycle, or any combination of these.

Perhaps the simplest component of a rotaxane to change is the macrocyclic component, and a wide variety of macrocycles have been used in literature. As the macrocycle can be synthesised separately (if using a capping, slipping or active-templating approach) and then threaded onto the rod, the macrocycle can be functionalised in almost any way required. One class of macrocycles, known as pillararenes, are versatile macrocycles formed from bridged hydroquinone units in the presence of a Lewis acid. Pillararenes, first reported in 2008 by Ogoshi,[73] can be easily functionalised by changing the hydroquinone unit's precursor.[74,75] The initial pillararene 1,4-dimethoxypillar[5]arene, is a pillarene formed in a condensation reaction from five 1,4-dimethoxybenzene units and paraformaldehyde in the presence of a Lewis acid. The simple nomenclature for pillarenes is that of (x)pillar[n]arene in which x is dictated by the initial functionalisation of the benzene group and n is the number of repeating units present in the ring structure. For example, if 1,4-diethoxybenzene is reacted to form a six-membered ring, it would have the given name 1,4-diethoxypillar[6]arene.

Work has been carried out building upon the simple pillararene design including copillararenes, which consist of more than one unit in the macrocyclic structure.[76–78] This has allowed two main advances in pillararene chemistry: first, the properties of the pillararenes themselves are able to be tailored to the a specific function, whether this be making water-soluble pillararenes[79–81] or to produce fluorescent pillararene structures,[82] and second; it allows for post synthetic modification to take place on the macrocycle (Scheme 1.7).

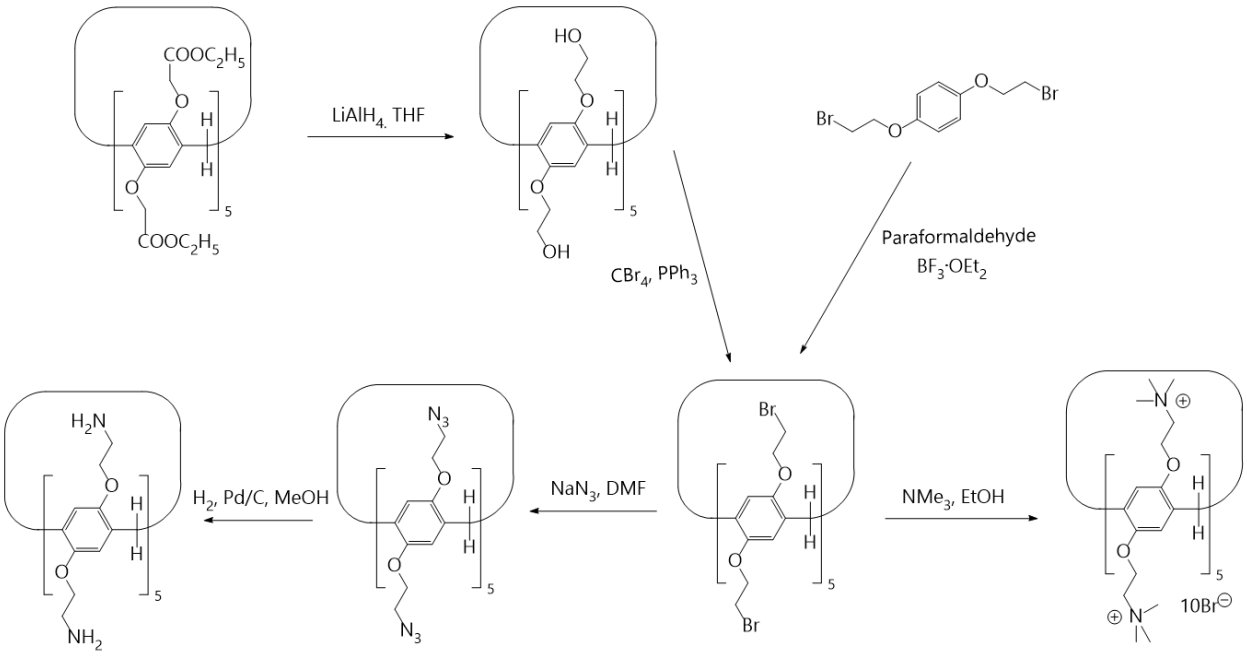

Scheme 1.7. An example of some synthetic modifications that can be performed on a pillar[5]arene molecule.

Functionalising the rod of a rotaxane can aid threading and therefore rotaxane formation. Using an electron deficient substituent can facilitate an interaction between this group and an electron rich macrocycle, which can provide a driving force for rotaxane threading, increasing reaction yields. A common motif used in literature is to use an imidazolium group as the electron-deficient component.[83–86] An example of this are reactions that use pillararene and an imidazolium group to form a [2]rotaxane (Scheme 1.8), which was first reported by Huang *et al.*[87] The pillararene cavity is electron rich, due to the electron donating nature of the ether linkages on the benzyl rings and if a positively charged (or electron deficient group) is introduced to this cavity, it will position itself inside, due to the electrostatic interaction between the two groups. This means that when the stopper reaction is performed, there is a much greater chance that the rod will be threaded and the rotaxane formed. This

imidazolium group/macrocycle interaction will be the basis of the rotaxanes reported herein and will be discussed further in the proceeding work.

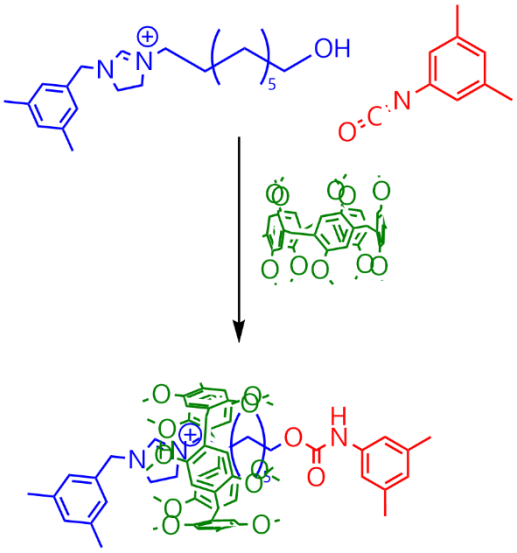

Scheme 1.8. The synthetic route to a [2]rotaxane employed by Huang *et al.* utilizing the pillarene/imidazolium motif.[87]

An interesting feature of imidazolium rods is the access to carbene chemistry that this provides. Imidazole groups propensity to form *N*-heterocyclic carbenes (NHCs)[88] in the presence of metal atoms/complexes allows for controlled molecular shuttling. In work by Champness *et al.*,[85] it was observed that by metalating the imidazolium groups on a rotaxane, shuttling can be controlled and monitored by NMR spectroscopic studies. It was observed in the ^{1}H NMR spectrum that there was a lack of peak splitting in the alkyl protons, meaning the pillararene macrocycle oscillates along the rod faster than the ^{1}H NMR timescale. By reaction with an Ag(I) or Pd(II) complex, shuttling can be restricted, and the individual alkyl proton signals observed. Once the metal complex is removed, the protons signals coalesce once again. This creates a controllable molecular shuttle that can be turned 'on and off' by metalation. These molecular shuttles are one of the simplest molecular machines.[65,89–92] The 2016 Nobel Prize was awarded to Jean-Pierre Sauvage, Sir J. Fraser Stoddart and Bernard L. Feringa for work on this class of molecules. An exciting possible application of molecular shuttles is for

data storage. In general, anything with an 'on/off' mode can be used for data storage. Molecular shuttles fit this criterion and therefore, could be used. This molecular storage approach has been employed using DNA nucleotide bases,[93–95] using base sequencing to represent bits in a binary storage scheme. By having a molecular shuttle that can actively be controlled, whether this be by coordination or solvent, this binary storage scheme can be employed in rotaxanes.

The final way in which rotaxanes can be functionalised is to change the stopper groups present on the rotaxane. This is sometimes to increase the solubility of the rotaxane structures. MIMs are by their nature, bulky structures and solubility can be an issue for further modification or analysis. A way around this is to add large polar or non-polar groups to the stoppers, which, while also acting as a good stopper to prevent dethreading, also aids the solubility. Published work by Amabilino *et al.*[96] describes the synthesis of a dendritic stoppers that were readily soluble in many different organic solvents (Figure. 1.7)

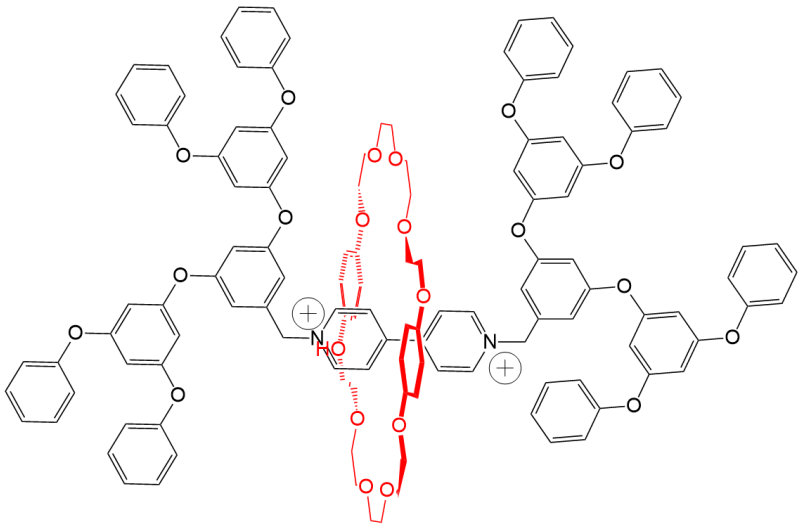

Figure 1.7. One of the rotaxanes bearing dendritic stoppers synthesised by Amabilino *et al.*[96]

If groups that can be coordinated to metal centres (such as carboxylic acids or nitrogen containing groups) are added to the stopper of the rotaxane, extended structures

incorporating rotaxanes can be produced. One class of these structures is metal-organic rotaxane frameworks and which now be discussed in detail.

1.7 Metal-Organic Rotaxane Frameworks

Metal-organic frameworks are three-dimensional porous materials that are formed from organic ligands joined coordinatively by metal centres.[97] These generally take the form of metal clusters known as structural build units (SBUs) and instead of being a single metal atom, they are inorganic fragments containing multiple metal atoms bridged together.[98–101] These can be formed upon reaction of an organic ligand with a metal salt, and this is most usual method for forming metal-organic frameworks. An almost infinite amount of ligand/metal combinations can be used and over 70,000 different MOF structures have been reported.[102]

In contrast, metal-organic rotaxane frameworks (MORFs), which incorporate rotaxanes as ligands, have far less reported examples, with fewer than ten structures found in literature.[103–111] These will now be discussed.

The first MORF structure was reported by Loeb in 2005.[112] This consisted of a bis(*N*-oxide) imidazolium rod and a crown ether macrocycle that formed a pseudorotaxane (Figure 1.8) (a threaded but uncapped rotaxane) that was then capped at both ends by Yb(III) metal centres to form the MORF structure. This MORF has an unusual structure formed of seven coordinate ytterbium centres, six rotaxanes and one triflate anion. This was followed by another reported MORF structure in 2010 by Loeb & Vukotic in which a singly charged pyridinium axle was used with the same benzyl crown ether macrocycle and then linked together using zinc ions to form a two-dimensional porous planar square framework.[103]

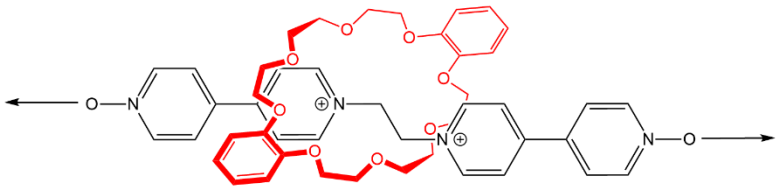

Figure 1.8. The pseudorotaxane linker unit used in the first MORF structure reported by Loeb in 2005.[112]

The first three-dimensional MORF structure was reported in 2011 by Sessler *et al.*[109] This was achieved in a one-step self-assembly reaction by combining a tetraimidazolium "molecular box"[113] macrocycle with 2,6-naphthalene carboxylate anions and zinc(II) cations. These self-assembled into a highly ordered cubic structure with the macrocyclic components threaded onto the naphthalene dicarboxylate dianions to give a "closed bicyclic, adamantane-like arrangement of zinc cations containing three coordination stabilized rotaxane motifs."

The following year another pseudorotaxane based MORF was synthesised by Yaghi *et al.,*[105] this time using a Cu(II) metal centre to coordinate the macrocycle and rod components together, which was then reacted with a zinc salt to form the MORF. A large macrocyclic ring was reacted with a Cu(II) salt to form a coordinated species and then this was reacted with a phenanthroline unit, which displaces the other two ligands forming a threaded species (Scheme 1.9). This produces a three-fold interpenetrated structure, meaning that three different individual networks within the MORF are catenated with one another in the final structure.[114]

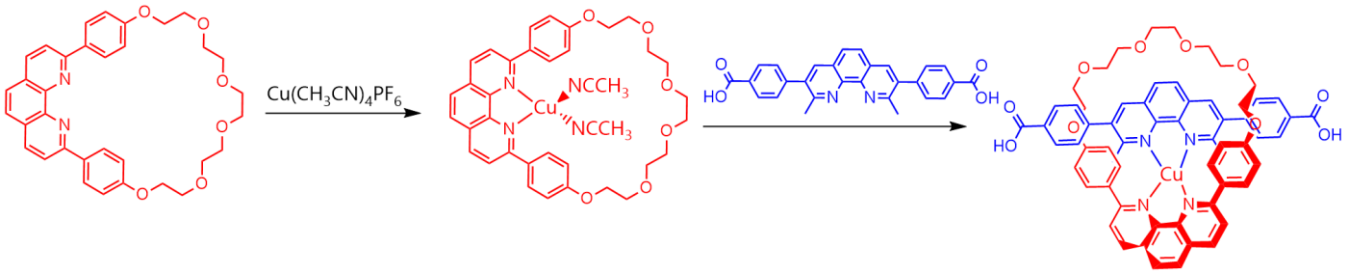

Scheme 1.9. The pseudorotaxane formation reaction using a Cu(II) centre to anchor the macrocycle and rod components to form the pseudorotaxane.[105]

Up to this point, the method of synthesising MORF structures was to form a pseudorotaxane and then coordinate these to metal centres to form a threaded rotaxane *in situ*. In 2012, Loeb *et al.* reported a MORF structure in which the rotaxane was previously synthesised with stopper groups allowing for complexation with metal centres.[104] A macrocycle was formed around a diphenyl ammonium ion, that had been functionalised with two carboxylic ester functionalities on each benzyl ring. The macrocycle was formed by a ring closing reaction olefin metathesis mediated by Grubbs' I catalyst, which was then reduced to give the final crown ether macrocycle and threaded onto the ammonium axle (Scheme 1.10). The ester groups were then deprotected the leave a tetracarboxylic acid functionalised rotaxane, able to bind to Cu(II) units to form the final MORF structure.

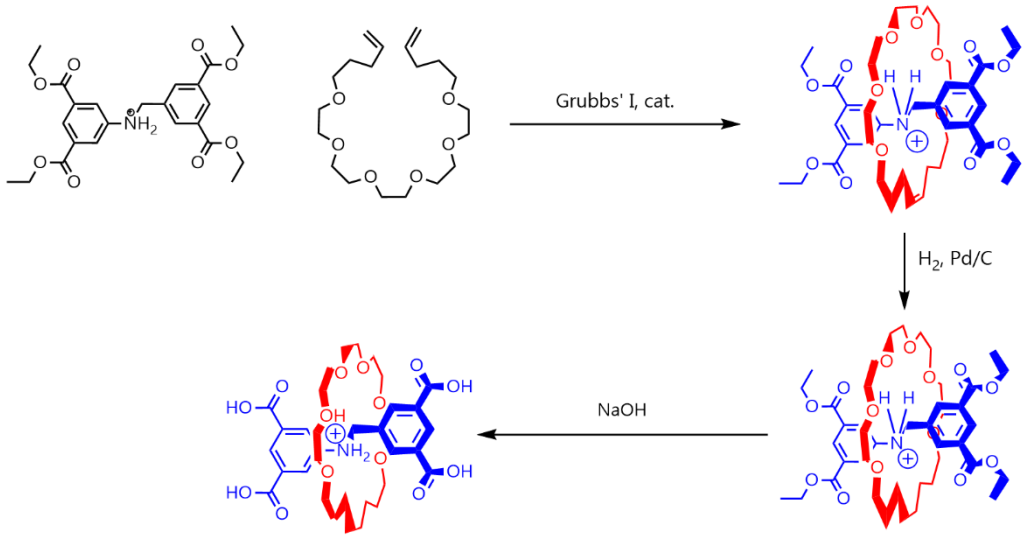

Scheme 1.10. The formation of the rotaxane used in the MORF structure reported by Loeb *et al.* in 2012.[104]

Until this point, research had focused on crown ether or modified crown ether type macrocycles in MORF assembly. In 2015, Su *et al.*[106] reported a MORF structure formed from cucurbituril-based pseudorotaxane rods. The pseudorotaxane was formed from a bipyridyl diammonium rod threaded through a cucurbit[6]uril macrocycle.

This was then reacted with a cadmium salt and a benzene dicarboxylic acid (either H_2BDC or H_2BPDC) to form a pillared MORF structure (Figure 1.9).

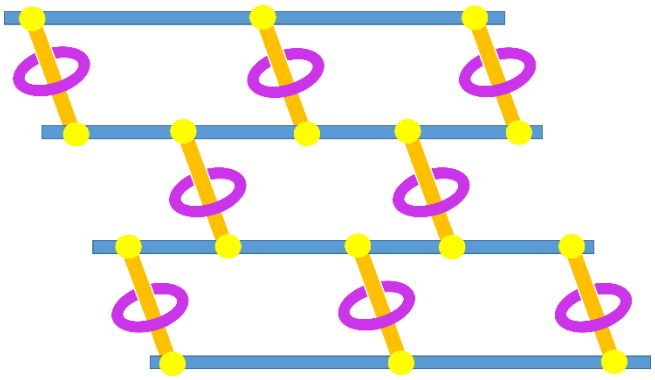

Figure 1.9. A 2D simplified representation of the pillared cucurbituril MORF in work published by Su *et al.*[106] (benzene dicarboxylic acid in blue, cadmium centres in yellow, cucurbituril in purple and bipyridyl diammonium rod in orange).

Another MORF structure, reported in 2016 by Loeb, uses the 'active templating' approach discussed earlier to assemble the rotaxane that is then subsequently used to create the final MORF structure.[115] A hexa-ester rotaxane (Scheme 1.11) is formed by a coupling reaction between two different constituents, one a formylphenyl imidazolium species and the other a diaminophenyl species, both attached to identical triphenyl backbones, respectively. This formed a symmetrical diimidazolium rod, threaded through an ester functionalised crown ether with the bulky triphenyl groups acting as stoppers. The rotaxane was then deprotected to form the hexa-acid rotaxane. This rotaxane was then joined together by Zn(II) metal centres, with two rotaxane ligands attached to each metal centre, to form an interpenetrated MORF.

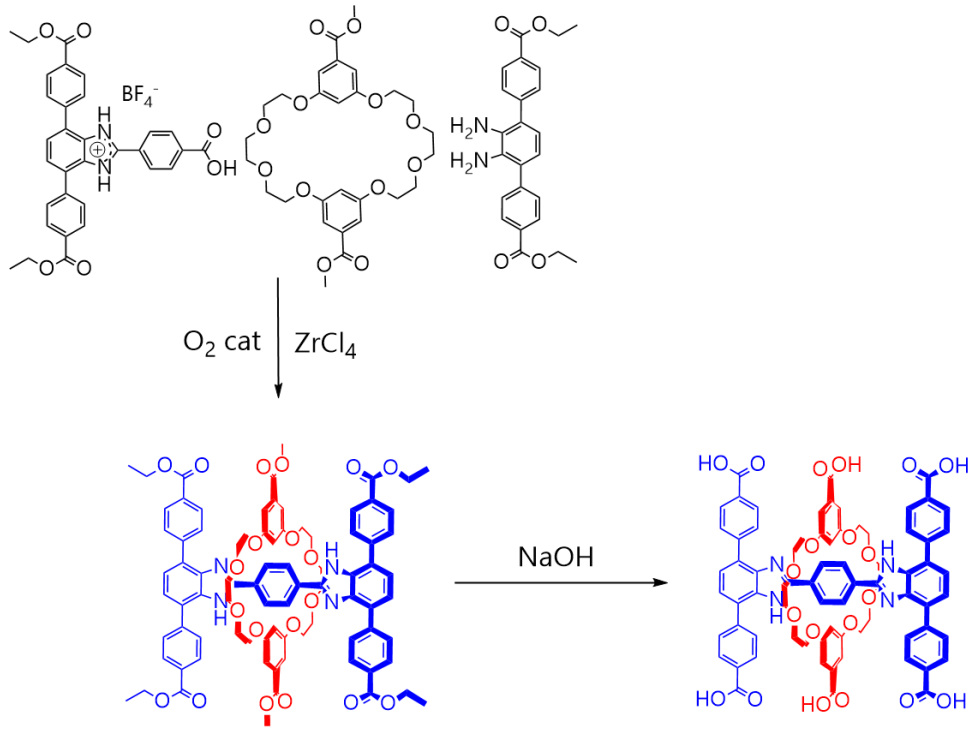

Scheme 1.11. The 'active templated' rotaxane used in the MORF reported by Loeb *et al.*[115]

Pyridine-functionalised rotaxanes have also been used to construct MORF structures. Loeb *et al.* used a dipyridyl rotaxane in conjunction with 4,4'-biphenyldicarboxylic acid and 4,4'-azodiphenyldicarboxylic acid to form mixed-linker MORF frameworks.[116] These were formed by a similar method to earlier work, with a crown ether diene intramolecularly coupled, using Grubbs' catalyst, to form a pseudorotaxane around a bisbromophenyl amine chain. A pyridyl group was then added to both ends of the chain using a Suzuki coupling[117] using the pyridyl boronic acid. The alkene macrocycle was then reduced to give the final pseudorotaxane structure. This was then combined with zinc nitrate and the cross-linking acid and allowed to self-assemble. These MORFs were found to also exhibit restricted motion of the crown ether in solution and free motion of the crown ether macrocycle upon removal of solvent. This was found to be a completely reversible and this control over the macrocycle motion in interlocked structures demonstrates the possibility for distinct modes in the structure, akin to a molecular switch. A porous MORF structure with switchable modes has also been

shown by Stoddart and co-workers with the synthesis of a molecular shuttle inside a MORF.[91]

1.8 Molecular Rotaxane Handcuffs

Molecular handcuffs are another class of interlocked supramolecular architectures.[118] These exist broadly in two groups, handcuff rotaxanes[119–124] and handcuff catenanes.[119,122,125–127] These form similarly to rotaxanes forming a pseudo-structure and then being either stoppered or, in the case of catenanes, a ring-forming reaction taking place to mechanically lock the structure in place.

Handcuff rotaxanes, which are largely like rotaxanes, are threaded and stoppered in multiple positions. Handcuff catenanes are interlocked ring structures which have two or more rings mechanically linked, and finally, higher handcuff structures, are larger, more complex structures are a mix of both catenane and rotaxane architectures in the same molecule. Due to the possible complexity of these structures, it is necessary to institute naming conventions to best describe them. This convention, suggested by Champness *et al.*[128] takes the form, (x)handcuff[y]rotaxane/catenane, where "x refers to the number of threaded macrocyclic hosts that are joined in the handcuff component of the mechanically interlocked molecule [and] y, refers to the number of mechanically bonded components of the rotaxane or catenane". Later in this thesis, a [2]handcuff [2]rotaxane (Figure 1.11) will be discussed and this type of handcuff rotaxane will now be examined in further detail.

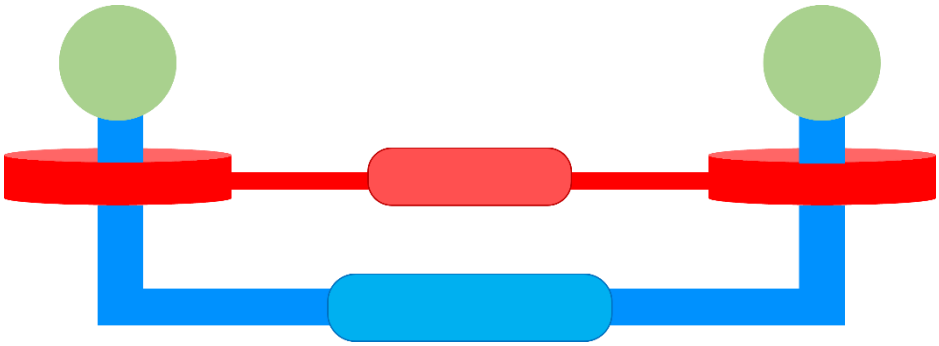

Figure 1.11. A simplified, generalised example of a [2]handcuff[2]rotaxane. Macrocyclic rod component shown in red, threaded rod component shown in blue, stoppers shown in green.

A [2]handcuff[2]rotaxane consists of two rods; one of which has two macrocyclic components and the other than has two electron-deficient groups that can thread through these macrocycles. These are then stoppered to prevent dethreading.

It may, at first sight, seem improbable that these complex structures would self-assemble but the rod can be functionalised with moieties that can interact, holding the macrocycles in place, allowing for threading to occur more readily. This, in combination with the interactions of the macrocycle and threading rod, allows for higher yields than may be expected for such complex structures.

The first proper [2]handcuff[2] rotaxane was synthesised in 2006 by Sato and Takata and was formed by bridging a [3]rotaxane with two dithiol linkers, creating the handcuff structure (Figure 1.12).[123]

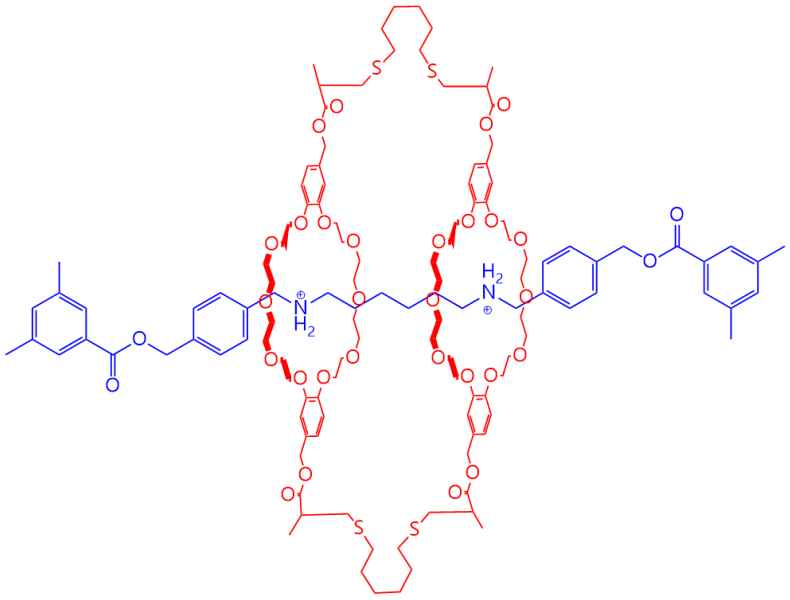

Figure 1.12. The structure of the first [2]rotaxane [2] handcuff reported in 2006 by Sato and Takata.[123]

Functionalising the chains of handcuff rotaxanes with planar, aromatic groups allows stacking to occur. This has a two-fold benefit: the first being that the increased interaction between these two molecules, increasing the driving force for the handcuff formation reaction to take place; and second, this configuration allows molecules to be held at such distances that the two molecules can interact with one another. Once the handcuffs are formed, the nature of the interactions between the two groups can be probed with techniques such as UV-visible spectroscopy, fluorescence, cyclic voltammetry (CV) and spectroelectrochemistry. These techniques allow the electronic properties of the functional groups to be studied both separately and then in relation to each other, in an environment where these groups are situated close to one another probing the effects they have on one another's electronic properties.

An example of this is the work by Champness *et al.*[129] in which a [2]rotaxane[2]handcuff including both perylene diimide (PDI) and naphthalene diimide (NDI) functionalities in the same molecule. The proximity of these molecules allows for them to interact with one another but also the structural flexibility to allow the molecules to move together and apart. This facilitates the formation of a radical anion π-dimer upon double reduction of the same molecule. A PDI/PDI handcuff was also synthesised and found to form similar dimers.

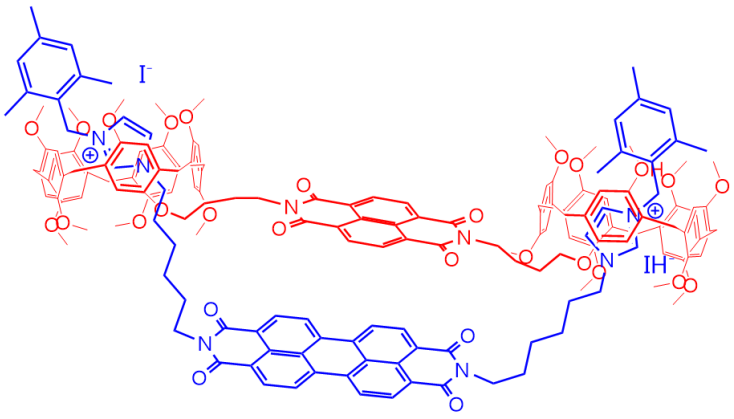

Figure 1.13. The structure of the NDI/PDI handcuff synthesised by Champness *et al.*[129]

1.9 Research Aims & Objectives

A novel zinc MOF NDI-nanotube had been synthesised previously in the group as a by-product of a MOF formation reaction. No examples of a similar structure could be found in literature at the time that the structure was synthesised, and, for this reason, the NDI nanotube was to be synthesised again to see of it could be regularly replicated and if the nanotubes could be reproduced reliably, considering the electronic properties that NDI possesses[130–133], UV/Vis spectroscopic measurements could be taken to see if a radical is formed during this process and stabilised in the nanotube structure.

Second, taking inspiration from previous MORF assembly methods,[103,104] a rotaxane formed by utilising the pillararene/imidazolium interaction with carboxylic acid-functionalised stopper groups is to be assembled using a stepwise method; with the imidazolium rod assembled first, a pillararene macrocycle threaded onto this rod and then capped to form a rotaxane. This rotaxane could then potentially be combined with metal salts to from a MORF. If these structures form crystalline products, they can be analysed using single-crystal X-ray techniques. These novel MORF structures will further the understanding of MORF formation as a whole and more specifically, those incorporating the pillararene group.

Finally, an NDI/porphyrin handcuff rotaxane molecule synthesis will be attempted in a similar method to that of the acid rotaxane discussed above. A MOF containing NDI and porphyrin ligands had previously been synthesised in the group and the synthesis of the handcuff rotaxane analogue can offer a direct comparison between the rigid, ordered MOF structure and a flexible handcuff. Once synthesised, the handcuff can be probed using cyclic voltammetry to explore the electronic effect the NDI and porphyrin have on one another, respectively, and see if a similar structure to π-dimer reported by Champness *et al.* is formed.[129]

2. Synthesis of an NDI-MOF Nanotube

2.1 Naphthalene Diimide Containing Metal-Organic Framework Nanotubes

Naphthalene diimides (NDIs) are a class of organic molecules that have been well studied due to their electronic behaviour and have subsequently been utilised as n-type semiconductors in field-effect transistors.[133–136] NDIs consist of an aromatic core, formed from four fused rings with four carbonyl moieties. This core is easily functionalised using simple addition reactions, granting access to a vast array of different materials.[130,137–139] By changing the substituents on an NDI molecule, the physical properties can be changed. Substitutions on NDIs can occur at several different positions (Figure 2.1), and it has been shown that different substituents not only effect the orbital energies of an NDI but also the electron transfer properties.[140,141] By selecting substituents correctly, NDI molecules can be tuned to fit their desired purpose. An illustration of this is the use of substituted NDI molecules as synthetic photosystems.[142–144]

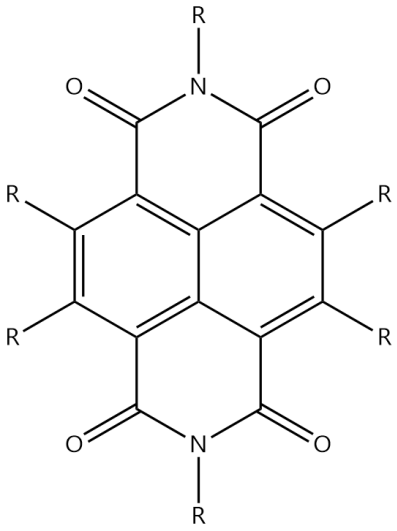

Figure 2.1. The generic structure of an NDI molecule. The positions marked in 'R' are positions available for substitution.

NDIs can form stable radical species. This radical formation can take the form of a chemical oxidation using an oxidising agent such as lead(IV) dioxide,[132] however radicals can also be formed by ultraviolet or visible light radiation[145] as well as mechanical methods.[133] One example of interest is that of work by Zhang et al. They reported a highly stable radical NDI species, stabilised by incorporation into a supramolecular system.

Herein, a zinc NDI-MOF nanotubular structure that self-assembles from a methyl pyridine substituted NDI and naphthalene dicarboxylic acid in the presence of zinc nitrate is reported. The NDI-MOF nanotubes were characterised by single-crystal X-ray diffraction (SCXRD) and imaged using scanning-electron microscopy (SEM).

The zinc/NDI nanotubes were synthesised from a mixture of $Zn(NO_3)_2 \cdot 6H_2O$, 1,4-naphthalene dicarboxylic acid (NDA) and dipyridyl methyl naphthalene diimide (DPMNDI), in dimethylformamide, which was heated at 100 °C for 24 hours. This produced clear colourless needles (Figure 2.2) that were characterised using single-crystal X-ray diffraction.

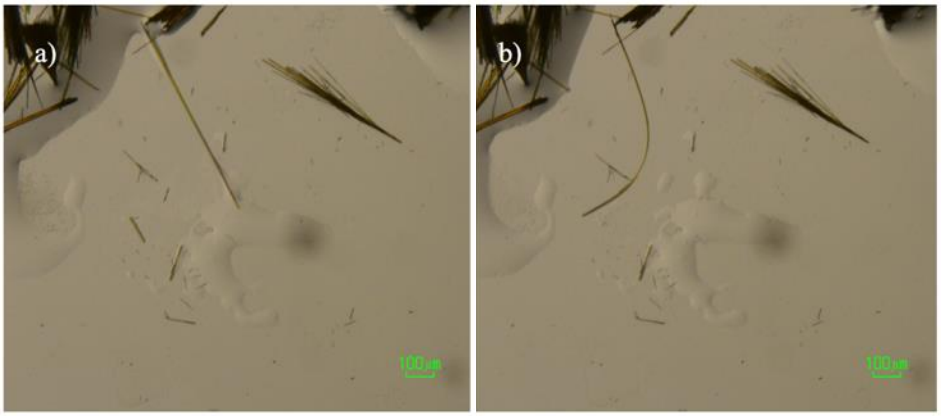

Figure 2.2. Microscope images of in the NDI-MOF nanotubes. It can be seen that the nanotubes are discrete and flexible needles.

The nanotubes crystallise in the tetragonal $P4_2$ space group with an asymmetric unit consisting of two DPMNDI molecules, each bound to a Zn centre which is then bound to a 1,4-naphthalene dicarboxylic acid molecule (Figure 2.4). Upon expansion of the structure (Figure 2.5), a two walled, helical nanotube can be observed. The inner wall is formed of entirely NDA units and the outer wall is formed by DPMNDI units with both being linked by a pseudo-tetrahedral four-coordinate zinc centre. The observed coordination angles in the zinc centres (Figure 2.3) are unusual in geometry as they lie somewhere between a uniform tetrahedral geometry (six angles of 109.5 °), as seen in a four coordinate zinc complex like zincblende, and a split geometry (two pairs of three identical angles) as observed in a four coordinate complex, such as that in carbonic anhydrase.[146] In the Zn centres in the nanotubes, there are four N-Zn-O bond angles; of which two are smaller than that of a regular tetrahedron and two are larger. The Zn-N bond lengths are consistent with literature values (between 2.007 – 2.025 Å) .[146] The Zn-O bond lengths have between those measured in a ZnO monolayer by Gao *et al.*[147] (1.92 Å) and those of ZnO bulk material (2.01 Å). This could be expected given the distorted tetrahedral geometry, being somewhere between the tetrahedral ZnO structure and the planar ZnO monolayer.

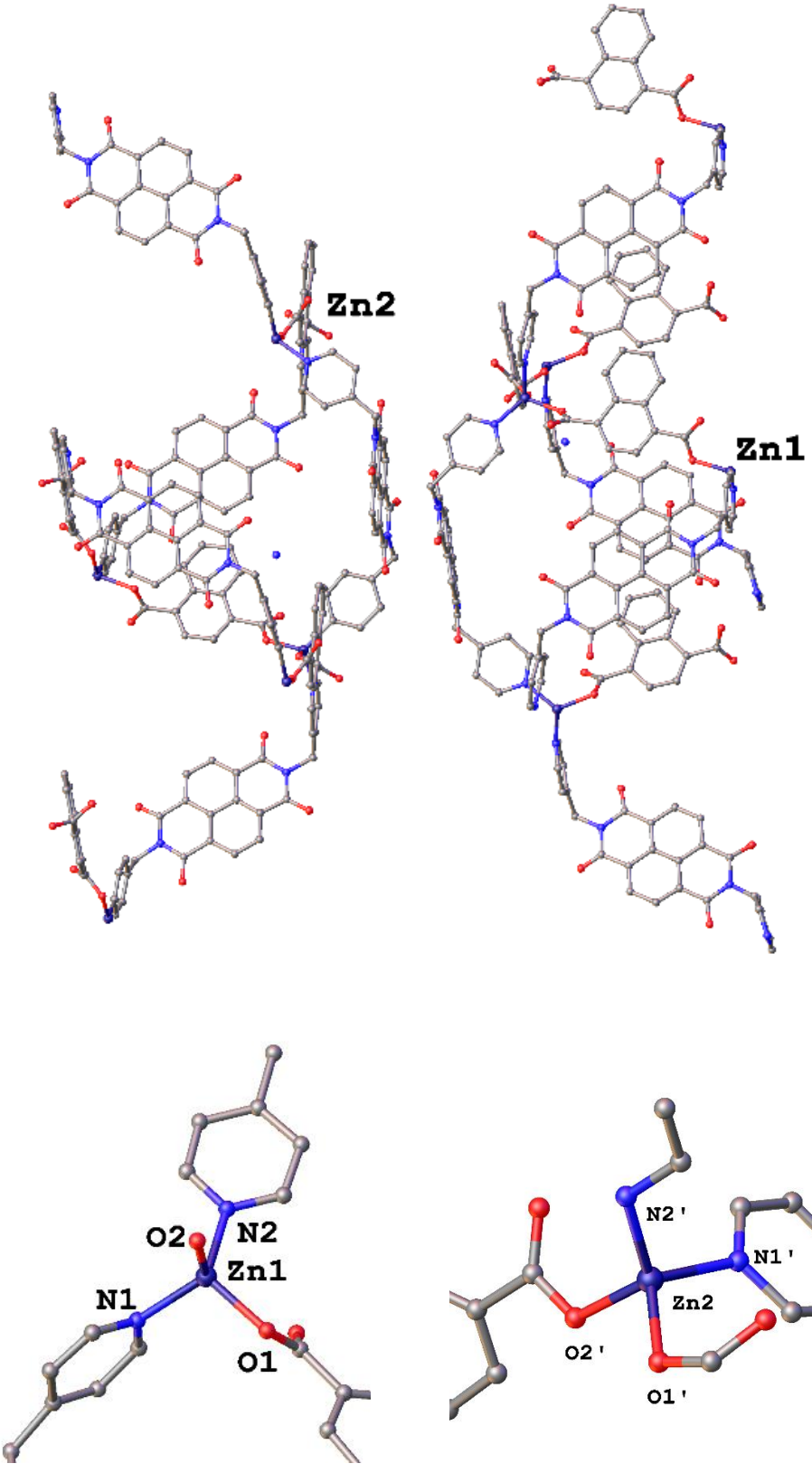
Zn2
Zn1
O2
N2
Zn1
N1
O1
N2'
N1'
Zn2
O2'
O1'

Atoms	Bond Length (Å)	Atoms	Bond Angle (°)
Zn1-N1	2.014(9)	O1-Zn1-O2	97.3(3)
Zn1-N2	2.030(9)	O1-Zn1-N1	108.1(3)
Zn2-N1′	2.023(9)	O1-Zn1-N2	118.7(4)
Zn1-O1	1.924(8)	O2-Zn1-N2	103.0(3)
Zn1-O2	1.980(8)	O2-Zn1-N1	115.3(4)
Zn2-O1′	1.935(8)	N1-Zn1-N2	113.5(3)
		O1′-Zn2-O2′	97.9(3)
		O1′-Zn2-N1′	114.4(4)
		O1′-Zn2-N2′	103.1(3)
		O2′-Zn2-N1′	107.7(3)
		O2′-Zn2-N2′	119.4(4)
		N1′-Zn1-N2′	113.4(4)

Figure 2.3. The Bond lengths and bond angles around the zinc centres in the NDI-MOF nanotubes (C – grey, N – blue, O – red, Zn – dark blue).

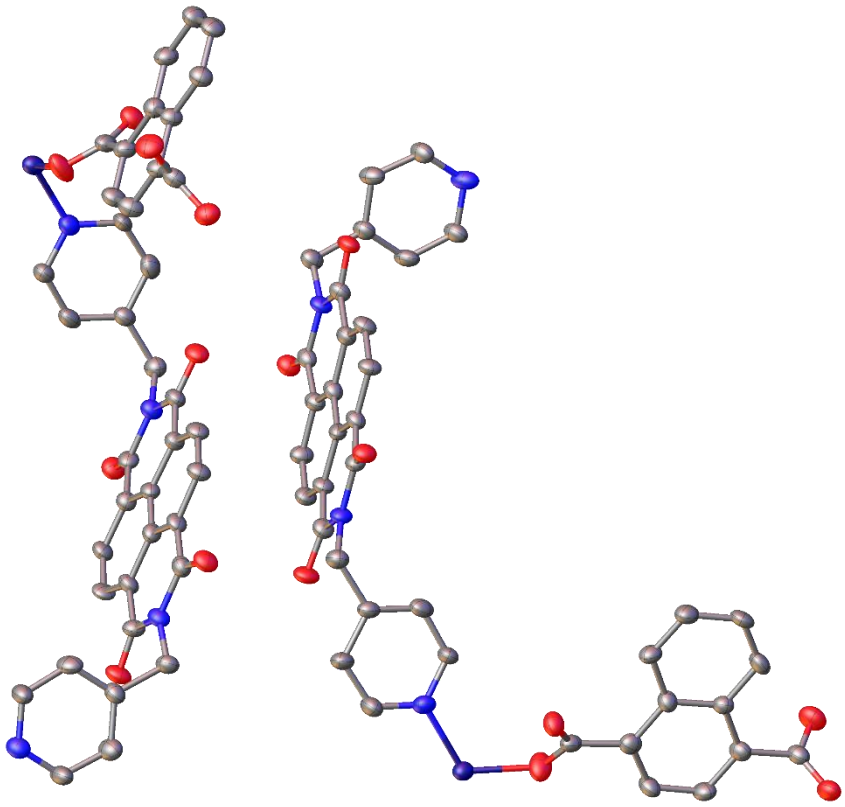

Figure 2.4. The asymmetric unit for the NDI-MOF nanotubes structure (50% ellipsoids). Zn – dark blue, O – red, N – blue, C – grey. Hydrogens omitted for clarity.

The NDI-MOF nanotubes crystalise in enantiomeric pairs. This means the two nanotubes are non-superimposable due to the differing direction of the helical spiral in each tube, with a fraction of each one of these visible in the asymmetric unit. Single-walled carbon nanotubes (SWCNTs) are chiral by their nature[148] and it could be expected that, as another example of a nanotube structure, the same chirality descriptions can be used. This is, however, not the case. Due to the uniform nature of SWCNTs, the surfaces can be seen as a continuous rolled sheet.[149] For the NDI-MOF nanotubes, with the helical shape, it more accurate to describe the chirality in a similar way to that of DNA.[150] The NDI-MOF nanotubes can be described as L- or R-helices depending on the relative direction of coiling. In each expanded asymmetric unit, there is one of each present.

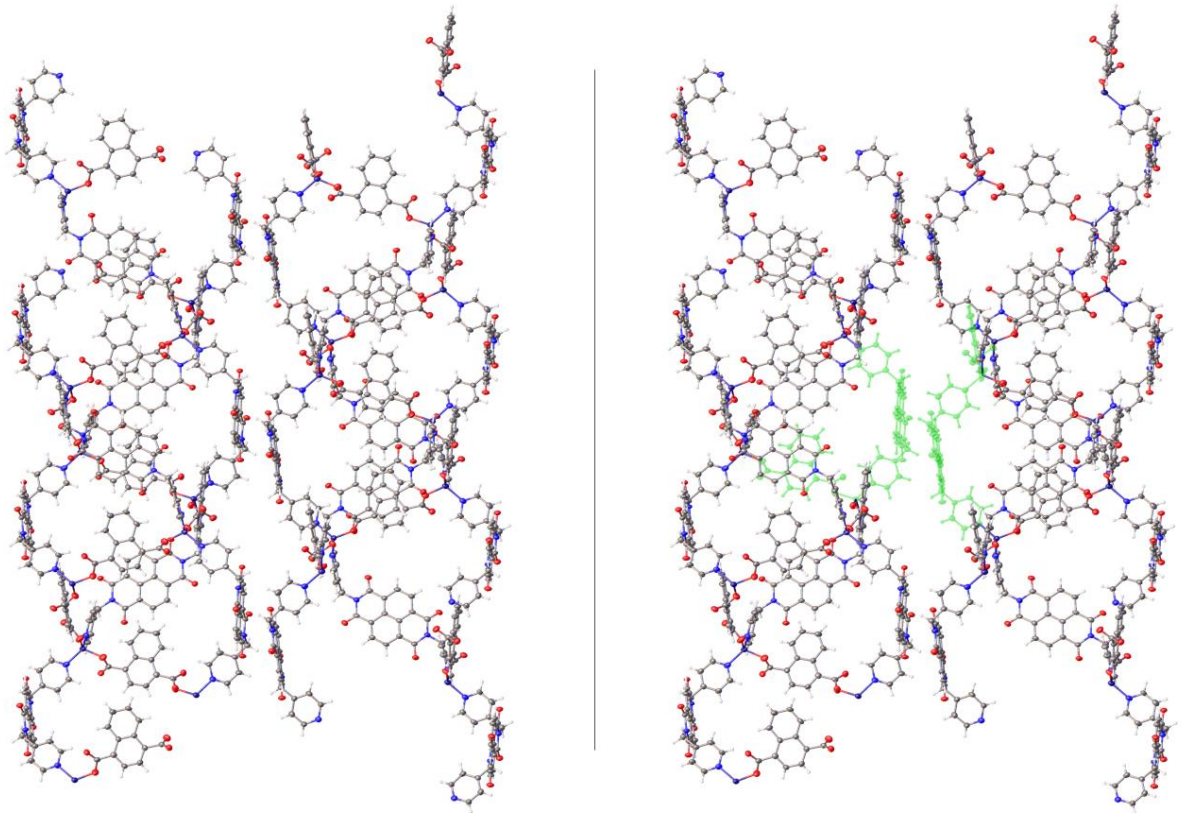

Figure 2.5. The expanded structure of the NDI-MOF nanotubes. Two different enantiomers can be seen. The structure on the right shows how the asymmetric unit (green) fits into the overall structure. Zn – dark blue, O – red, N – blue, C – grey. Hydrogens omitted for clarity.

The DPMNI molecules in the nanotubes all adopt the same cis geometry forming a U-shaped molecule. This conformation allows for $\pi - \pi$ interactions to be maximised for the nanotubes internally, between the NDI cores and the NDA units, and externally between the NDI outer walls of neighbouring nanotubes. $\pi - \pi$ interaction distances were measured using both atom-atoms distances and centroid-centroid distances by OLEX2.[151] The measured atom-atom distances are 3.548(3) Å, between the outer and inner tube walls, and 3.740(4)Å, between discrete nanotubes. The centroid-centroid $\pi - \pi$ distance calculations give interaction distances between 3.609(4)-3.999(4) Å with shifts between 1.172(8)-2.049(7) Å.

Upon packing of the nanotube structure, two different pores can be observed (Figure 2.6). The first, a square continuous channel measuring 10.844(9) Å × 10.844(9) Å, is present in the centre of each nanotube. The second is a larger continuous rectangular pore present between four different nanotubes with a pore opening measuring 13.268 Å × 13.065 Å. The accessible pore volumes were calculated with PLATON[152] and four different accessible pores are found with volumes of: 696Å^3 (8%), 881 Å^3 (10%), 881 Å^3 (10%), 692 Å^3 (8%), totalling 3150 Å^3 (36.9%). These values are calculated by the PLATON programme inserting a sphere into a void and then gradually increasing the volume until the sphere reaches the van der Waals radius of the atoms on the cavity edge. The subsequent volume of this sphere is the accessible pore volume.

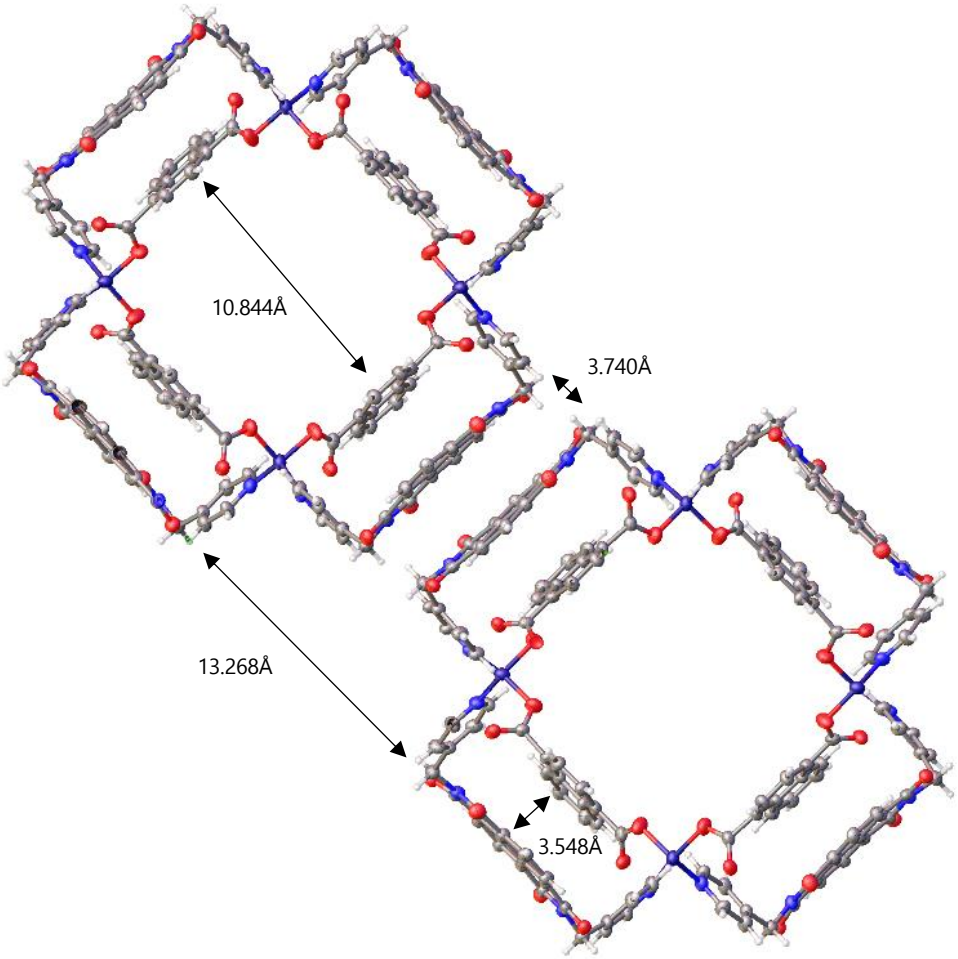

Figure 2.6. A partially extended structure of the NDI-MOF nanotubes. The ball and stick structure (top) show the double walled nature of the nanotubes with the atom-atom distances labelled both for the distance between the inner and outer walls of the nanotube and the distance between neighbouring nanotubes, respectively. These distances are consistent with $\pi - \pi$ interaction distances. (Zn – dark blue, O – red, N – blue, C – grey. Hydrogen atoms omitted for clarity).

Solid state UV/Vis spectroscopy measurements were taken, revealing a short-lived, reversible colour change. This novel two-walled helical nanotube structure is permanently porous and capable of producing semi-stable radicals in the presence of visible and ultraviolet light, persisting for around thirty minutes, before returning to the parent material. The NDI nanotubes undergo a reversible photoreduction upon exposure to ultraviolet (λ = 465 nm) radiation, signified by a visible colour change. This

visible colour change can be measured using solid state reflectance UV/Vis spectroscopy (Figure 2.7). Before irradiation, the MOF crystals were ground to form a homogenous powder and loaded into an UV/Vis Near-IR Agilent Cary Spectrometer with a solid-state UV/Vis attachment, at room temperature. The orange powder had the expected spectrum with high percentage reflectance in the visible region peaking around 650-700 nm, corresponding with the red/orange visible region of the electromagnetic spectrum, which would be expected due to the orange colour of the sample. Upon irradiation with a UV light source, the visible colour of the MOF powder changed, becoming much paler and less vibrant. This corresponded to a drop in reflectance in the spectrum in the visible region. The signals of the sample, pre- and post-irradiation, are almost identical in the ultraviolet region of the spectrum and begin to diverge in the visible region. The post-irradiation sample has a much lower reflectance in the visible region in general but is much lower in the orange/red region. The signal pre-irradiation is almost featureless with an incline in the visible region, peaking around 700 nm before, declining towards the infrared region. In the irradiated sample, many new features appear in the spectrum. These are most likely attributed to the radical formation.

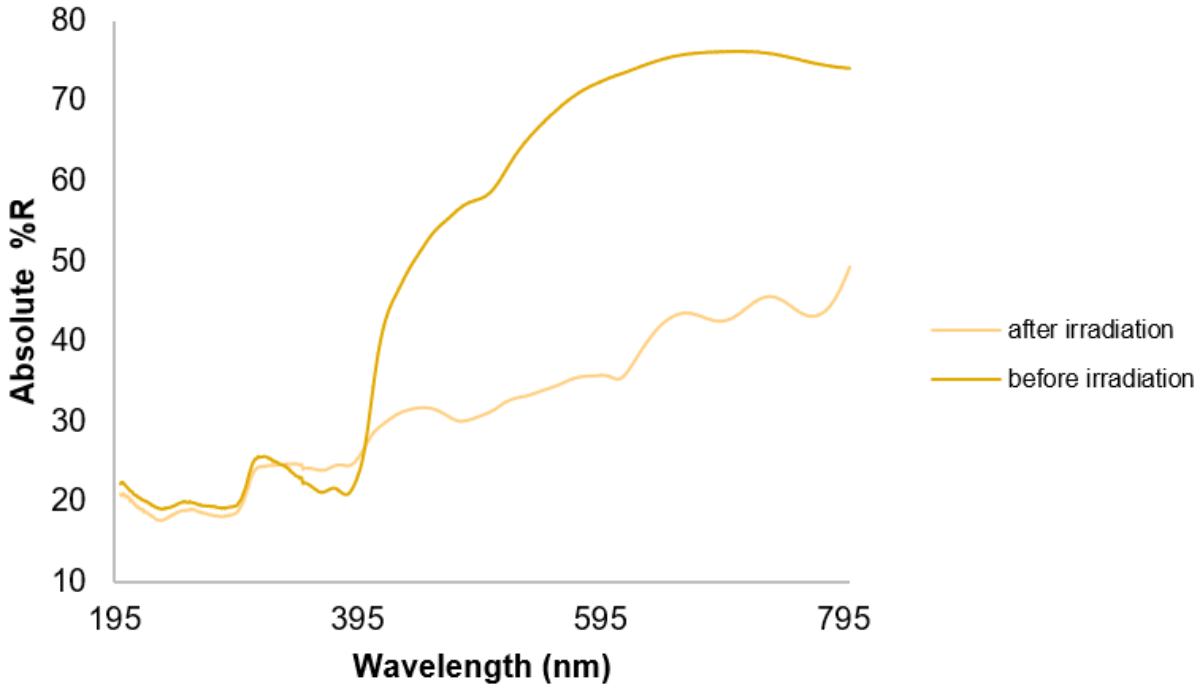

Figure 2.7. The solid-state UV/Vis reflectance spectrum of the MOF-NTs clearly shows that upon irradiation at 465 nm, a clear decrease in reflectance is observed, corresponding to an observed colour change. This plot shows the difference between the sample before and after irradiation.

2.2 SEM Measurements

The zinc MOF nanotubes were dried and further characterised by scanning electron microscopy (Figure 2.8). These SEM images show distinct, discrete nanotubular structures, bunched together. The fibres are very thin, with diameters no more than 20 μm and with lengths between 500 – 700 μm, much longer than previously reported MOF nanotube crystals.[153]

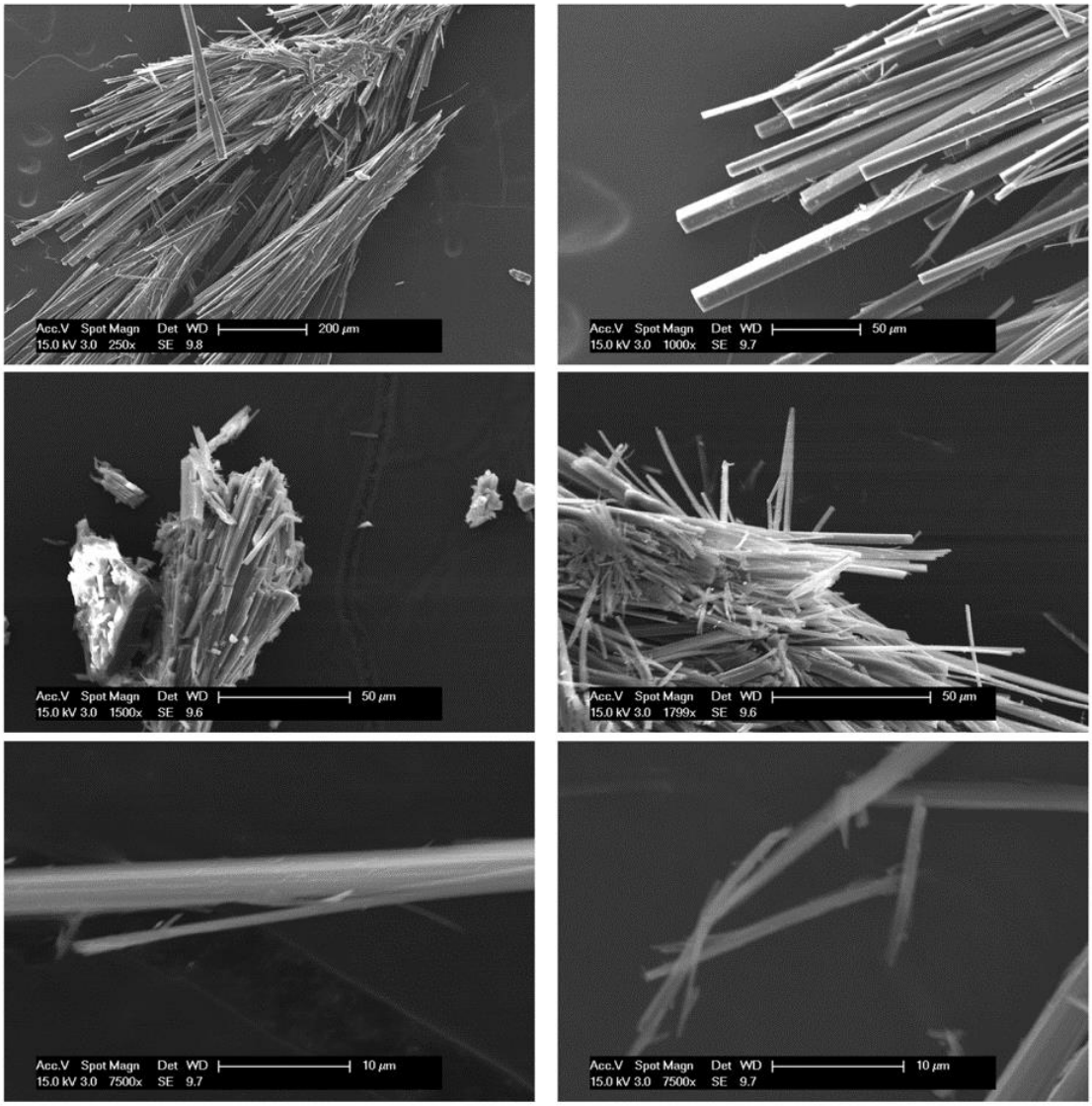

Figure 2.8. SEM images taken of the MOF-NTs. Single crystals can be seen both individually and as large bundles of hundreds of crystals.

2.3 Raman Measurements

Upon the discovery of the flexible nature of the nanotubes, it was decided that Raman measurements would be a suitable way of identifying if there was a chemical change in the nanotubes when bending occurs. The initial strategy for this was to find straight and bent nanotubes, record Raman measurements, and compare the spectra. If chemical differences, displayed in small wavenumber shifts as bonds elongate or contract, were present, it can be shown that physical bending changes the chemical properties of the nanotubes. For the straight tube measurements, seven suitable tubes were selected and measured (Figure 2.9). The results showed that six of the seven nanotubes had almost identical spectra and therefore it can be reasonably assumed that they are the same material. Many non-tubular artifacts were also present, but these were assumed to be precursor materials and thus not measured.

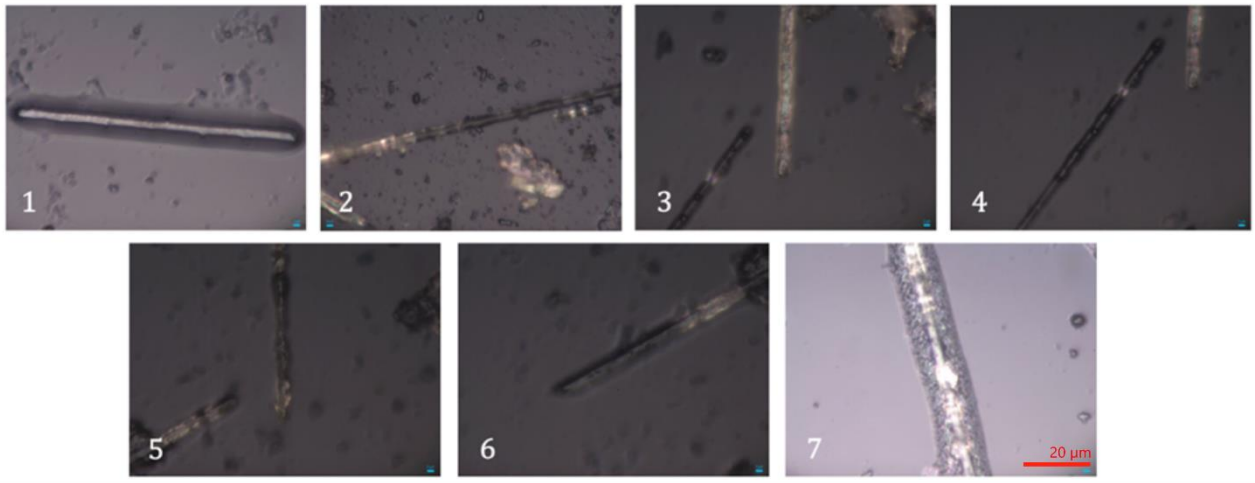

Figure 2.9. Images of the seven straight nanotube crystals that were initially chosen for Raman spectral analysis.

Attempts to locate bent tubes were unsuccessful. These 'bent' tubes were to be any tubes that were visibly curved. Three different candidates were chosen and all these subsequently gave different spectra, none of which were close to that of the straight tubes.

The next strategy that was attempted was to isolate a suitable straight crystal, take measurements, bend the crystal mechanically and repeat the measurement. After multiple attempts, this was deemed unfeasible as the nanotubes were only pliable while solvated and upon drying, crystals were prone to cracking or breaking. For this reason, it was decided that a higher resolution measurement would be taken using the previous method of identifying a straight and bent crystal and taking measurements of each one respectively.

Once these measurements are plotted and overlaid (Figure 2.10), and although the two spectra are similar, there is evidence of a Stokes redshift of around 1.4 cm^{-1} in the bent tube compared to straight tube. This suggests that the bent tube is under higher tensile strain than the straight tube. This would be supported by the observations of cracking and breaking when tubes are bent and desolvated. Possible evidence of polarisation can also be observed by increases in the peak magnitudes between 1600-1800 cm^{-1} in the bent tube spectrum. Polarization can be used to determine orientation in two-dimensional structures and azimuthal angles in 3D structures.[154] By observing this polarisation of the nanotubes, it indicates a change of angle, observed as bending.

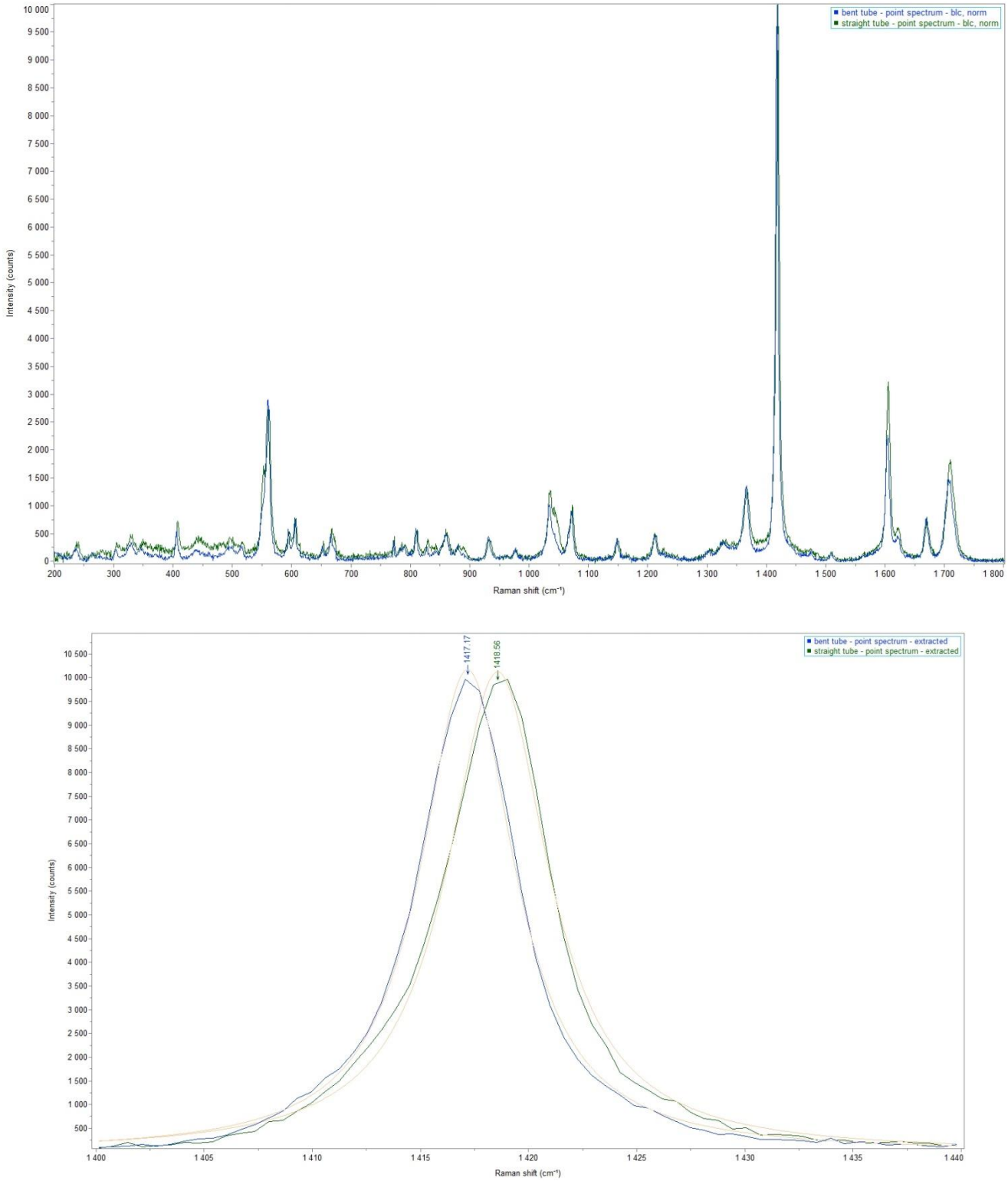

Figure 2.10. (Top) The overlay of the Raman spectra from the straight and bent tube measurements. (Bottom) A close up of the highest intensity peak, showing the 1.4 cm^{-1} shift between the straight (green) and bent (blue) tubes.

If a map is constructed similarly to before (Figure 2.11), areas with strain can be seen as red shift. For the straight tube, the band positions obtained from the edge of the tube are more red shifted that those at the centre, suggesting greater tensile strain at the edges. For the bent tube, it is more complex but generally the vibrational modes on the inner (concave) surfaces are more red shifted than those on the outer surface. The magnitude of the shift is also dependent on the position relative to the apex of the bend with points closer to the bend exhibiting more strain. The mean spectra are broadly consistent with the single point spectra data. As this is only one isolated measurement, it is possible that tube twisting is observed rather than bending and more measurements would have to be taken to verify if this is the case.

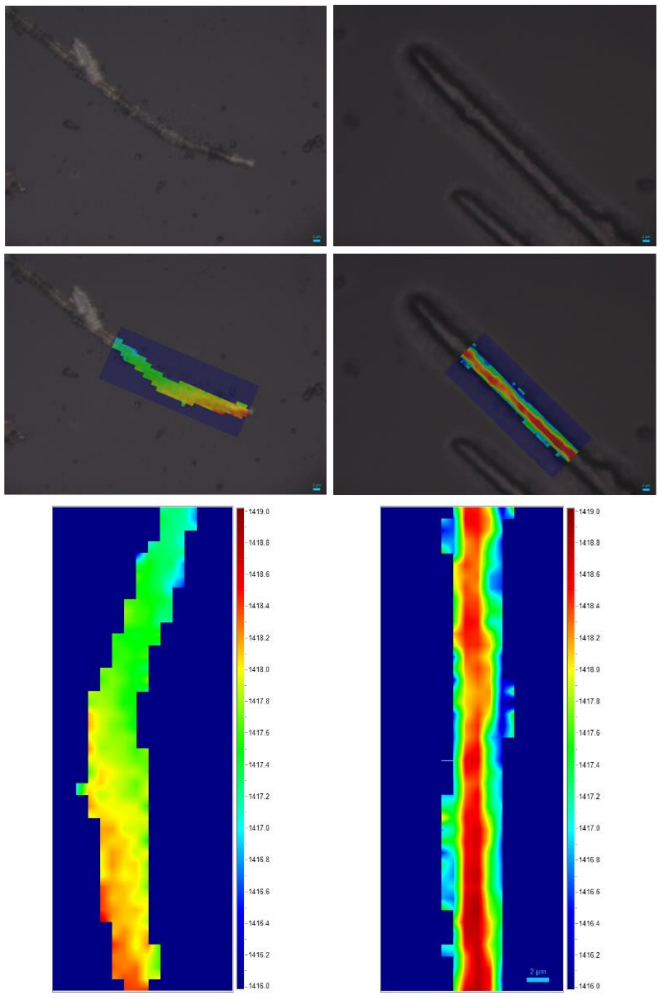

Figure 2.11. A comparison of the bent and straight tubes with the peak positions plotted as a function of position.

2.4 Conclusions

A helical zinc-NDI nanotube was successfully re-synthesised reliably and its identity confirmed using single crystal X-ray methods. These nanotubes were imaged using SEM methods and found to be 500 – 700 μm in length, much larger than any MOF nanotubes reported previously in the literature. The UV/visible properties of these were then probed using solid-state reflectance UV/visible methods and it was observed that upon irradiation, the reflectance spectrum shows a clear decrease in the 400 – 800 nm range, accompanied by a visible colour change from a dark orange to a paler yellow colour.

The nanotubes were also found to be flexible upon mechanical manipulation and this was further explored using Raman spectroscopy. A Stokes redshift of around 1.4 cm^{-1} was observed when the bent nanotubes spectrum was compared with that of the straight tubes, suggestion greater tensile strain on the bent nanotubes. A map of the relative shifts was constructed and displayed that the outer edges of the nanotubes exhibited greater shifts, corresponding to a greater strain. Further measurement could be made in the future to give a better idea of the bending strain.

2.5 Experimental

N,N'-Bis(4-pyridylmethyl)-1,4,5,8-naphthalenetetracarboxydiimide (DPMNI)

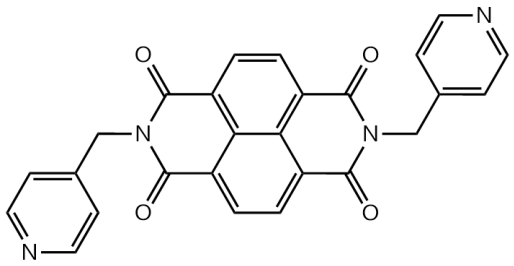

The synthesis of DPMNI was adapted from literature methods[155]. 4-(aminomethyl)pyridine (2.33 g, 11.5 mmol), 1,4,5,8-naphthalene tetracarboxylic dianhydride (2.46 g, 4.6 mmol) and *N,N*-dimethylformamide (40 mL) were combined and heated under reflux overnight at 120 °C. The dark brown solution was cooled to room temperature and precipitate was filtered off by vacuum filtration. The pale brown solid was washed with dichloromethane (2 × 10 mL) and acetone (2 × 10 mL). The product was recrystallised from hot DMF to give a pale brown powder as a product. (1.83 g, 4.08 mmol, 89% yield). ^{1}H NMR (400 MHz; $CDCl_3$) δH ppm 8.83 (4 H, s), 8.59 (4 H, d, *J* = 7 Hz), 7.41 (4 H, d, *J* = 7 Hz), 5.41 (4 H, s) ·MS (MALDI-TOF): m/z calculated for $[C_{26}H_{16}N_4O_4]$- 448.12, found 448.03.

NDI-MOF Nanotubes

$Zn(NO_3)_2{\cdot}6H2O$ (30 mg, 0.1 mmol), 1,4-naphthalene dicarboxylic acid (11 mg, 0.05 mmol), DPMNDI (22 mg, 0.05 mmol) and DMF (2 mL) were combined in a sealed scintillation vial. The mixture was heated in an oven at 100 °C for 24 hours to yield orange, needle crystals.

General characterisation methods and materials

All chemicals were purchased from commercial sources and used without further purification. ^{1}H and ^{13}C nuclear magnetic resonance (NMR) spectra were collected using a Bruker AV(III)400 spectrometer at room temperature. The chemical shifts are reported in ppm with respect to the $CDCl_3$ solvent shifts at 7.26 ppm for ^{1}H NMR spectra or 77.00 ppm for ^{13}C NMR spectra. For ^{1}H NMR spectra, peaks are reported using following abbreviations; n H = number of hydrogen atoms in the environment, s = singlet, d = doublet, *J*= coupling constant, reported in Hertz (Hz). Matrix-assisted laser desorption ionization time of flight mass spectrometry (MALDI-TOF MS) was collected using Bruker Ultraflex III mass spectrometer instrument using *trans*-2-[3-(4-tert-Butylphenyl)-2-methyl-2-propenylidene] malononitrile (DCTB) as the matrix (m/z 250.34) at room temperature and collected data is reported in m/z units.

Crystallography

Details of crystallographic methods can be found in the appendix.

Solid-state UV/vis Spectroscopy

Solid state UV/Vis reflectance spectra were collected using a UV/Vis Near-IR Agilent Cary Spectrometer, with a thin-layer solid-state UV/Vis attachment, at room temperature. MOF samples were ground to a homogeneous powder and their percentage reflectance (%R) was recorded both before and after 30 minutes of UV radiation (λ= 465 nm).

Raman Spectroscopy

Raman spectroscopy was performed using a HORIBA LabRAM HR Raman microscope. Spectra were obtained using a 785 nm laser (at ~20 mW power), a 600 lines/mm grating, a 100× objective and a 50 µm confocal hole. The spectral resolution in this configuration is better than 0.6 cm^{-1}

Scanning electron microscopy

SEM images were taken using Philips (FEI) XL30 scanning electron microscope at room temperature. Prior to loading on the microscope, the samples were coated with a conductive layer of fine carbon, that is transparent to the electron beam, through deposition *via* thermal evaporation of carbon.

Table 1 Crystal data and structure refinement for ZNCRQA_sq (1).

Identification code	ZNCRQA_sq (1)
Empirical formula	$C_{110}H_{190}N_{28}O_{32}Zn$
Formula weight	2482.26
Temperature/K	120.00(10)
Crystal system	tetragonal
Space group	$P4_2$
a/Å	31.3893(6)
b/Å	31.3893(6)
c/Å	8.67473(14)
α/°	90
β/°	90
γ/°	90
Volume/Å^3	8547.1(3)
Z	8
ρ_{calc}g/cm^3	3.858
μ/mm^{-1}	2.890
F(000)	10656.0
Crystal size/mm^3	0.347 × 0.024 × 0.022
Radiation	CuKα (λ = 1.54184)
2Θ range for data collection/°	7.966 to 153.472
Index ranges	-39 ≤ h ≤ 39, -39 ≤ k ≤ 39, -5 ≤ l ≤ 10
Reflections collected	30297
Independent reflections	11723 [R_{int} = 0.0503, R_{sigma} = 0.0438]
Data/restraints/parameters	11723/1/920
Goodness-of-fit on F^2	1.017
Final R indexes [I>=2σ (I)]	R_1 = 0.0416, wR_2 = 0.1098
Final R indexes [all data]	R_1 = 0.0483, wR_2 = 0.1134
Largest diff. peak/hole / e Å^{-3}	0.48/-0.66
Flack parameter	0.11(3)

Experimental

Single crystals of $C_{110}H_{190}N_{28}O_{32}Zn$ **[ZNCRQA_sq (1)]** were mounted in fomblin on a micromount. A suitable crystal was selected and on a Bruker diffractometer. The crystal was kept at 120.00(10) K during data collection. Using Olex2 [1], the structure was solved with the Unknown [2] structure solution program using Unknown and refined with the Unknown [3] refinement package using Unknown minimisation.

1. Dolomanov, O.V., Bourhis, L.J., Gildea, R.J, Howard, J.A.K. & Puschmann, H. (2009), J. Appl. Cryst. 42, 339-341.
2. Sheldrick, G.M. (2015). Acta Cryst. A71, 3-8. 3.
3. Sheldrick, G.M. (2015). Acta Cryst. C71, 3-8.

Crystal structure determination of [ZNCRQA_sq (1)]

Crystal Data for $C_{110}H_{190}N_{28}O_{32}Zn$ (M =2482.26 g/mol): tetragonal, space group $P4_2$ (no. 77), a = 31.3893(6) Å, c = 8.67473(14) Å, V = 8547.1(3) Å^3, Z = 8, T = 120.00(10) K, μ(CuKα) = 2.890 mm^{-1}, $Dcalc$ = 3.858 g/cm^3, 30297 reflections measured (7.966° ≤ 2Θ ≤ 153.472°), 11723 unique (R_{int} = 0.0503, R_{sigma} = 0.0438) which were used in all calculations. The final R_1 was 0.0416 (I > 2σ(I)) and wR_2 was 0.1134 (all data).

Refinement model description

Number of restraints - 1, number of constraints - unknown.

Details:

1. Twinned data refinement
Scales: 0.89(3) 0.11(3)
2. Fixed Uiso
At 1.2 times of:
All C(H) groups, All C(H,H) groups
3.a Secondary CH2 refined with riding coordinates:
C6A(H6AA,H6AB), C21A(H21A,H21B), C6B(H6BA,H6BB), C21B(H21C,H21D)
3.b Aromatic/amide H refined with riding coordinates:
C1A(H1A), C2A(H2A), C4A(H4A), C5A(H5A), C12A(H12A), C13A(H13A), C17A(H17A), C18A(H18A), C22A(H22A), C23A(H23A), C25A(H25A), C26A(H26A), C29A(H29A), C30A(H30A), C33A(H33A), C34A(H34A), C35A(H35A), C36A(H36A), C1B(H1B), C2B(H2B), C4B(H4B), C5B(H5B), C12B(H12B), C13B(H13B), C17B(H17B), C18B(H18B), C22B(H22B), C23B(H23B), C25B(H25B), C26B(H26B), C29B(H29B), C30B(H30B), C33B(H33B), C34B(H34B), C35B(H35B), C36B(H36B)

Bond Lengths for ZNCRQA_sq (1).

Atom	Atom	Length/Å	Atom	Atom	Length/Å
Zn01	O00E	1.935(8)	C00X	C01C	1.400(15)
Zn01	O00I1	1.961(8)	C010	C01K	1.433(15)
Zn01	N00N2	2.023(9)	C010	C01M	1.392(14)
Zn01	N00R	2.009(9)	C011	C01A	1.444(14)
Zn02	O00F3	1.980(8)	C011	C01J	1.415(15)
Zn02	O00H	1.924(8)	C012	C027	1.369(14)
Zn02	N00M	2.014(9)	C013	C01R	1.514(14)
Zn02	N00P4	2.030(9)	C015	C021	1.520(14)
O003	C01B	1.219(11)	C017	C01F	1.461(13)
O004	C00Y	1.222(12)	C017	C01R	1.418(16)
O005	C01H	1.237(12)	C017	C029	1.396(15)
O006	C016	1.237(13)	C018	C024	1.520(15)
O007	C013	1.217(12)	C018	C02J	1.335(14)
O008	C01L	1.253(13)	C018	C02U	1.443(16)
O009	C02K	1.236(12)	C019	C01E	1.396(15)
O00A	C014	1.230(12)	C019	C01G	1.478(13)
O00B	C01G	1.218(12)	C01A	C01B	1.476(13)
O00C	C01V	1.236(12)	C01C	C026	1.415(14)
O00D	C01U	1.238(13)	C01D	C025	1.508(14)
O00E	C015	1.298(13)	C01D	C02H	1.392(16)
O00F	C02K	1.289(13)	C01D	C02I	1.404(14)
O00G	C015	1.222(12)	C01E	C01I	1.384(14)
O00H	C013	1.285(13)	C01F	C01T	1.442(14)
O00I	C01V	1.268(13)	C01F	C02A	1.391(15)
N00J	C016	1.381(13)	C01H	C01M	1.470(14)
N00J	C01G	1.400(14)	C01I	C01K	1.384(14)
N00J	C02C	1.485(13)	C01J	C01L	1.465(14)
N00K	C00Y	1.398(12)	C01J	C026	1.384(14)

N00K	C014	1.422(14)	C01K	C01U	1.457(13)
N00K	C01Z	1.476(13)	C01M	C027	1.406(15)
N00L	C01H	1.423(14)	C01N	C01R	1.377(15)
N00L	C01U	1.393(12)	C01N	C02R	1.409(14)
N00L	C025	1.481(13)	C01O	C02A	1.394(15)
N00M	C02D	1.388(13)	C01O	C02O	1.397(15)
N00M	C02L	1.351(15)	C01P	C02G	1.396(15)
N00N	C01P	1.346(14)	C01Q	C023	1.411(14)
N00N	C020	1.357(13)	C01Q	C028	1.419(15)
N00O	C01B	1.395(13)	C01S	C02Q	1.370(16)
N00O	C01L	1.393(13)	C01T	C02K	1.505(14)
N00O	C024	1.493(13)	C01T	C02R	1.369(15)
N00P	C02M	1.337(14)	C01V	C023	1.518(13)
N00P	C02P	1.346(14)	C01W	C01Z	1.509(14)
C00Q	C00V	1.390(15)	C01W	C022	1.399(16)
C00Q	C012	1.417(14)	C01W	C02G	1.399(14)
C00Q	C016	1.477(13)	C01X	C028	1.387(16)
N00R	C02S	1.374(14)	C01X	C02Q	1.417(15)
N00R	C02T	1.324(15)	C01Y	C02D	1.388(16)
C00S	C00T	1.408(15)	C01Y	C02E	1.397(16)
C00S	C00X	1.380(14)	C020	C022	1.394(15)
C00S	C011	1.430(13)	C021	C02F	1.369(15)
C00T	C00Y	1.449(13)	C023	C02N	1.362(15)
C00T	C00Z	1.405(14)	C029	C02O	1.374(16)
C00U	C01Q	1.435(13)	C02B	C02E	1.379(14)
C00U	C01S	1.417(14)	C02B	C02L	1.385(15)
C00U	C021	1.410(15)	C02C	C02E	1.530(15)
C00V	C010	1.435(14)	C02F	C02N	1.412(14)
C00V	C019	1.402(14)	C02H	C02P	1.394(16)
C00W	C00Z	1.404(14)	C02I	C02M	1.420(15)

C00W	C01A	1.371(15)	C02J	C02T	1.403(15)
C00X	C014	1.465(13)	C02S	C02U	1.374(16)

Bond Angles for ZNCRQA_sq (1).

Atom	Atom	Atom	Angle/˚	Atom	Atom	Atom	Angle/˚
O00E	Zn01	O00I1	97.9(3)	O003	C01B	N00O	120.7(9)
O00E	Zn01	N00N2	107.7(3)	O003	C01B	C01A	122.0(9)
O00E	Zn01	N00R	119.4(4)	N00O	C01B	C01A	117.2(8)
O00I1	Zn01	N00N2	114.4(4)	C00X	C01C	C026	118.8(9)
O00I1	Zn01	N00R	103.1(3)	C02H	C01D	C025	120.3(9)
N00R	Zn01	N00N2	113.4(4)	C02H	C01D	C02I	118.4(10)
O00F3	Zn02	N00M	115.3(4)	C02I	C01D	C025	121.2(10)
O00F3	Zn02	N00P4	103.0(3)	C019	C01E	C01I	119.9(10)
O00H	Zn02	O00F3	97.3(3)	C017	C01F	C01T	118.3(9)
O00H	Zn02	N00M	108.1(3)	C02A	C01F	C017	119.3(9)
O00H	Zn02	N00P4	118.7(4)	C02A	C01F	C01T	122.4(9)
N00M	Zn02	N00P4	113.5(3)	O00B	C01G	N00J	120.3(9)
C015	O00E	Zn01	117.3(7)	O00B	C01G	C019	122.8(10)
C02K	O00F	Zn025	114.9(7)	N00J	C01G	C019	116.9(9)
C013	O00H	Zn02	119.1(7)	O005	C01H	N00L	119.4(9)
C01V	O00I	Zn016	117.6(7)	O005	C01H	C01M	123.7(10)
C016	N00J	C02C	117.3(9)	N00L	C01H	C01M	116.9(9)
C01G	N00J	C016	124.3(8)	C01K	C01I	C01E	122.2(10)
C01G	N00J	C02C	118.2(8)	C011	C01J	C01L	119.4(9)
C00Y	N00K	C014	123.5(8)	C011	C01J	C026	119.8(9)
C00Y	N00K	C01Z	116.7(9)	C026	C01J	C01L	120.5(10)
C014	N00K	C01Z	119.7(8)	C010	C01K	C01U	118.3(9)
C01H	N00L	C025	119.5(8)	C01I	C01K	C010	119.3(9)
C01U	N00L	C01H	123.0(8)	C01I	C01K	C01U	122.2(9)
C01U	N00L	C025	116.9(9)	O008	C01L	N00O	119.4(9)

C02D	N00M	Zn02	119.6(8)
C02L	N00M	Zn02	121.0(7)
C02L	N00M	C02D	118.6(9)
C01P	N00N	Zn017	120.1(7)
C020	N00N	Zn017	120.7(8)
C020	N00N	C01P	118.3(9)
C01B	N00O	C024	118.4(8)
C01L	N00O	C01B	124.9(8)
C01L	N00O	C024	116.2(8)
C02M	N00P	Zn028	119.2(7)
C02P	N00P	Zn028	121.3(8)
C02P	N00P	C02M	119.3(10)
C00V	C00Q	C016	119.3(9)
C012	C00Q	C00V	120.9(9)
C012	C00Q	C016	119.8(9)
C02S	N00R	Zn01	121.8(8)
C02T	N00R	Zn01	121.4(7)
C02T	N00R	C02S	116.5(10)
C00T	C00S	C011	118.7(9)
C00X	C00S	C00T	121.9(9)
C00X	C00S	C011	119.4(10)
C00S	C00T	C00Y	119.8(9)
C00Z	C00T	C00S	119.8(9)
C00Z	C00T	C00Y	120.4(10)
C01S	C00U	C01Q	117.6(9)
C021	C00U	C01Q	119.1(9)
C021	C00U	C01S	123.3(9)
C00Q	C00V	C010	118.3(9)
C00Q	C00V	C019	121.7(9)
C010	C00V	C019	120.0(9)
O008	C01L	C01J	122.4(9)
N00O	C01L	C01J	118.1(9)
C010	C01M	C01H	120.6(9)
C027	C01M	C010	119.8(9)
C027	C01M	C01H	119.5(9)
C02R	C01N	C01R	121.8(10)
C02A	C01O	C02O	118.3(11)
N00N	C01P	C02G	122.7(10)
C023	C01Q	C00U	118.4(9)
C028	C01Q	C00U	119.7(9)
C028	C01Q	C023	121.9(8)
C017	C01R	C013	122.8(9)
C01N	C01R	C013	116.8(10)
C01N	C01R	C017	120.5(9)
C02Q	C01S	C00U	122.0(9)
C01F	C01T	C02K	119.0(9)
C02R	C01T	C01F	120.8(9)
C02R	C01T	C02K	120.1(10)
O00D	C01U	N00L	118.4(9)
O00D	C01U	C01K	122.1(9)
N00L	C01U	C01K	119.5(9)
O00C	C01V	O00I	125.5(9)
O00C	C01V	C023	120.9(9)
O00I	C01V	C023	113.5(9)
C022	C01W	C01Z	121.9(9)
C022	C01W	C02G	117.7(9)
C02G	C01W	C01Z	120.3(9)
C028	C01X	C02Q	119.5(11)
C02E	C01Y	C02D	120.9(10)
C01W	C01Z	N00K	111.8(8)

C01A	C00W	C00Z	120.1(10)
C00S	C00X	C014	120.1(9)
C00S	C00X	C01C	121.6(9)
C01C	C00X	C014	118.2(9)
O004	C00Y	N00K	118.8(9)
O004	C00Y	C00T	123.3(9)
N00K	C00Y	C00T	117.8(9)
C00T	C00Z	C00W	121.5(10)
C00V	C010	C01K	118.4(9)
C01M	C010	C00V	120.3(10)
C01M	C010	C01K	121.3(9)
C01A	C011	C00S	119.9(9)
C01J	C011	C00S	119.4(9)
C01J	C011	C01A	120.7(9)
C027	C012	C00Q	119.9(10)
O007	C013	O00H	123.4(10)
O007	C013	C01R	121.8(10)
O00H	C013	C01R	114.8(9)
O00A	C014	N00K	119.0(9)
O00A	C014	C00X	124.1(10)
N00K	C014	C00X	116.9(8)
O00E	C015	C021	114.2(9)
O00G	C015	O00E	124.7(9)
O00G	C015	C021	121.2(9)
O006	C016	N00J	118.8(9)
O006	C016	C00Q	123.2(9)
N00J	C016	C00Q	118.0(9)
C01F	C017	C01R	118.5(9)
C029	C017	C01F	116.8(10)
C029	C017	C01R	124.7(9)
N00N	C020	C022	122.0(11)
C00U	C021	C015	123.5(9)
C02F	C021	C00U	120.5(9)
C02F	C021	C015	116.0(10)
C020	C022	C01W	119.8(10)
C01Q	C023	C01V	119.9(9)
C02N	C023	C01Q	121.3(9)
C02N	C023	C01V	118.8(9)
N00O	C024	C018	112.1(8)
N00L	C025	C01D	111.6(8)
C01C	C026	C01J	121.0(10)
C012	C027	C01M	120.8(10)
C01X	C028	C01Q	120.7(9)
C02O	C029	C017	122.3(10)
C01O	C02A	C01F	122.0(9)
C02L	C02B	C02E	120.3(10)
N00J	C02C	C02E	110.6(8)
N00M	C02D	C01Y	120.1(11)
C01Y	C02E	C02B	117.7(10)
C01Y	C02E	C02C	121.7(9)
C02B	C02E	C02C	120.6(10)
C021	C02F	C02N	120.5(10)
C01P	C02G	C01W	119.2(10)
C02P	C02H	C01D	120.3(10)
C02M	C02I	C01D	117.8(10)
C02T	C02J	C018	119.1(11)
O009	C02K	O00F	126.6(10)
O009	C02K	C01T	121.4(9)
O00F	C02K	C01T	112.0(9)
N00M	C02L	C02B	122.2(10)

C02J	C018	C024	122.5(10)	N00P	C02M	C02I	122.8(10)
C02J	C018	C02U	119.4(10)	C023	C02N	C02F	120.1(10)
C02U	C018	C024	118.1(9)	C029	C02O	C01O	121.2(11)
C00V	C019	C01G	119.6(9)	N00P	C02P	C02H	121.5(11)
C01E	C019	C00V	120.3(9)	C01S	C02Q	C01X	120.4(11)
C01E	C019	C01G	120.0(9)	C01N	C02R	C01T	120.0(10)
C00W	C01A	C011	119.9(9)	C02U	C02S	N00R	123.6(11)
C00W	C01A	C01B	120.8(9)	N00R	C02T	C02J	124.2(10)
C011	C01A	C01B	119.2(9)	C02S	C02U	C018	117.2(10)

3. Synthesis of Acid-capped Rotaxanes for Metal-Organic Rotaxane Synthesis

3.1 Synthesis of a tetraacid-functionalised rotaxane: TAR4

A tetracarboxylic acid pillarene rotaxane was synthesised one component at a time and then assembled, the process of which will now be detailed. This rotaxane was used as the primary linker in the proposed MORF structure. This rotaxane was chosen due to the tetracarboxylic acid functionality present in the rotaxane making it ideal for metal coordination. The pillarene used in subsequent reactions, pillar[5]arene, was also synthesised and kindly donated by Philipp Langer, Marysia Tarnowska, Alexander Lewis and Nathan Andersen.

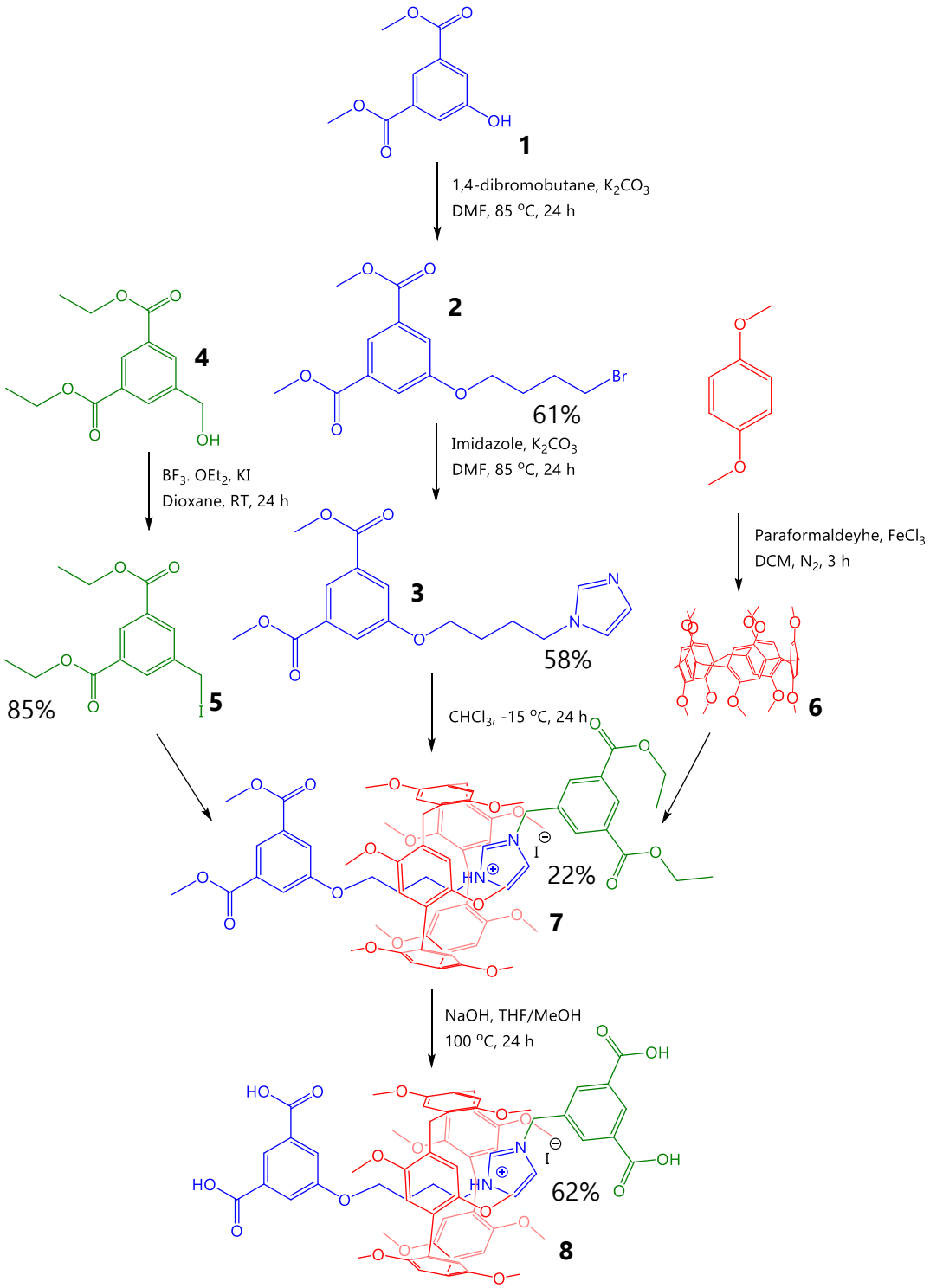

Scheme 3.1. The complete reaction scheme for the formation of TAR4. The three separate component syntheses are shown in different colours. Green – stopper, Blue – imidazolyl rod, Red – pillar[5]arene.

The first step in the formation of the diacid rotaxane **8** was to synthesise the imidazole rod **3** (Scheme 3.1). This began with 5-hydroxyisophthalate **1**, a bulky diester with sufficient bulk to prevent dethreading which will be deprotected once the rotaxane has formed to give the acid groups for MORF synthesis.

1,4-dibromobutane and dimethyl 5-hydroxyisophthalate were stirred with potassium carbonate in dimethylformamide at 85 °C for 24 hours. Potassium carbonate is used as a base to deprotonate the phenolic O-H group, allowing S_N2 substitution of the dibromide chain to occur. A large excess of bromoalkane was used to prevent the formation of the di-substituted 'dumbbell' molecule which is unusable for the next step of the reaction. The reaction proceeded to give a crude product that was a yellow oil. This oil was purified by silica column chromatography to give the product as a pale-yellow oil. The identity of this compound was confirmed to be dimethyl 5-(4-bromobutoxy)isophthalate by ^{1}H NMR spectroscopy.

Once the dimethyl 5-(4-bromobutoxy)isophthalate **2** was synthesised, it was a relatively simple transformation to form the imidazolyl analogue. Dimethyl 5-(4-bromobutoxy)isophthalate **2** and imidazole were stirred with potassium carbonate in dimethylformamide at 85 °C for 24 h. After purification by silica gel column chromatography, a pale-yellow oil was obtained crystallised to a white solid. This is most likely due to the amount of solvent remaining after purification being a much smaller fraction of the final product.

To stopper the rod once threading has occurred during assembly, a similar starting material, diethyl 5-(hydroxymethyl)isophthalate **4** was iodinated to produce an asymmetric rotaxane. Asymmetric rotaxanes illustrate the flexibility of the toolbox approach.

To a solution of both diethyl 5-(hydroxymethyl)isophthalate **4** and potassium iodide in dioxane was added $BF_3.Et_2O$. This was then stirred in darkness, at room temperature, for 24 h. The reaction was carried out in the absence of light due to the instability of

the iodinated product. The iodinated stopper group **5** was stored in the absence of light to prevent decomposition.

Now that the imidazolyl rod and stopper had been synthesised, they could combine with the pillar[5]arene macrocycle **6** in cold chloroform and allowed to self-assemble. 5-(4-(1H-imidazol-1-yl)butoxy)isophthalate **3** and pillar[5]arene **6** were dissolved in the minimal amount of chloroform (~2 mL) and cooled to -15 °C (Figure 5). Chloroform is used for this reaction due to the increased binding affinity of the pillarene to the imidazolium group with respect to other more competitive solvents such as acetonitrile. Chloroform is much less strongly bound to the pillarene in solution meaning it can be displaced much more easily. In the absence of light, a solution of diethyl 5-(iodomethyl)isophthalate **5** in chloroform was added. This mixture was allowed to warm up to room temperature and stirred over-night. The product was purified by column chromatography to afford a yellow solid.

To form the final tetraacid rotaxane **8**, the two diester stoppers needed to be deprotected. This is done by a simple base deprotection reaction. **7** was dissolved in a methanol/tetrahydrofuran mixture and sodium hydroxide added dropwise. This was left to stir at reflux for 24 h. After this time, the reaction mixture was acidified with hydrochloric acid. The mixture was cooled until precipitate was formed and filtered to give a pale-brown powder. From ^{1}H NMR spectroscopy data, a characteristic shift in the imidazole, and some of the aliphatic protons, can be observed[86], brought about by the shielding effect of the pillarene, with the shifting of the most shielded protons into the almost negative region of the NMR spectrum. These shifts can be seen in Figure 3.1, and this is evidence that the rotaxane had been formed. If a proton environment lies inside the cavity of the macrocycle, in this case the pillarene, the signal will be shifted towards the negative region of the spectrum. Proton environments that lie directly to the side of the pillararene will be deshielded and shifted to a higher ppm.

The alkyl protons d, e and f are shifted, showing that they are positioned inside the cavity of the pillarene.

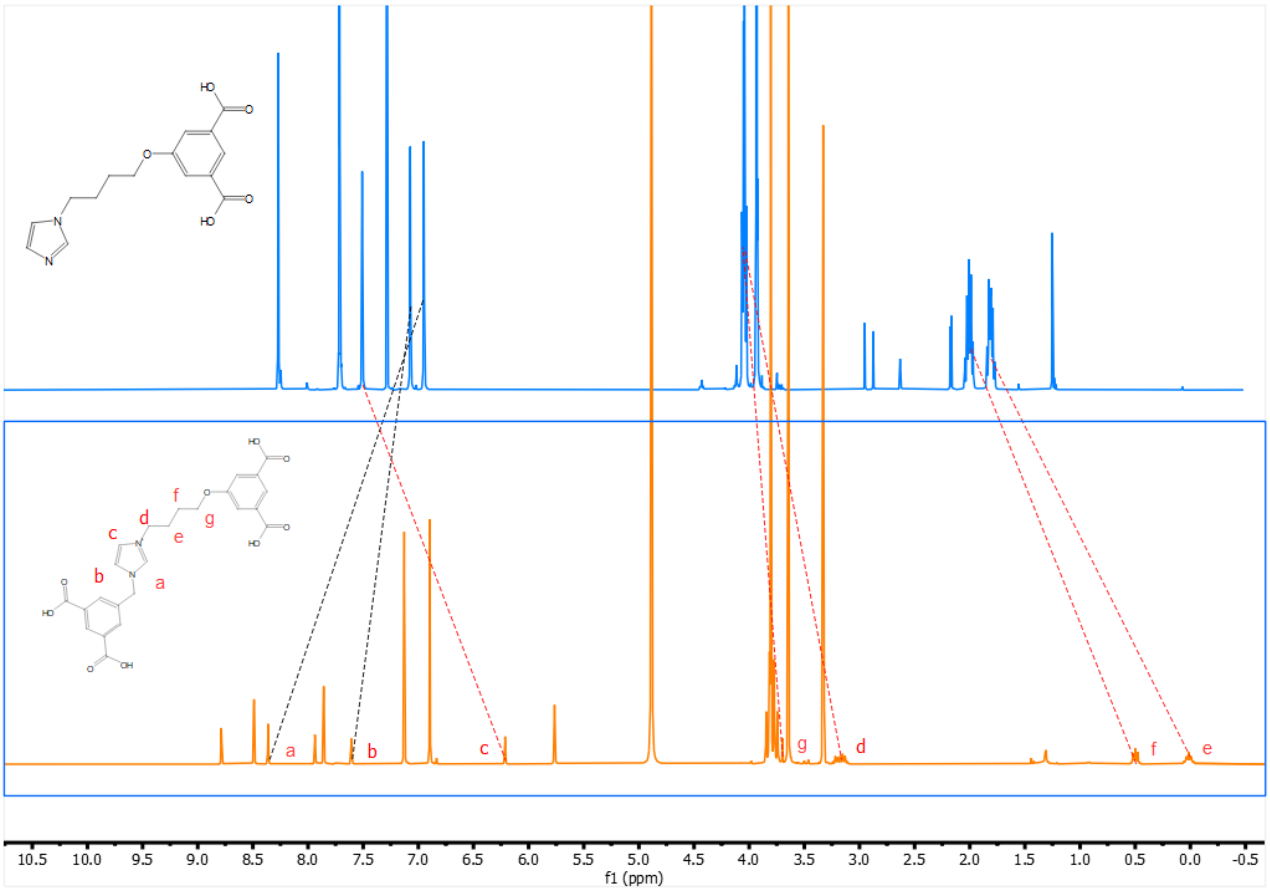

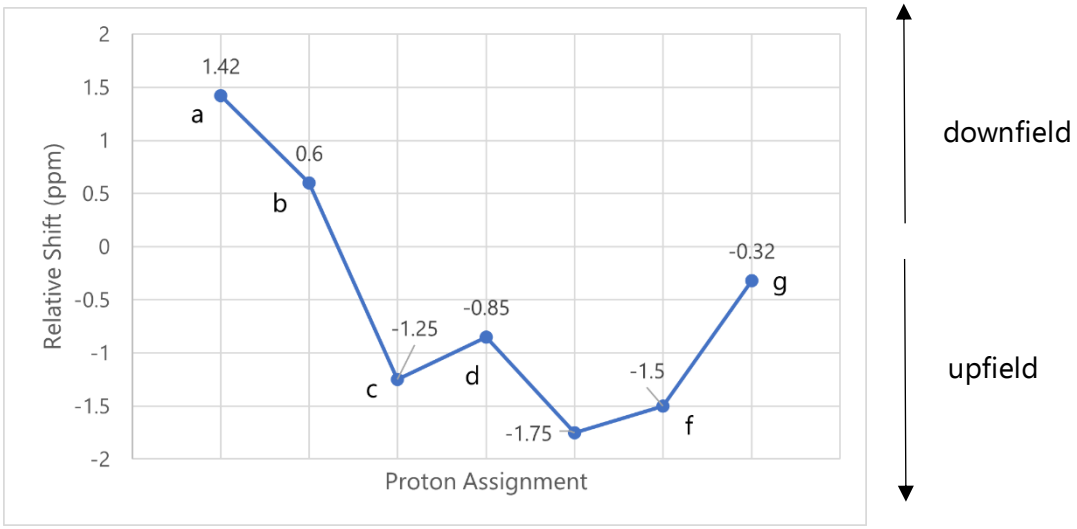

Figure 3.1: The ^{1}H NMR spectra in $CDCl_3$/MeOD for the un-stoppered imidazolium rod (top) and TAR4 (bottom). It can be clearly seen that protons c, d, e, fand g have been downshifted by the shielding of the pillarene once assembly occurs.

3.2 Attempted Synthesis of a rotaxane-containing metal-organic framework

Although efforts to synthesise a rotaxane using TAR4 were overall unsuccessful, through the different experimental practices employed in this report, much was learned about the structure and properties of TAR4, the problems associated with MORF assembly and how to possibly overcome these. The primary method of analysis intended to be used was single-crystal X-ray (SCXRD) diffraction and therefore crystalline material was required. For this reason, any method that did not produce feasible crystals were deemed unsuccessful. For characterisation, powder diffraction or elemental analysis could show the chemical composition but due to the three-dimensional structure being so key the MORF formation process, SCXRD offers information that these other techniques cannot.

Solvothermal Synthesis Methods

Solvothermal synthesis is the method of heating reagents together with solvent in a sealed vessel to generate autogenous pressure. This method is perhaps the most common method used in the generation of MOFs due to the simplicity and ease of the technique. For this reason, it was the first synthetic method used.

Initially, solvothermal synthesis methods were employed in conditions similar to those used by Loeb and co-workers[115] combining TAR4 and zinc nitrate with different polar solvents; DMF, dioxane, ethanol and water. It was found that the rotaxane would not dissolve in a polar solvent alone and addition of acid was required for the rotaxane to dissolve. Although the addition of acid would protonate the carboxylic acids present in the rotaxane structure and allow them to more easily dissolve in the polar solvents used, unfortunately, protonating the acid means that the carboxylate groups are less available to bind to a metal centre, which is barrier to MORF self-assembly. Despite this, the insolubility of TAR4 was the first major problem encountered and it was decided that this problem be tackled first. Three acids in an attempt solubility by protonation: hydrochloric, nitric and trifluoroacetic acid. All of these were unsuccessful

in producing crystalline material of any kind. Different d-block metals: cadmium, nickel, cobalt and copper, were then tried giving similar results, as seen on Figure 3.2.

Metal Complex	Solvent	Additive	Result
$Zn(NO_3)_2 \cdot 6H_2O$	DMF	-	Not dissolved
$Zn(NO_3)_2 \cdot 6H_2O$	Dioxane	-	Not dissolved
$Zn(NO_3)_2 \cdot 6H_2O$	Ethanol	-	Not dissolved
$Zn(NO_3)_2 \cdot 6H_2O$	Water	-	Not dissolved
$Zn(NO_3)_2 \cdot 6H_2O$	DMF	HCl	No product formed
$Zn(NO_3)_2 \cdot 6H_2O$	DMF	HNO_3	No product formed
$Zn(NO_3)_2 \cdot 6H_2O$	DMF	TFA	No product formed
$Cd(NO_3)_2 \cdot 4H_2O$	DMF	HNO_3	No product formed
$Ni(NO_3)_2 \cdot 6H_2O$	DMF	HNO_3	No product formed
$Cu(NO_3)_2 \cdot 2.5H_2O$	DMF	HNO_3	No product formed
$Ni(NO_3)_2 \cdot 6H_2O$	DMF	HNO_3	No product formed
$Ce(NO_3)_3 \cdot 6H_2O$	DMF	HNO_3	No product formed
$Pr(NO_3)_3 \cdot 6H_2O$	DMF	HNO_3	No product formed
$Sm(NO_3)_3 \cdot 6H_2O$	DMF	HNO_3	No product formed
$Er(NO_3)_3 \cdot 6H_2O$	DMF	HNO_3	No product formed
$Nd(NO_3)_3 \cdot 6H_2O$	DMF	HNO_3	No product formed
$Zn(NO_3)_2 \cdot 6H_2O$	DMF	NaOH	No product formed
$Zn(NO_3)_2 \cdot 6H_2O$	DMF	2,6-lutidine	White powder ppt.
$Cd(NO_3)_2 \cdot 4H_2O$	DMF	2,6-lutidine	White powder ppt.
$Ni(NO_3)_2 \cdot 6H_2O$	DMF	2,6-lutidine	White powder ppt.
$Cu(NO_3)_2 \cdot 2.5H_2O$	DMF	2,6-lutidine	White powder ppt.
$Ni(NO_3)_2 \cdot 6H_2O$	DMF	2,6-lutidine	White powder ppt.
$Ce(NO_3)_3 \cdot 6H_2O$	DMF	2,6-lutidine	White powder ppt.
$Pr(NO_3)_3 \cdot 6H_2O$	DMF	2,6-lutidine	White powder ppt.
$Sm(NO_3)_3 \cdot 6H_2O$	DMF	2,6-lutidine	White powder ppt.
$Er(NO_3)_3 \cdot 6H_2O$	DMF	2,6-lutidine	White powder ppt.
$Nd(NO_3)_3 \cdot 6H_2O$	DMF	2,6-lutidine	White powder ppt.

Figure 3.2. A list of the different individual MORF assembly reacts attempted with TAR4.

Due to the size of the rotaxane ligands, it was decided that larger lanthanide metal centres should be attempted, similar to work by Loeb *et al.*[112] A series of lanthanide metal nitrates and chlorides were used, however all gave similar results to the d-block metals. Lanthanides by their nature are much larger atoms than the early d-block metals usually used for MOF synthesis. Cerium, praseodymium, samarium, erbium and neodymium were tried but none of these yielded any crystalline products.

As acids aided solubility but limited the availability of the carboxylate groups, it was decided that adding base should be the next approach taken. Inorganic base was tried first in the form of sodium hydroxide, with water and DMF used as reaction solvents, but no crystalline products were formed. As an inorganic base did not give the desired effect, it was decided that a gentler organic base may be a suitable alternative. 2,6-Lutidine was chosen as an organic base with sufficient steric bulk to prevent coordination to the metal centres but be sufficiently basic enough to deprotonate the acid groups present on TAR4. 2,6-Lutidine and TAR4 were heated with many different metals in DMF. It was found that upon addition of lutidine, a white powder was formed, seemingly in much greater amounts that starting material used. This result was replicated in repeat experiments. This powder was thought to have possibly been a non-crystalline MORF. Infrared spectroscopy was carried out on this powder and the rotaxane starting material with a strong peak corresponding to the carboxylic acid -OH stretch was observed in both, with comparable intensity. This was sufficient evidence that the rotaxane starting material was present in the sample suggesting that MORF had not formed in any of the samples.

Sterics are key to the way that crystals arrange themselves. Given this, it was theorised that by using purely the pillarene rotaxane as the linker in a proposed MORF, the pillarene may be too sterically large to allow the rotaxanes to arrange into a stable framework. Pillared MOFs are widely known[156–158] and consist of a framework of two-dimensional layers of one type of linker coordinated to metal centres which are then in turn 'pillared' by a different linker that join these layers together forming a three-

dimensional porous structure. Using these secondary linkers creates a larger amount of space between each of the bulky pillararene rotaxanes, relieving some of the steric strain between them. Several secondary linkers of differing lengths were added to the reactions listed above, with both acid and base additives, but no crystalline material was formed. These were chosen as they were single coordinate and were of a similar length to the TAR4 rotaxane. These were added to the MORF formation reactions previously stated (Figure 3.3). This was initially in a 1:1 ratio with TAR4, but after these attempts did not yield any suitable products, the ratio was upped to 2:1. These also yielded no product, and no further reactions of this type were attempted.

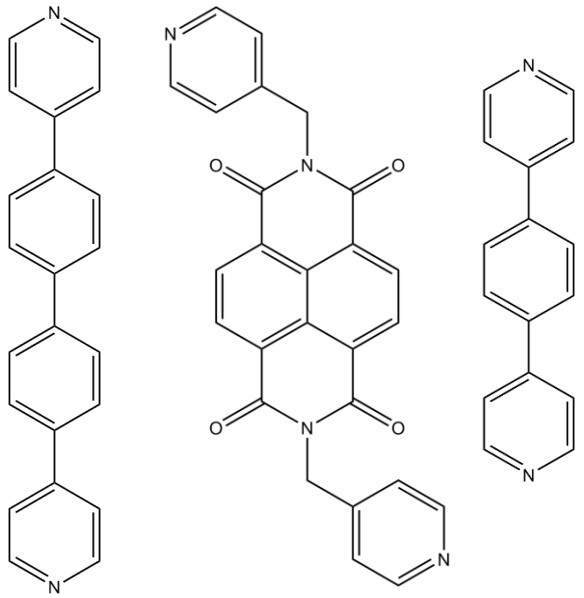

Figure 3.3. The structure of some of the secondary linkers added to the solvothermal synthesis reactions detailed above; (left to right) 4,4'-di(pyridin-4-yl)-1,1'-biphenyl, DPMNDI and 1,4-di(pyridin-4-yl)benzene.

3.3 Metal-Organic Rotaxane Framework Synthetic Methods

Diffusion methods can also be employed in the synthesis of self-assembling porous structures. In this method, the starting reagents are dissolved in solvent and then exposed to an 'anti-solvent', a substance that will not dissolve the starting materials. This introduction of the anti-solvent causes the starting materials to slowly precipitate out of solution, crystallising as they do so. The method of diffusion synthesis chosen for the following reaction was that of a slow evaporation of an organic non-polar anti-solvent into a solution containing the reagents of the reaction.

Three different solvent systems were used, these were methanol/chloroform, acetonitrile/isopropanol, and water/dichloromethane as the solvent/antisolvent for each respectively with several different metals. After being left for six months to slowly evaporate, no crystals were formed from any of these reactions, even after all solvent has evaporated fully.

Slow evaporation methods are, practically, the simplest method of crystallisation. These methods consist of dissolving the starting materials of the crystallisation in solvent and then allowing the solvent to slowly evaporate with crystallisation occurring as the solution gets more and more concentrated. Several different solvent systems were used for these evaporations. Acidified water was used as a solvent initially but was deemed to evaporate too slowly to be efficient. For this reason, solvents with higher volatilities were used. Acetonitrile and methanol, both acidified with nitric acid to aid solubility, were used as alternatives. The crystallisations with acetonitrile gave colourless crystals that upon analysis by single crystal X-ray diffraction, were found to be metal nitrate starting materials, showing MORF formation had not occurred the methanol evaporations however gave some much more promising results.

A crystallisation of a solution of TAR4, $Cu(NO_3)_2$, nitric acid and methanol was left for five months until clear red needles appeared. These crystals were analysed by single

crystal X-ray diffraction and found to be exclusively the rotaxane starting material (Figure 3.4). This system crystallised with a nitrate as the counter ion to the imidazolium in the rotaxane rod. The tetra ester precursor to TAR4 was seemingly found to have crystallised which is unexpected as this should have been eliminated during the deprotection step of the tetracarboxylic acid rotaxane synthesis. It was later realised that although the deprotection step has indeed proceeded as expected, the addition of methanol in the presence of an acid has re-esterified the acid functional groups. This re-esterification is even more likely due to all presence of only methyl esters. The protected tetra ester precursor of TAR4 possesses ethyl esters and if deprotection was not successful, these would still be present. As they are not, it once again suggests a reaction with the methanol used as the crystallisation solvent. This explains why complexation was not occurring; with the carboxylate binding sites not available to bind to metal centres, a MORF structure cannot form.

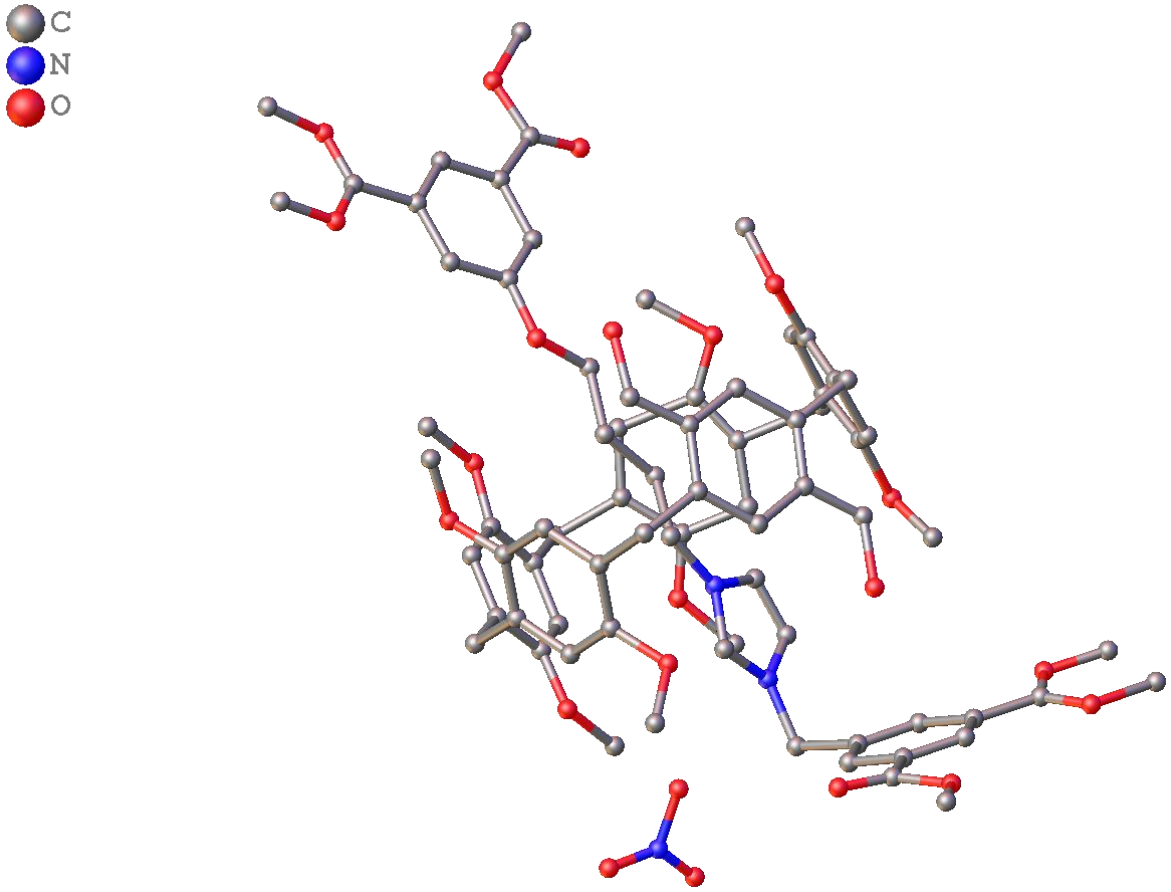

Figure 3.4. The crystal structure that resulted from single crystal X-ray diffraction of the product of the slow evaporation of a solution of TAR4 **8**, $Cu(NO_3)_2$ and nitric acid in methanol. The methyl ester groups can be seen present on the stopper groups of the rotaxane. Hydrogen atoms have been omitted for clarity.

Another slow evaporation of a solution of TAR4 $AgNO_3$ and nitric acid in methanol was left to evaporate slowly for five months and clear square plate-like crystals formed. Upon analysis by single crystal X-ray diffraction, it was found that the tetracarboxylic acid rotaxane was present (Figure 3.5). This structure crystallised into the $P2_1$ space group with an R_1 value of 5.60%. This structure crystallised with two DMF molecules and a nitrate ion as the counter ion for the imidazolium group in the rotaxane rod.

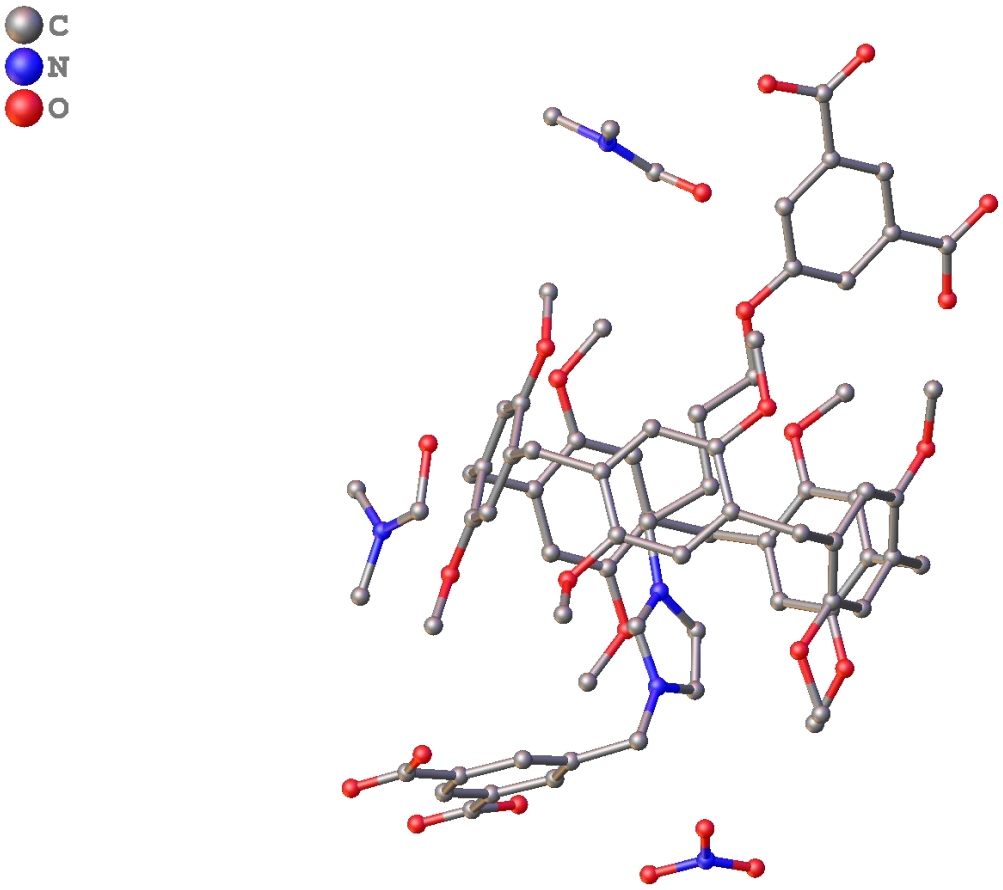

Figure 3.5. The crystal structure that resulted from single crystal X-ray diffraction of the product of the slow evaporation of a solution of TAR4 **8**, $AgNO_3$ and nitric acid in methanol. Hydrogen atoms have been omitted for clarity.

Due to the acid groups present on TAR4 and the proximity of the molecules in the crystal packing, hydrogen bonding can be observed (Figure 3.6). There are two intermolecular hydrogen bonds present between adjacent TAR4 molecules: with one between the acid groups on neighbouring TAR4 molecules and another hydrogen bond present, between the acid groups and a nitrate ion. These have bond lengths of 1.805(3) Å and 1.750(6) Å, respectively. The acid-acid hydrogen bond value is much smaller than the hydrogen bond lengths observed in most acid crystal structures with usual values between 2.5-2.8 Å[159]. This signifies that the hydrogen binding interactions in the TAR4 crystal structure between acid molecules are strong, suggesting that MORF

complexation is not occurring due to the strength of the reactions between the rotaxanes themselves. The hydrogen bonds between the acid groups and the nitrate counterion may also prevent metal centre coordination.

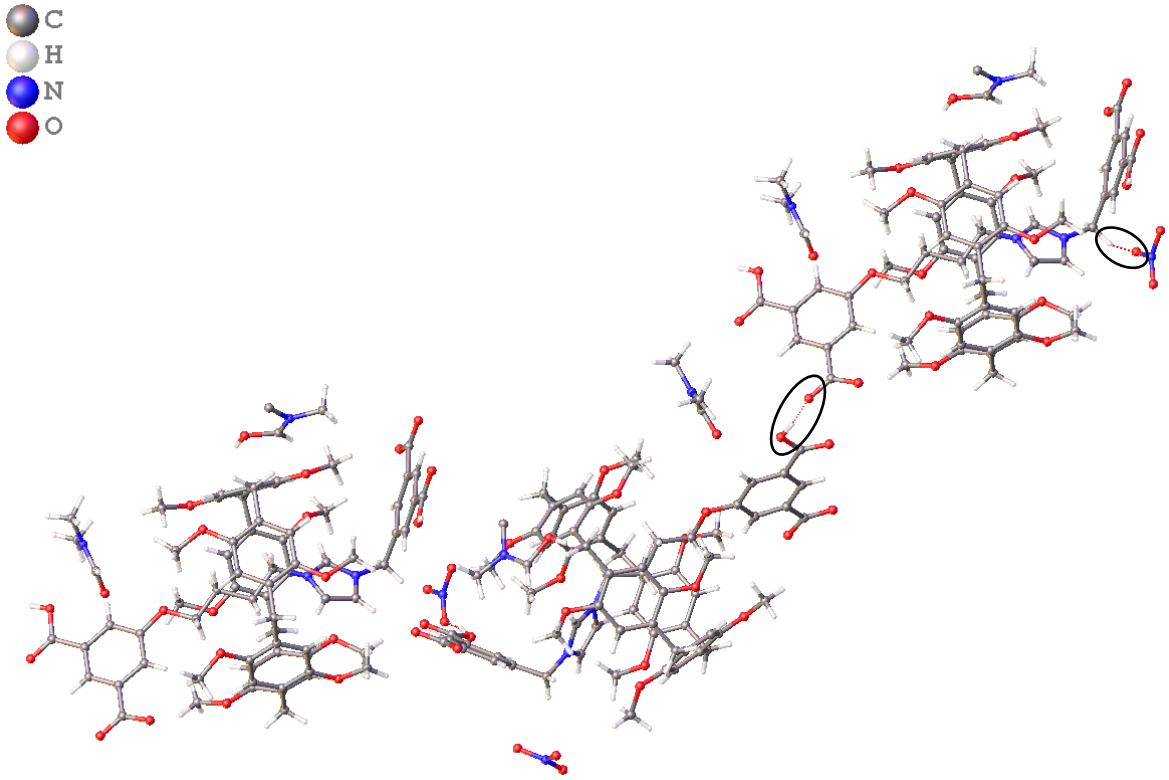

Figure 3.6. The hydrogen bonding scheme of TAR4 **8**. A hydrogen bond can be observed between acids groups on two different rotaxanes and between a nitrate group and an acid group.

Intramolecular hydrogen bonding is also observed in the TAR4 structure (Figure 3.7). These are relatively short hydrogen bonds (2.474(2)Å) are between the acid groups and the hydrogen atoms on the pillarene. When this crystal sample was measured by X-ray diffraction, the R-value of the data was 5.79%. This value is much lower than would be anticipated for a structure of this complexity and amount of free movement. The more complex a structure is, the larger the R-value typically becomes. Rotaxanes are complex and due to the movement of the macrocycle around the rod, R-values are typically higher than the value observed for TAR4. As crystallographic data is the

representation of average position of atoms in a molecule, the rotation of the rotaxane macrocycle creates disorder as atom positions overlap This low R-value suggest that the intramolecular hydrogen bonding 'anchors' the pillarene in place and reduces rotation of the macrocycle. This was also evident in the process of solving the measured crystal structure which required very few refinement cycles to achieve the finished structure.

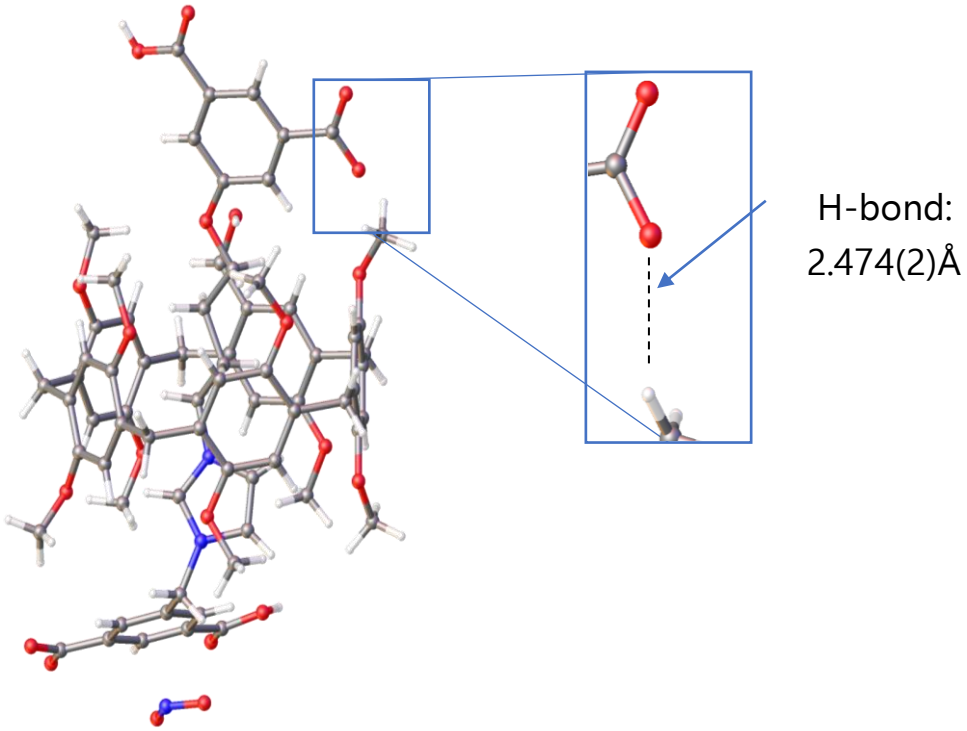

Figure 3.7. The crystal structure of TAR4 with the intramolecular hydrogen bonding atoms magnified for clarity.

The difference in these two crystal structures illustrates one key limitation of single crystal X-ray diffraction; when only one crystal from a sample is analysed, only the molecules present in that crystal are seen. This means that if crystals with different compositions are present in the sample, they may be ignored. For this reason, it is not unreasonable to say that both the tetra acid and tetra ester rotaxanes are present in both samples.

After unsuccessful attempts to produce a MORF using TAR4, it was decided that due to the steric bulk of the pillarene macrocycle, a longer rotaxane with a longer alkyl chain may provide the enough space to allow MORF formation to occur. For this reason, an octyl-analogue of TAR4, named TAR8, was synthesised in an almost identical fashion to TAR4. The synthesis of which will now be discussed.

3.4 Synthesis of a tetraacid rotaxane: TAR8

A tetra-acid capped rotaxane was synthesised using a modified active templating approach utilising an imidazolium/pillararene interaction to facilitate threading and then capped to form the rotaxane architecture. This was achieved by synthesising a mono-stoppered ester pseudorotaxane, formed from a mono-stoppered imidazole rod threaded into a pillarene molecule and then capping with another, iodinated group to form the rotaxane and then deprotecting the ester groups to form the final acid-capped rotaxane. The step-by-step process of this will now be detailed.

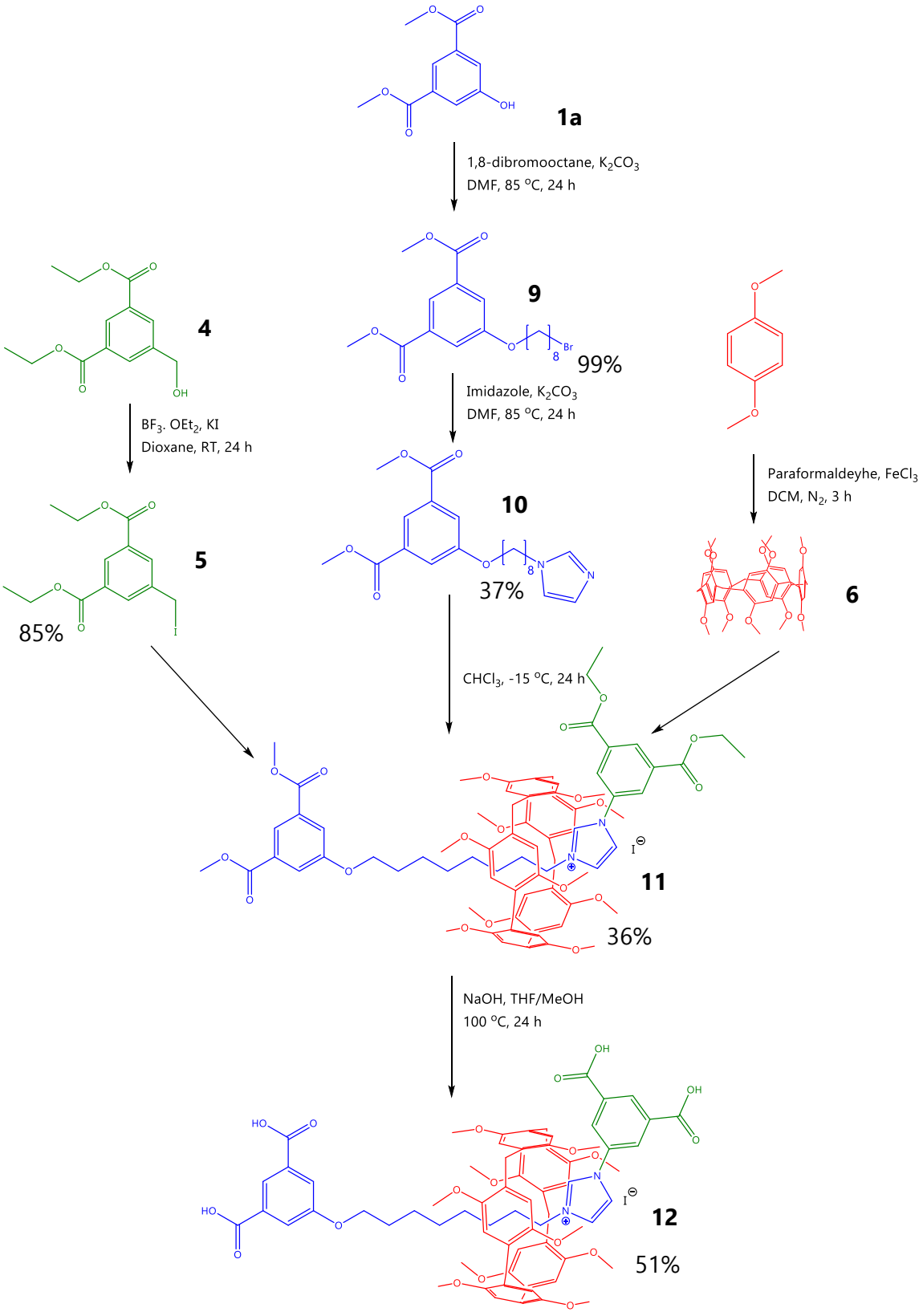

Scheme 3.2. The complete reaction path for the formation of TAR8

The synthesis of TAR8 **12** is almost identical to that of TAR4 with some small changes (Scheme 3.2). This first step uses the same basic conditions for the alkyl coupling reaction but with a reagent containing an octyl chain; in this case, dibromooctane. The bromooctyl rod **9** was then reacted with imidazole to form the imidazolyl rod. 5-(4-bromooctoxy)isophthalate then purified *via* silica gel chromatography to give dimethyl 5-(4-(1H-imidazol-1-yl)octoxy)isophthalate **10**.

The stopper group synthesis for TAR8 uses the same method for that of TAR4, with the iodination of a hydroxyisophthalate molecule.

Dimethyl 5-(4-(1H-imidazol-1-yl)octoxy)isophthalate **10** and dimethoxypillar[5]arene **6** were dissolved in minimal chloroform and cooled to -15 °C. Under the exclusion of light, diethyl 5-(iodomethyl)isophthalate **5** was added and the mixture was left to warm to room temperature while being stirred overnight. The product mixture was purified to afford the product, tetra-ester rotaxane (TER8). Dimethoxypillar[5]arene was kindly provided by Alexander Lewis.

The tetra ester intermediate (TER8) **11** rotaxane formation can be once again confirmed by ^{1}H NMR spectral analysis. Characteristic peaks are present in the negative region of the ^{1}H NMR spectra. By synthesising a 'dumbbell' molecule, which is a stoppered rod without a macrocycle, relative shifts that are attributed to the pillarene shielding can be compared. By plotting this graphically it can be seen which protons are shifted the most and therefore, where the pillarene most likely lies in the rotaxane molecule. The reason that TER8 **11** was used and not the final acid rotaxane, is that, due to the limited solubility of TAR8 **12**, two different solvents must be used. TER8 can be easily dissolved in chloroform and therefore is much easier to use for these kinds of comparative measurements. Initially, it was thought that TER8 and TAR8 would have similar NMR spectra but as detailed later, this is not the case.

Proton environments 'b-h' (Figure 3.8) are all shifted upfield due to shielding by the pillararene molecules. It can be seen by the shift data, that the alkyl protons 'e' are by

far the most upfield shifted in the rotaxane molecule. From this, it can be inferred that the pillararene molecule is centred over this proton environment ‘e’, close to the imidazolium charge which is expected.

Once this tetra-ester acid was synthesised, it needed to be deprotected to form the final tetra-acid rotaxane, suitable for possible MORF assembly. This will now be detailed, as well as some of possible differences in structure between TER8 and TAR8.

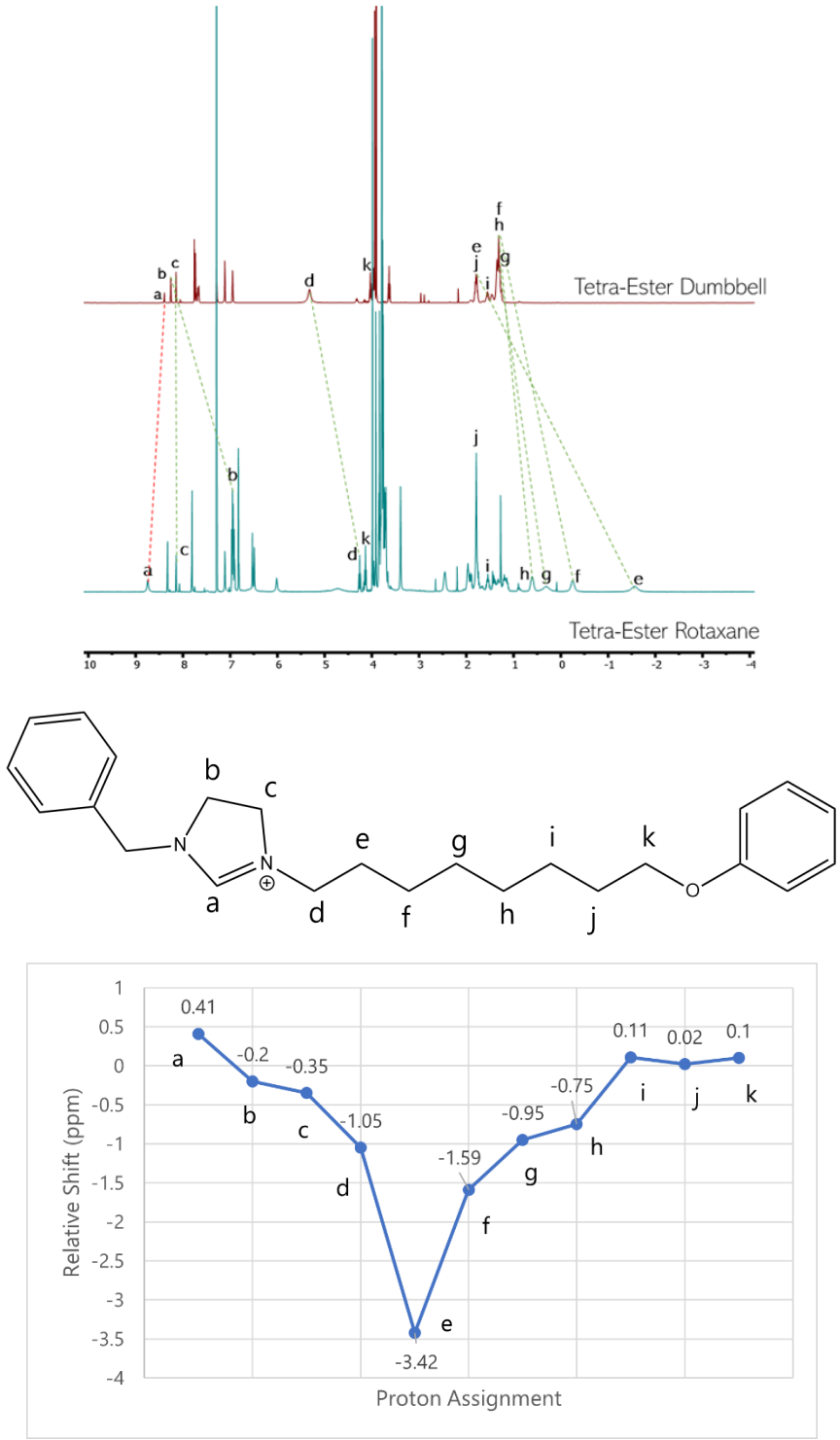

Figure 3.8. The ^{1}NMR shift data in $CDCl_3$/MeOD comparing TER8 rotaxane to the TER8 dumbbell. The shift of proton environments is shown (top), with upfield shifted proton signals shown by green dashed lines and downfield shifted proton signals shown by red dashed lines. The proton environments that these correspond to on the rotaxane/dumbbell rod can be see as well as their relative ppm shift (bottom).

TER8 was dissolved in methanol/tetrahydrofuran, 2 M sodium hydroxide was added and the mixture heated at reflux for 24 h. Solvents were removed under reduced pressure and the residue was dissolved in water. The solution was adjusted to pH 4 by the dropwise addition of HCl. The resulting mixture was left at 4 ^{o}C for 24 h and the formed precipitate filtered under gravity, washed with water and diethyl ether and dried to afford the product as a white solid.

TAR8 has the same characteristic negative alkyl peaks as TER8 in the proton ^{1}H NMR spectrum, confirming that the rotaxane is still mechanically threaded after the deprotection process.

As the only modification made to the rotaxane is the ester deprotection, the NMR data of the alkyl protons, the rotaxane structure would be expected to remain consistent (due to the distance between the ester/acid groups and the alkyl protons). However, when the difference between the alkyl protons from TAR8 and TER8 is calculated (Figure 3.9), the imidazolium protons and the directly adjacent alkyl protons are more shielded in TAR8 than in TER8. This implies that the pillarene in TAR8 lies closer to the imidazolium group in TAR8. This suggests that the hydrogen bonding is still present

in TAR8, similarly to TAR4. Attempts to crystalise a TAR8 sample were made but were unsuccessful.

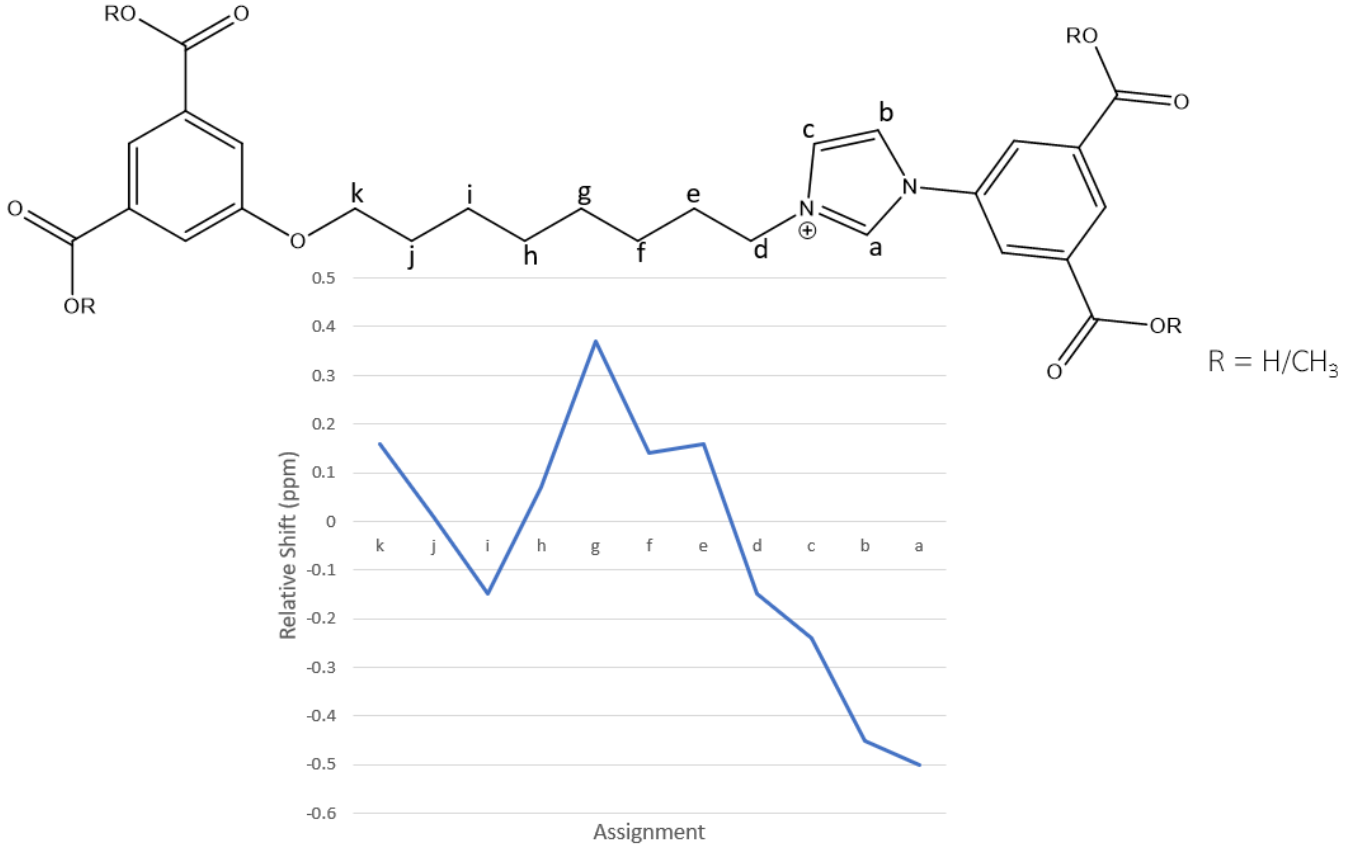

Figure 3.9. The relative shift data for TAR8 and TER8 rotaxanes. The rotaxane rod structure can be seen (top) labelled with the proton assignments. The shifts are shown graphically (middle) with the equation used to calculate these (bottom).

Efforts to synthesise MORF structures with this rotaxane have been unsuccessful, mainly due to solubility problems. It was decided that a xylenol (dimethylphenol) based stopper would be designed and synthesised (Scheme 3.3). The methyl groups should have had sufficient bulk to trap a pillarene macrocycle during rotaxane formation and the hydroxyl group is susceptible to addition of an alkyl chain to form a mono-stoppered rod. From this starting point, a methyl ester group was added *via* a Duff reaction[160] with HMTA to add an aldehyde functionality in a *para*-position, which then

was oxidised to a carboxylic acid *via* a Jones oxidation[161] with chromic acid and then protected to form the methyl ester. This reaction was facilitated by protection and deprotection of the hydroxyl group to form the final desired stopper group. This was then functionalised with a dibromoalkyl chain and then reacted with imidazole to form a rotaxane rod, suitable for rotaxane formation, when reacted with a suitable stopper and pillararene. The details of these syntheses will now be reported.

3.5 Synthesis of a di-acid rotaxane

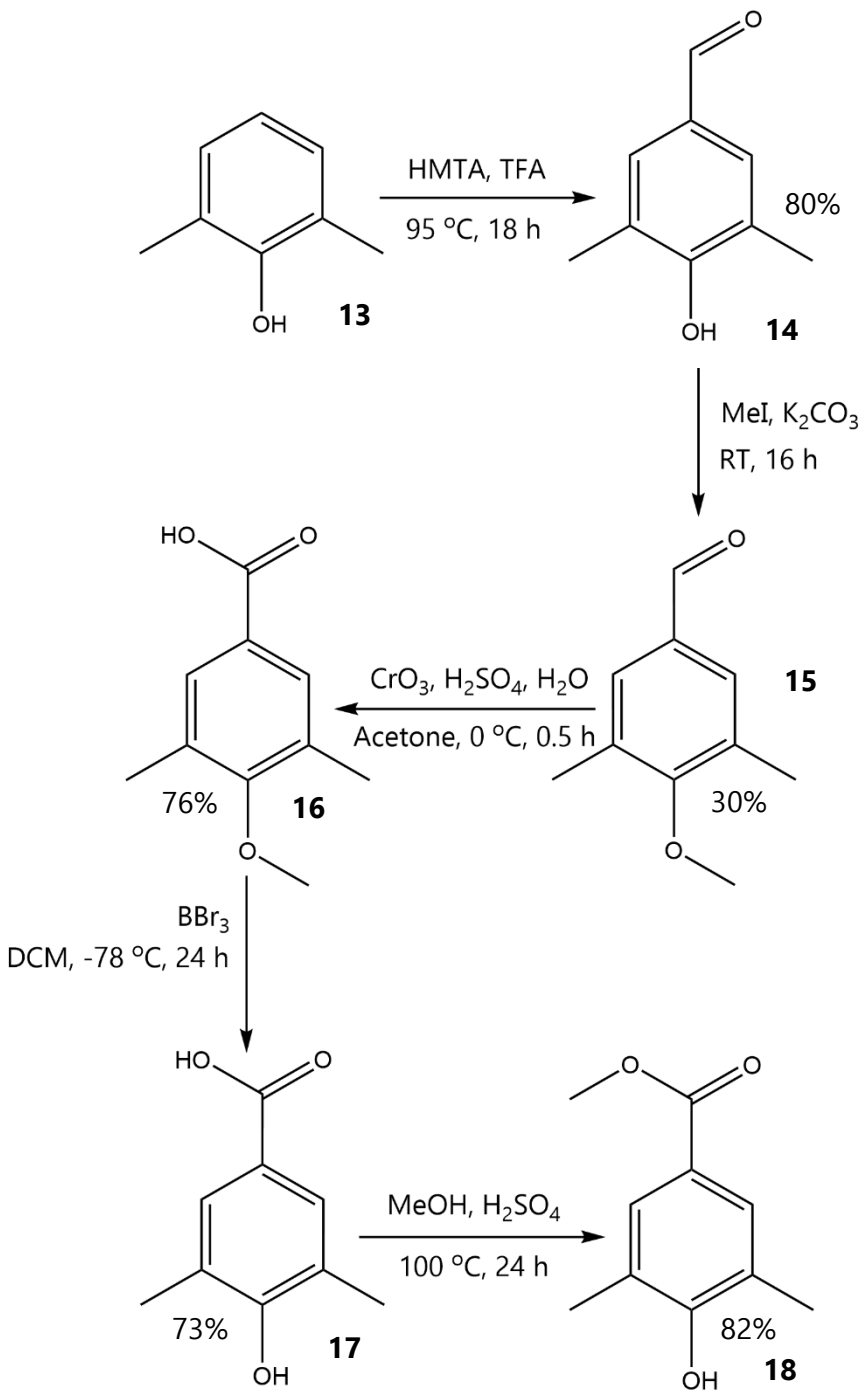

Scheme 3.3. The 5-step reaction scheme for the formation of methyl 4-hydroxy-3,5-dimethylbenzoate **18**, a molecule designed to be a viable stopper group for a di-acid rotaxane for MORF preparation.

2,6-Dimethylphenol, hexamethylenetetramine and trifluoroacetic acid were mixed and refluxed for 18 hours. The resulting red solution was quenched with water and stirred for a further one hour at room temperature. This red/orange solution was neutralised with solid sodium hydrogen carbonate until at pH 7. Once filtered under vacuum this afforded a pale-yellow solid. This solid was then dissolved in diethyl ether and the white solid impurity filtered off under gravity. The brown solution was evaporated under reduced pressure to give an orange solid. This was dried in air to give a pale brown solid.

Once the Duff reaction was completed successfully, the alcohol group needed to be protected before the oxidation of the aldehyde to an acid to prevent this being also converted by the Jones oxidation. 4-Hydroxy-3,5-dimethylbenzaldehyde **14**, methyl iodide and potassium carbonate were stirred at room temperature in DMF for 16 hours. This afforded an orange solid and was purified by column chromatography to give a yellow oil.

For the oxidation of the aldehyde to a carboxylic acid, chromic acid was created using chromium(VI) oxide, sulfuric acid, and water, and added dropwise to 4-methoxy-3,5-dimethylbenzaldehyde **15** in acetone and stirred at 0 °C for 30 minutes. After this time, the resulting brown solution was quenched with ethanol until a green colour was seen throughout. This reaction was filtered and washed with ether to yield a pale-yellow powder.

To leave the alcohol group free for addition by a dibromoalkane, the ether must be deprotected. 4-Methoxy-3,5-dimethylbenzoic acid **16** and dichloromethane were cooled to -78 °C and BBr_3 (1M in DCM) was added dropwise. This mixture was then allowed to stir at RT for 24 h. The pale brown solution was added dropwise to water over ice. A white precipitate was formed. This was then filtered under reduced pressure and washed with water, DCM and dried in air to afford a white powder.

The final step in the stopper synthesis was to protect the acid group the acid group by esterification. 4-Hydroxy-3,5-dimethylbenzoic acid **17** in methanol and conc. sulfuric acid was heated to reflux for 24 hours. This pale-yellow solution was cooled, and the solvent removed under pressure to afford a white solid.

Now that the starting material for both the rod and stopper was complete. A dibromoalkane can be added using the similar basic addition method for both the TAR4 and TAR8 rods, respectively. Methyl 4-hydroxy-3,5-dimethylbenzoate **18**, 1,4-dibromobutane and potassium carbonate were stirred in DMF at 85 $^{\circ}$C for 24 hours. The resulting mixture was extracted with chloroform and washed with water and brine. The pale-yellow solution was dried over magnesium sulfate and reduced in volume under vacuum to afford an orange oil. This solid was purified by column chromatography to give a yellow oil.

Methyl 4-(4-bromobutoxy)-3,5-dimethylbenzoate was then reacted with imidazole and potassium carbonate in DMF at 85 °C for 24 hours. The resulting mixture was extracted with chloroform and washed with water and brine. The pale-yellow solution was dried over magnesium sulfate and reduced in volume under vacuum to afford an orange oil, similar in appearance to that of the starting material. Upon, ^{1}H NMR analysis, it was found that the reaction had not proceeded. This reaction was repeated several times, with the starting material remaining unconverted each time.

3.6 Di-acid Rotaxanes: Syringol-based Rotaxane

Another di-acid rotaxane architecture was devised and partially synthesised. This utilises syringol, a cheap, commercially available molecule as a stopper group for the rotaxane which removes the need for multi-step synthesis, pre-rotaxane rod formation. The formation of the rotaxane rod consisted of an esterification of the acid, which could be deprotected later once the final rotaxane was formed. This esterification was followed by the addition of a bromobutyl-chain on the alcohol group, which was then functionalised with an imidazole group. Once this was achieved in appreciable yield, a di-ester rotaxane was to be assembled using this rod, dimethoxypillar[5]arene and iodosyringate as a stopper. This would then be deprotected to form a di-acid rotaxane suitable for MORF formation.

To form the syringate ester, syringic acid **19** was dissolved in methanol, concentrated sulfuric acid added, and heated at reflux for 16 hours. The solvent was removed under reduced pressure and the resulting off-white solid was dissolved in chloroform and washed with water and brine. The pale brown solution was dried over magnesium sulfate and the solvent removed under vacuum to afford an off-white solid.

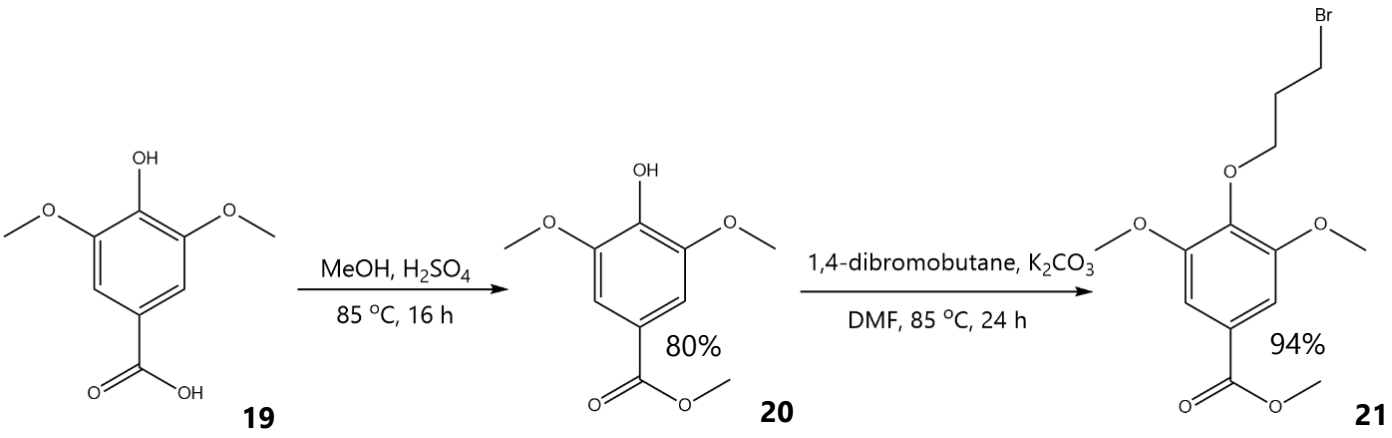

Scheme 3.4. The esterification reaction to form syringate.

To produce the rotaxane rod; syringate **20**, 1,4-dibromobutane and potassium carbonate were stirred in DMF at 85 °C for 24 h (Scheme 3.4). The resulting mixture was extracted with chloroform and washed with water and brine. The yellow solution was dried over magnesium sulfate and reduced in volume under vacuum to afford a dark yellow solid. This solid was purified by column chromatography to give a clear oil **21**.

To synthesise the stopper group, syringate **20**, potassium iodide and boron trifluoroboron diethyl etherate were stirred overnight in 1,4-dioxane in the absence of light (Scheme 3.5). The residue was extracted in ether, washed and dried to afford a brown solid **22**.

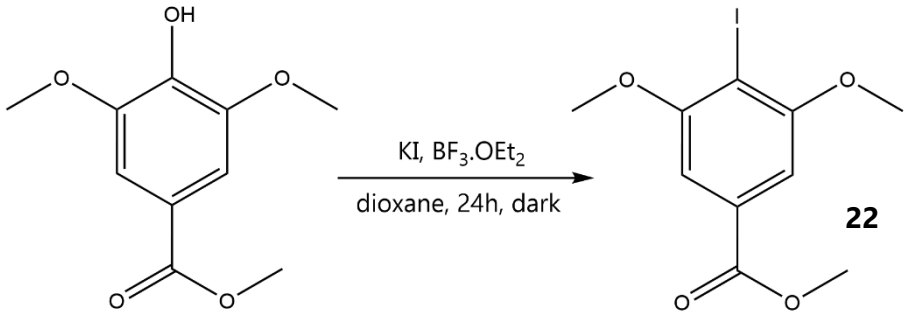

Scheme 3.5. The synthesis of iodosyringate.

When an assembly reaction was attempted using the iodinated stopper, the syringate rod and pillararene, a threaded rotaxane was not formed. This is most likely because the substituents on the ring did not offer enough steric bulk to prevent dethreading. It was at this point that it was decided that this diacid rotaxane framework was not a viable route forward due the lack of steric bulk for the commercially available syringate motif and the synthetic complexity of the previously synthesised analogue.

3.7 Conclusions

Two different tetra acid rotaxanes, TAR4 and TAR8, have been synthesised using a stepwise toolbox approach. Both these rotaxanes utilise the imidazolium cation/pillar[5]arene interaction to spontaneously self-assemble to form a threaded macrocycle. Once these rotaxanes were synthesised, attempts were made to combine these with metals to form a stable MORF. Many metal reagents and reaction conditions were used, however, all of which were unsuccessful.

Crystal structures of TAR4 were obtained by single crystal X-ray crystallography, revealing that both inter and intra molecular hydrogen bonding can be observed. Using ^{1}H NMR spectroscopic shift data, the hydrogen bonding shifts the macrocycle from the expected position due to this hydrogen bonding.

A diacid rotaxane was designed using a different stopper group which was synthesised from dihydroxyphenyl by a six-step reaction scheme. This produced the desired stopper, however, upon assembly of the rotaxane, a final threaded rotaxane was not formed. Another syringate based stopper group was also synthesised but also gave no threaded product upon attempted self-assembly.

3.8 Experimental

Synthesis of a rod precursor: Dimethyl 5-(4-bromobutoxy)isophthalate (**2**)

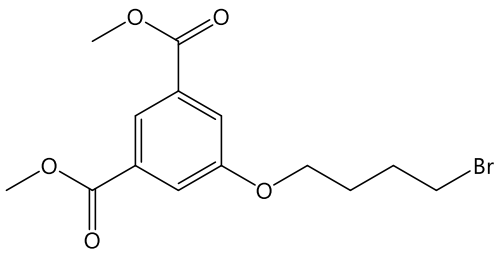

1,4-Dibromobutane (3.40 mL, 8.79 mmol) and dimethyl 5-hydroxyisophthalate (1.00 g, 4.74 mmol) were mixed with potassium carbonate (1.00 g, 7.24 mmol) in dimethylformamide (40 mL) at 85 ºC for 24 hours. After 24 hours had passed, solvent was removed under reduced pressure and the solid remaining was extracted into chloroform, washed with water and brine, dried over magnesium sulfate and filtered. The solvent was removed under pressure to give a crude product that was a yellow oil. This oil was purified by silica column chromatography (hexane/ethyl acetate (9:1)) to give the product as a pale-yellow oil. (0.991 g, 2.88 mmol, 61%) ^{1}H NMR (400 MHz, Chloroform-d) δ 8.28 (t, *J* = 1.4 Hz, 1H), 7.75 (d, *J* = 1.4 Hz, 2H), 4.10 (t, *J* = 5.9 Hz, 2H), 3.95 (s, 6H), 3.51 (t, *J* = 6.5 Hz, 2H), 2.16 – 2.02 (m, 2H), 2.00 (dtd, *J* = 7.2, 6.4, 5.0 Hz, 2H), 0.87 (s, 1H), 0.09 (s, 1H).

Synthesis of imidazole rod: dimethyl 5-(4-(1H-imidazol-1-yl)butoxy)isophthalate (**3**)

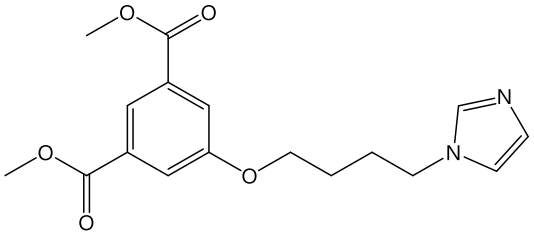

Dimethyl 5-(4-bromobutoxy)isophthalate (1.00 g, 2.91 mmol) and imidazole (0.40 g, 5.88 mmol) were mixed with potassium carbonate (0.6 g, 4.34 mmol) in

dimethylformamide (40 mL) at 85 ºC for 24 hours. After 24 hours had passed, solvent was removed under reduced pressure and solid remaining was extracted into chloroform, washed with water and brine, and dried over magnesium sulfate then filtered. The solvent was removed under pressure to give a crude product that was a yellow oil. This oil was purified by silica column (chloroform/acetone (65:35)) to give the product as a pale-yellow oil. It was found that when synthesised in larger amounts, the oil crystallised to a white solid. (0.56g, 1.69 mmol, 58%) ^{1}H NMR (400 MHz, Chloroform-d) δ 8.27 (t, *J* = 1.4 Hz, 1H), 7.71 (d, *J* = 1.5 Hz, 2H), 7.51 (t, *J* = 1.2 Hz, 1H), 7.07 (d, *J* = 1.1 Hz, 1H), 6.95 (t, *J* = 1.3 Hz, 1H), 4.05 (td, *J* = 7.1, 6.5, 3.4 Hz, 4H), 3.93 (s, 6H), 2.07 – 1.95 (m, 2H), 1.87 – 1.75 (m, 2H). ^{13}C NMR (101 MHz, Chloroform-d) δ 166.10, 158.81, 137.12, 131.80, 129.64, 123.10, 119.69, 118.75, 77.30, 67.69, 52.47, 46.68, 27.97, 26.15.

Synthesis of stopper group: Diethyl 5-(iodomethyl)isophthalate (**5**)

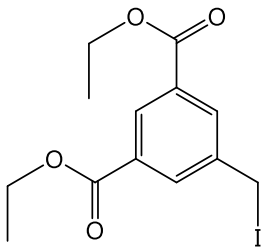

To a solution of both diethyl 5-(hydroxymethyl)isophthalate (0.25 g, 0.99 mmol) and potassium iodide (0.18 g, 1.08 mmol) in 1,4-dioxane (20 mL) was added $BF_3.Et_2O$ (0.134 mL, 1.09 mmol). This was then stirred in darkness, at room temperature, for 24 hours. The solvent was removed, and the product extracted in diethyl ether, washed with water and brine, dried over magnesium sulfate and filtered. The solvent was then removed to afford an orange solid. (0.28 g, 0.84 mmol, 85%) ^{1}H NMR (400 MHz, Chloroform-d) δ 8.63 (t, *J* = 1.6 Hz, 1H), 8.29 – 8.20 (m, 4H), 4.53 (s, 2H), 4.44 (q, *J* = 7.1 Hz, 8H), 1.34 – 1.19 (m, 6H).

Assembly of the tetraethyl ester pillarene rotaxane: TER4 (**7**)

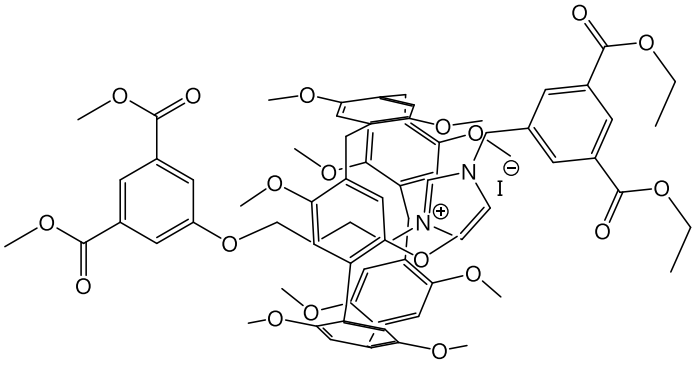

5-(4-(1H-imidazol-1-yl)butoxy)isophthalate (0.50 g, 1.50 mmol) and pillar[5]arene (1.25 g, 1.67 mmol) were dissolved in the minimal amount of chloroform (2 mL) and cooled to -15 °C. In the absence of light, a saturated solution of diethyl 5-(iodomethyl)isophthalate in chloroform (1 mL) was added. This mixture was allowed to warm up to room temperature and stirred over-night. The products were purified by silica gel column chromatography (acetone/chloroform 1:9) to afford a yellow solid. (0.71 g, 0.49 mmol, 22%).

Deprotection to a tetracarboxylic acid rotaxane: TAR4 (**8**)

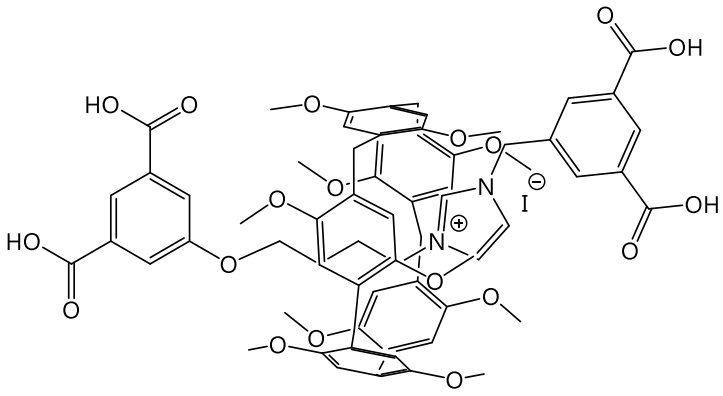

TER4 (0.50 g, 0.34 mmol) was dissolved in a methanol/tetrahydrofuran (24 mL/12 mL)

and 2M NaOH (6 mL) added dropwise. This was left to stir at reflux for 24 hours. Solvents were removed under reduced pressure and the solid residue dissolved in water. The pH was adjusted to 1 by addition of hydrochloric acid. The mixture was cooled until precipitate was formed and filtered under gravity and dried in a vacuum oven (70 °C, ~10 bar) to give a pale-brown powder (0.303 g, 0.21 mmol, 62%). ^{1}H NMR (400 MHz, Methanol-d_4) δ 8.79 (t, *J* = 1.6 Hz, 1H), 8.49 (d, *J* = 1.6 Hz, 2H), 8.36 (t, *J* = 1.4 Hz, 1H), 7.94 (t, *J* = 1.8 Hz, 1H), 7.86 (d, *J* = 1.4 Hz, 2H), 7.61 (t, *J* = 1.7 Hz, 1H), 7.13 (s, 4H), 6.90 (s, 4H), 6.21 (t, *J* = 1.8 Hz, 1H), 5.76 (s, 2H), 3.87 – 3.76 (m, 8H), 3.80 (s, 13H), 3.72 (d, *J* = 17.3 Hz, 2H), 3.65 (s, 12H), 3.26 – 3.09 (m, 1H), 1.31 (s, 1H), 0.50 (dd, *J* = 10.4, 7.6 Hz, 2H), -1.72 (dt, *J* = 16.8, 7.8 Hz, 1H).

MORF Synthetic Methods

$Cu(NO_3)_2.2.5H_2O$ (2 mg, 8.60 × 10^{-3} mmol) and TAR4 (4 mg, 3.24 × 10^{-3} mmol) were dissolved in MeOH (1 mL) and conc. HNO_3 (0.1 mL) and left to slowly evaporate for 5 months.

Ag/TAR4 Crystallisation

$Ag(NO_3)$ (2 mg, 0.012 mmol) and TAR4 (4 mg, 3.24 × 10^{-3} mmol) were dissolved in MeOH (1 mL) and conc. HNO_3 (0.1 mL) and left to slowly evaporate for 5 months. After such time, clear, colourless plates were formed.

TAR8 Experimental

Dimethyl 5-(4-bromooctoxy)isophthalate (**9**)

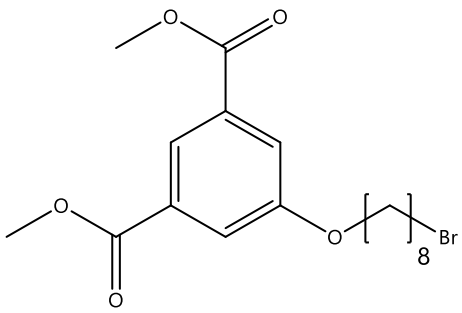

Dimethyl 5-hydroxyisophthalate (2.00g, 9.52 mmol), 1,8-dibromooctane (10.5 mL, 56.9 mmol) and potassium carbonate (2.00g, 14.5 mmol) were dissolved in DMF (60 mL) and the mixture heated to 85 ºC overnight. The solvent was then removed under reduced pressure and the residue taken up in water and dichloromethane. The organic layer was washed with water (2 × 100 mL) and brine (1 × 100mL) before being dried over anhydrous magnesium sulfate and filtered. The solvent was removed under reduced pressure and the crude residue subjected to column chromatography (SiO_2/ hexane: hexane: ethyl acetate 90: 10) to afford the product as a clear oil (3.784g, 99%). ^{1}H NMR (400 MHz, Chloroform-d) δ 8.27 (t, *J* = 1.4 Hz, 1H), 7.75 (d, *J* = 1.4 Hz, 2H), 4.18 (td, *J* = 6.7, 0.9 Hz, 3H), 4.05 (t, *J* = 6.4 Hz, 2H), 3.95 (s, 6H), 1.73 – 1.61 (m, 4H), 1.46 (dtd, *J* = 6.8, 3.6, 1.8 Hz, 5H), 1.27 (d, *J* = 1.2 Hz, 2H). ^{13}C NMR (101 MHz, Chloroform-d) δ 166.23, 161.20, 159.22, 131.72, 122.79, 119.84, 76.73, 68.53, 64.01, 52.40, 33.96, 33.93, 32.78, 32.74, 29.71, 29.13, 29.04, 28.98, 28.68, 28.61, 28.58, 28.47, 28.09, 28.04, 25.88, 25.72.

Dimethyl 5-(4-(1H-imidazol-1-yl)octoxy)isophthalate (**10**)

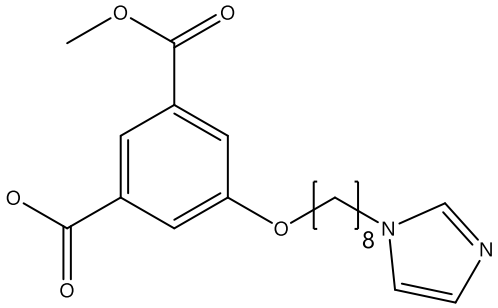

Dimethyl 5-(4-bromooctoxy)isophthalate (1.7g, 4.24 mmol), imidazole (0.29g, 4.26 mmol) and potassium carbonate (0.69g, 4.99 mmol) were dissolved in DMF (40 mL) and the mixture heated to 85 ºC overnight. The solvent was then removed under reduced pressure and the residue taken up in water and dichloromethane. The organic layer was washed with water (2 × 100 mL) and brine (1 × 100mL) before being dried over anhydrous magnesium sulfate and filtered. The solvent was removed under reduced pressure and the crude residue subjected to column chromatography (SiO_2/chloroform: acetone 65 : 35) to afford the product as a pale yellow solid (0.61g, 37%). ^{1}H NMR (400 MHz, Chloroform-d) δ 7.97 (s, 4H), 7.69 (dd, *J* = 2.7, 1.5 Hz, 2H), 7.00 (t, *J* = 1.1 Hz, 2H), 6.87 (dq, *J* = 2.6, 1.3 Hz, 2H), 4.12 (tdd, *J* = 6.7, 3.5, 0.9 Hz, 2H), 3.99 (t, *J* = 6.4 Hz, 2H), 3.90 (s, 6H), 1.89 (s, 1H), 1.74 (d, *J* = 10.2 Hz, 3H), 1.42 (td, *J* = 7.7, 6.5, 3.6 Hz, 2H), 1.29 – 1.27 (m, 2H), 1.22 (s, 2H). ^{13}C NMR (101 MHz, Chloroform-d) δ 166.16, 162.50, 161.16, 159.16, 137.03, 131.68, 129.31, 122.73, 119.77, 118.76, 68.44, 52.37, 46.97, 31.02, 30.99, 30.95, 29.07, 28.39, 25.64.

Tetra-ester Rotaxane (TER8) (**11**)

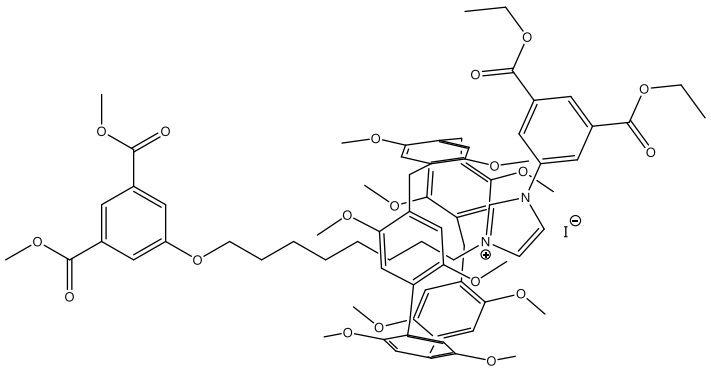

Dimethyl 5-(4-(1H-imidazol-1-yl)octoxy)isophthalate (175mg, 0.45 mmol) and dimethoxypillar[5]arene (338 mg, 0.45 mmol) were dissolved in chloroform (2 mL) and cooled to -15 °C. Under the exclusion of light, a solution of diethyl 5-(iodomethyl)isophthalate (163 mg, 0.51 mmol) in chloroform (1 mL) was added and the mixture was left to warm to room temperature and stirred overnight. The product mixture was subjected to column chromatography (SiO_2/ acetone: chloroform 10 : 90) to afford the product as a yellow solid (221mg, 36%). ^{1}H NMR (400 MHz, Chloroform-d) δ 8.75 (s, 2H), 8.32 (t, *J* = 1.4 Hz, 1H), 8.11 (d, *J* = 27.2 Hz, 1H), 7.81 (d, *J* = 1.5 Hz, 2H), 7.13 – 6.87 (m, 10H), 6.82 (s, 2H), 6.51 (d, *J* = 16.0 Hz, 4H), 4.26 (td, *J* = 6.7, 0.9 Hz, 2H), 4.17 – 4.09 (m, 2H), 3.95 (d, *J* = 28.6 Hz, 10H), 3.87 – 3.81 (m, 12H), 3.79 – 3.74 (m, 30H), 1.79 (s, 2H), 1.55 (p, *J* = 7.8 Hz, 2H), 0.61 (s, 2H), 0.31 (s, 2H), -0.25 (s, 2H), -1.56 (s, 2H).

Tetra-acid Rotaxane (TAR8) (**12**)

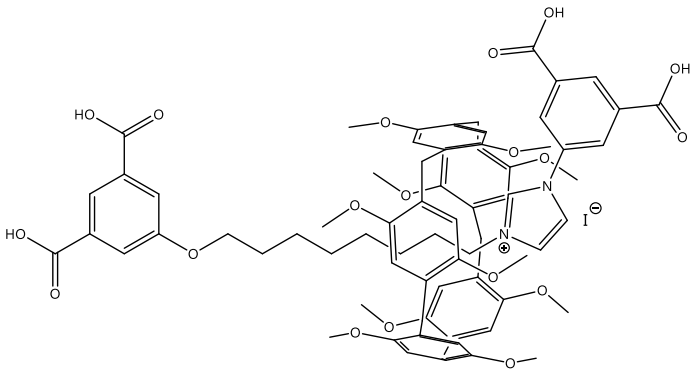

TER8 (145mg, 0.11 µmol) was dissolved in methanol/tetrahydrofuran (24/12 mL) and 2 M sodium hydroxide (4 mL) was added dropwise to the stirring solution which was subsequently heated to reflux for 24 hours. Solvents were removed under reduced pressure and the residue was redissolved in water (30 mL). The pH of the solution was adjusted to 4 by the dropwise addition of 2 M HCl. The resulting mixture was left at 4 ^{0}C for 24 hours and the formed precipitate was filtered under gravity, washed with water and diethyl ether and dried to afford the product as a pale brown solid (70mg, 51%). ^{1}H NMR (400 MHz, Chloroform-d) δ 8.28 (s, 1H), 7.66 (s, 1H), 7.57 (s, 1H), 7.02 – 6.87 (m, 10H), 6.81 (dd, *J* = 8.9, 4.8 Hz, 4H), 6.46 (s, 2H), 4.30 (s, 2H), 4.11 (t, *J* = 6.1 Hz, 2H), 3.97 – 3.83 (m, 10H), 3.81 – 3.77 (m, 31H), 1.40 (dt, *J* = 11.8, 7.3 Hz, 2H), 0.78 – 0.59 (m, 4H), -0.11 (s, 2H), -1.40 (s, 2H).

Di-acid rotaxane synthetic methods

Synthesis of 4-hydroxy-3,5-dimethylbenzaldehyde (**14**)

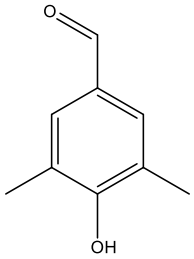

2,6-dimethylphenol (11.4 g, 0.093 mol), hexamethylenetetramine (HTMA) (13.3g, 0.950 mols) and trifluoroacetic acid (70 mL) were mixed and refluxed for 18 hours. The resulting red solution was quenched with 150 mL water and stirred for a further one hour at room temperature. This red/orange solution was neutralised with solid sodium hydrogen carbonate until at pH 7. Once filtered under vacuum this afforded a pale yellow solid. This solid was then dissolved in diethyl ether and the white solid impurity filtered off under gravity. The brown solution was evaporated under reduced pressure to give an orange solid. This was dried in air to give a wet brown solid. (11.48 g, 80%) ^{1}H NMR (400 MHz, Chloroform-d) δ 9.83 (s, 1H), 7.56 (s, 2H), 2.33 (s, 6H). ^{13}C NMR (101 MHz, Chloroform-d) δ 191.41, 158.03, 130.99, 129.39, 123.73, 76.72, 15.82. ESI-MS: (MALDI-TOF) [$C_9H_{10}O_2$] Measured: 149.010 ($C_9H_9O_2^+$) . IR: 3223 cm^{-1} (OH), 2974 cm^{-1} (CH), 2839 cm^{-1} (CH), 2795 cm^{-1} (CH, aldehyde), 1660 cm^{-1} (CO, aldehyde).

Synthesis of 4-methoxy-3,5-dimethylbenzaldehyde (**15**)

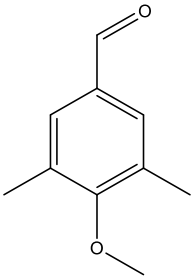

4-Hydroxy-3,5-dimethylbenzaldehyde (10.0 g, 0.067 mol), methyl iodide (5 mL, 0.080 mol) and potassium carbonate (11.1 g, 0.080 mol) were stirred at room temperature in

DMF (100 mL) for 16 hours. After this time, the solvent was removed under pressure and the dark orange solid remaining was extracted with ethyl acetate, washed with water and brine and the solvent removed under pressure. This afforded an orange solid. This solid was purified by column chromatography (hexane: ethyl acetate (9:1)) to give a yellow oil. (3.33g, 30%) ^{1}H NMR (400 MHz, Chloroform-d) δ 9.87 (s, 1H), 7.55 (s, 2H), 3.78 (s, 3H), 2.34 (s, 6H). ^{13}C NMR (101 MHz, Chloroform-d) δ 191.61, 162.40, 132.26, 131.91, 130.69, 130.67, 59.68, 16.15.

Synthesis of 4-methoxy-3,5-dimethylbenzoic acid (**16)**

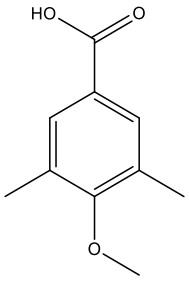

Chromic acid was made using chromium oxide (2.73 g, 0.027 mol), sulfuric acid (2.50 mL) and water (12 mL) and added dropwise to 4-methoxy-3,5-dimethylbenzaldehyde (3.00 g, 0.018 mol) in acetone (90 mL) and stirred at 0 °C for 30 min. After this time, the resulting brown solution was quenched with ethanol until a green colour was seen throughout. The solvent was removed under reduced pressure to give a green powder. This powder was extracted with diethyl ether, washed with water and brine and dried over magnesium sulfate. This solvent was removed to give a pale-yellow powder. (2.722 g, 76 %). ^{1}H NMR (400 MHz, chloroform-d) δ 7.82 (m, 2H), 7.16, 3.80 (s, 1H), 2.34 (s, 6H). ^{13}C NMR (101 MHz, CDCl3) δ 172.14, 161.84, 131.24, 131.17, 124.53, 59.69, 16.16. ESI-MS: (MALDI-TOF) $C_{10}H_{12}O_3$ Measured: 179.071 ($C_{10}H_{11}O_3^+$) . IR: 2950 cm^{-1} (OH, acid), 2922 cm^{-1} (CH), 2853 cm^{-1} (CH), 2617 cm^{-1} (CH), 1677 cm^{-1} (CO, acid).

Synthesis of 4-hydroxy-3,5-dimethylbenzoic acid (**17**)

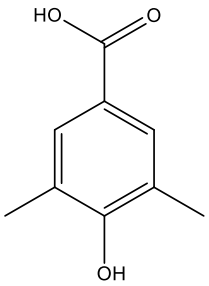

4-methoxy-3,5-dimethylbenzoic acid (2.00g, 0.120 mol) and DCM (25 mL) was cooled to -78 °C and BBr_3 (1M in DCM) (33 mL, 33 mmol) was added dropwise. This mixture was then allowed to stir at RT for 24 hours. The pale brown solution was added dropwise to water (50 cm^3) over ice. A white precipitate was formed. This was then filtered under reduced pressure and washed with water, DCM and dried in air to afford a white powder. (1.32g, 0.88 mol, 73%) ^{1}H NMR (400 MHz, Methanol-d_4) δ 7.63 (s, 2H), 2.24 (s, 6H). ESI-MS: (MALDI-TOF) $C_9H_{10}O_3$ Measured: 165.0551 ($C_9H_9O_3^+$). IR: 3419 cm^{-1} (OH, alcohol), 2977 cm^{-1} (OH, acid), 2956 cm^{-1} (CH), 2907 cm^{-1} (CH), 1655 cm^{-1} (CO acid).

Synthesis of methyl 4-hydroxy-3,5-dimethylbenzoate (**18**)

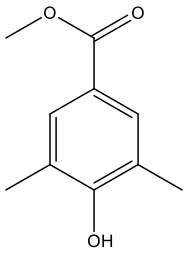

4-Hydroxy-3,5-dimethylbenzoic acid (3.00g, 15.1 mmol) in methanol (25 mL) and conc. sulfuric acid (0.50 mL) was heated to reflux for 24 hours. This pale-yellow solution was cooled and the solvent removed under pressure to afford a white solid. (1.90g, 59%). ^{1}H NMR (400 MHz, Methanol-d4) δ 7.62 (d, *J* = 7.2 Hz, 2H), 3.84 (d, *J* = 1.6 Hz, 3H), 2.24 (d, *J* = 1.9 Hz, 6H). ^{13}C NMR (101 MHz, CD_3OD) δ 169.08, 167.71, 158.04, 157.92, 130.18, 129.89, 123.86, 123.73, 120.94, 120.47, 50.77, 48.27, 48.05, 47.84, 47.63, 47.42, 47.21, 46.99, 15.23.

Synthesis of methyl 4-(4-bromobutoxy)-3,5-dimethylbenzoate:

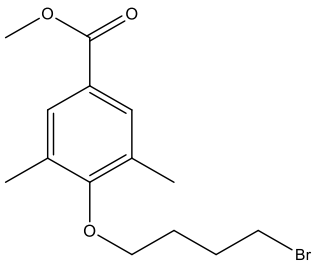

Methyl 4-hydroxy-3,5-dimethylbenzoate (1.00g, 6.02 mmol), 1,4-dibromobutane (0.80 mL, 0.74 mmol) and potassium carbonate (1.00g, 7.24 mmol) were stirred in DMF (20 mL) at 85 ºC for 24 hours. The resulting mixture was extracted with chloroform and washed with water and brine. The pale-yellow solution was dried over magnesium sulfate and reduced in volume under vacuum to afford an orange oil. This solid was purified by column chromatography (hexane: ethyl acetate (9:1)) to give a yellow oil. (1.91 g, 0.61 mmol, 82%)^{1}H NMR (400 MHz, Chloroform-d) δ 7.73 (d, *J* = 4.1 Hz, 2H), 4.33 (tdt, *J* = 18.5, 12.2, 5.7 Hz, 1H), 3.94 – 3.79 (m, 4H), 3.57 – 3.44 (m, 1H), 2.33 (s, 4H), 2.21 – 1.82 (m, 4H). ^{13}C NMR (101 MHz, Chloroform-d) δ 166.45, 159.95, 125.42, 125.39, 125.37, 63.78, 51.94, 31.94, 31.44, 30.32, 29.06, 27.46, 16.37, 14.13.

Synthesis of syringate (**20**)

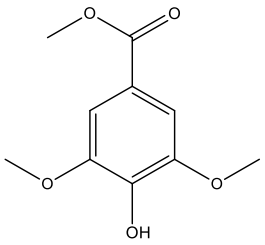

Syringic acid (10.0g, 0.050 mols) was dissolved in methanol (150 mL) with concentrated sulfuric acid (2.00 mL) and heated at reflux for 16 hours. The solvent was removed under reduced pressure and the resulting off-white solid was dissolved in chloroform and washed with water and brine. The pale brown solution was dried over magnesium sulfate and the solvent removed under vacuum to afford an off-white solid. (8.56g, 0.040 mol, 80%). 1H NMR (400 MHz, Chloroform-d) δ 7.34 (d, *J* = 1.4 Hz, 2H), 3.94 (dd,

J = 16.7, 1.4 Hz, 9H). ESI-MS: (MALDI-TOF) $C_{10}H_{12}O_5$ Measured: 235.0583 $C_{10}H_{12}O_5Na$ (+Na)

Synthesis of methyl 4-(4-bromobutoxy)-3,5-dimethoxybenzoate (**21**)

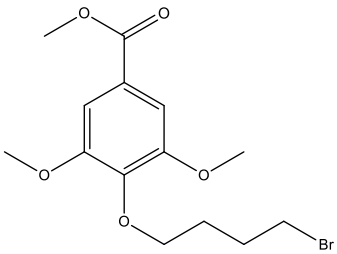

Syringate (3.00g, 14.1 mmol), 1,4-dibromobutane (7.8 mL, 7.23 mmol) and potassium carbonate (2.5g, 18.1 mmol) were stirred in DMF (75 mL) at 85 ºC for 24 hours. The resulting mixture was extracted with chloroform and washed with water and brine. The yellow solution was dried over magnesium sulfate and reduced in volume under vacuum to afford a dark yellow. This solid was purified by column chromatography (chloroform: acetone 99:1) to give a clear oil. (2.36g, 94%) ^{1}H NMR (400 MHz, Chloroform-d) δ 7.29 (d, *J* = 2.3 Hz, 2H), 4.05 (t, *J* = 6.1 Hz, 2H), 3.90 (dd, *J* = 6.4, 1.7 Hz, 9H), 3.53 (t, *J* = 6.9 Hz, 2H), 2.19 – 2.08 (m, 2H), 1.91 (tt, *J* = 13.3, 6.7 Hz, 2H) 13C NMR (101 MHz, CDCl3) δ 166.69, 160.96, 153.13, 141.19, 125.17, 106.75, 76.79, 72.15, 62.91, 56.21, 52.22, 33.73, 32.93, 32.55, 30.96, 29.37, 29.12, 28.69, 27.17.

Synthesis of iodosyringate (**22**)

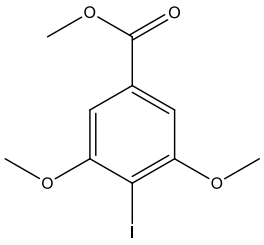

Syringate (2.00g, 9.42 mmol), potassium iodide (1.17g, 7.05 mmol) and boron trifluorodiethyletherate (0.87 mL, 7.05 mmol) were stirred overnight in 1,4-dioxane (120 mL) in the absence of light. The solvent from this brown solution was removed, the solid residue extracted in ether, washed in water and brine. This solution was dried

with magnesium sulfate and the solvent removed under reduced pressure to afford a brown solid. (2.85g (wet)). 1H NMR (400 MHz, Chloroform-d) δ 7.35 (s, 2H), 3.94 (d, *J* = 17.4 Hz, 9H). 13C NMR (101 MHz, CDCl3) δ 146.63, 139.18, 121.11, 106.65, 76.71, 75.65, 56.44, 52.11. MS: $C_{10}H_{11}O_4I$ 197.0447 (Compound –I, +H)

Cu/TAR4 Crystallographic Information

Experimental

Single crystals of $C_{74}H_{84}N_3O_{23}$ [CUMANA]. A suitable crystal was selected and mounted in a fomblin film on a micromount on a SuperNova, Atlas S2 diffractometer. The crystal was kept at 120(2) K during data collection. Using Olex2 [1], the structure was solved with the ShelXT [2] structure solution program using Unknown and refined with the ShelXL [3] refinement package using Unknown minimisation.

1. Dolomanov, O.V., Bourhis, L.J., Gildea, R.J, Howard, J.A.K. & Puschmann, H. (2009), J. Appl. Cryst. 42, 339-341.
2. Sheldrick, G.M. (2015). Acta Cryst. A71, 3-8. 3.
3. Sheldrick, G.M. (2015). Acta Cryst. C71, 3-8.

Identification code	CUMANA
Empirical formula	$C_{74}H_{84}N_3O_{23}$
Formula weight	1229.07
Temperature/K	120(2)
Crystal system	triclinic
Space group	P-1
a/Å	12.1298(11)
b/Å	16.3875(15)
c/Å	19.3412(15)
α/°	96.604(7)
β/°	106.892(7)
γ/°	104.979(8)
Volume/Å^3	3477.7(6)
Z	2
ρ_{calc}g/cm^3	1.174
μ/mm^{-1}	0.836
F(000)	1306.0
Crystal size/mm^3	0.257 × 0.069 × 0.052
Radiation	CuKα (λ = 1.54184)
2Θ range for data collection/°	7.862 to 149.392
Index ranges	-15 ≤ h ≤ 10, -20 ≤ k ≤ 19, -23 ≤ l ≤ 24
Reflections collected	25966
Independent reflections	13697 [R_{int} = 0.0364, R_{sigma} = 0.0623]
Data/restraints/parameters	13697/0/939
Goodness-of-fit on F^2	1.318
Final R indexes [I>=2σ (I)]	R_1 = 0.1445, wR_2 = 0.4041

Final R indexes [all data]	R_1 = 0.2090, wR_2 = 0.4543
Largest diff. peak/hole / e Å^{-3}	0.87/-0.53

Ag/TAR4 Crystallographic Information

Experimental

Single crystals of $C_{75}H_{83}N_5O_{24}$ [AGMANC]. A suitable crystal was selected and mounted in a fomblin film on a micromount on a SuperNova, Atlas S2 diffractometer. The crystal was kept at 120(2) K during data collection. Using Olex2 [1], the structure was solved with the ShelXT [2] structure solution program using Unknown and refined with the ShelXL [3] refinement package using Unknown minimisation.

1. Dolomanov, O.V., Bourhis, L.J., Gildea, R.J, Howard, J.A.K. & Puschmann, H. (2009), J. Appl. Cryst. 42, 339-341.
2. Sheldrick, G.M. (2015). Acta Cryst. A71, 3-8. 3.
3. Sheldrick, G.M. (2015). Acta Cryst. C71, 3-8.

Identification code	AGMANC
Empirical formula	$C_{75}H_{83}N_5O_{24}$
Formula weight	1402.84
Temperature/K	120(2)
Crystal system	monoclinic
Space group	$P2_1$
a/Å	16.5043(2)
b/Å	12.08540(10)
c/Å	19.2985(2)
α/°	90
β/°	108.0460(10)
γ/°	90
Volume/Å^3	3659.94(7)
Z	2
ρ_{calc}g/cm^3	1.273
μ/mm^{-1}	1.048
F(000)	1480.0
Crystal size/mm^3	0.202 × 0.154 × 0.065
Radiation	Cu Kα (λ = 1.54184)
2Θ range for data collection/°	7.32 to 147.82
Index ranges	-20 ≤ h ≤ 20, -15 ≤ k ≤ 14, -23 ≤ l ≤ 20
Reflections collected	30797

Independent reflections	13771 [R_{int} = 0.0213, R_{sigma} = 0.0241]
Data/restraints/parameters	13771/1/944
Goodness-of-fit on F^2	1.058
Final R indexes [I>=2σ (I)]	R_1 = 0.0563, wR_2 = 0.1622
Final R indexes [all data]	R_1 = 0.0579, wR_2 = 0.1650
Largest diff. peak/hole / e $Å^{-3}$	1.79/-0.56
Flack parameter	0.02(4)

Intermolecular H-bond distance: 1.807 Å

4. Towards a Naphthalene Diimide/Porphyrin [2]handcuff Rotaxane

4.1 Towards the synthesis of a porphyrin/naphthalene diimide [2]handcuff rotaxane

Molecular handcuffs are mechanically interlocked molecules that comprise of two or more molecules held together by mechanical bonds, not covalent bonds. Handcuff rotaxanes are complex structures that allow for molecules to stack in a controlled, but still flexible way, allowing molecular interactions to be studied.[128] Some of the more chemically interesting molecules to incorporate into molecular handcuffs are dye molecules such as naphthalene and perylenediimides (NDIs, PDIs) because of their strong colour and ability to be oxidised and reduced.[162–165] Both NDI and PDI have well defined redox potentials and have been extensively studied by cyclic voltammetry,[162,164] both free and in complex systems, including metal-organic frameworks (MOF).[166,167]

One of the key advantages of NDIs are their synthetic flexibility (Figure 4.1). Naphthalene dianhydride can be functionalised by reaction with a large variety of amines to produce ligands that are ideal for incorporation into complex systems.[163,167–168] For example, if an acid or amine group is added, an NDI can be coordinated to a metal centre to form a MOF[167], and if functionalised with pillararene moieties and reacted with a diimidazolium rod, it can form a handcuff rotaxane[128].

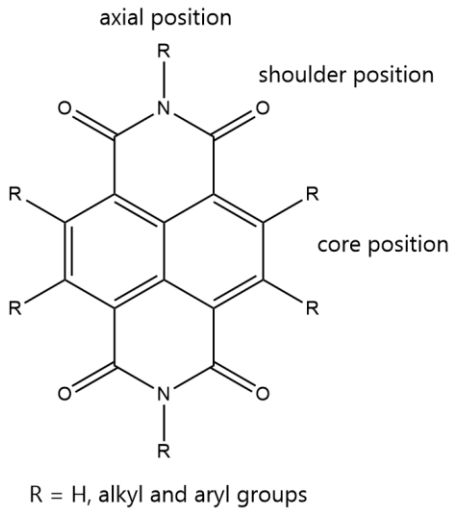

Figure 4.1. The chemical structure of naphthalene diimide. Substitution can occur at the axial, shoulder, and core position. Adapted from work by Mukhopadhyay and Shukla.[168]

A Zn/NDI/porphyrin metal-organic framework has been previously synthesised in the Champness group. The MOF structure arranges the NDI and porphyrin groups in rigid staggered arrangement (Figure 4.2). After seeing this MOF structure and taking the principals of handcuff rotaxane synthesis from the group, a [2]rotaxane handcuff molecule with both an NDI and a porphyrin was designed. The synthesis of this molecule was started and will now be detailed.

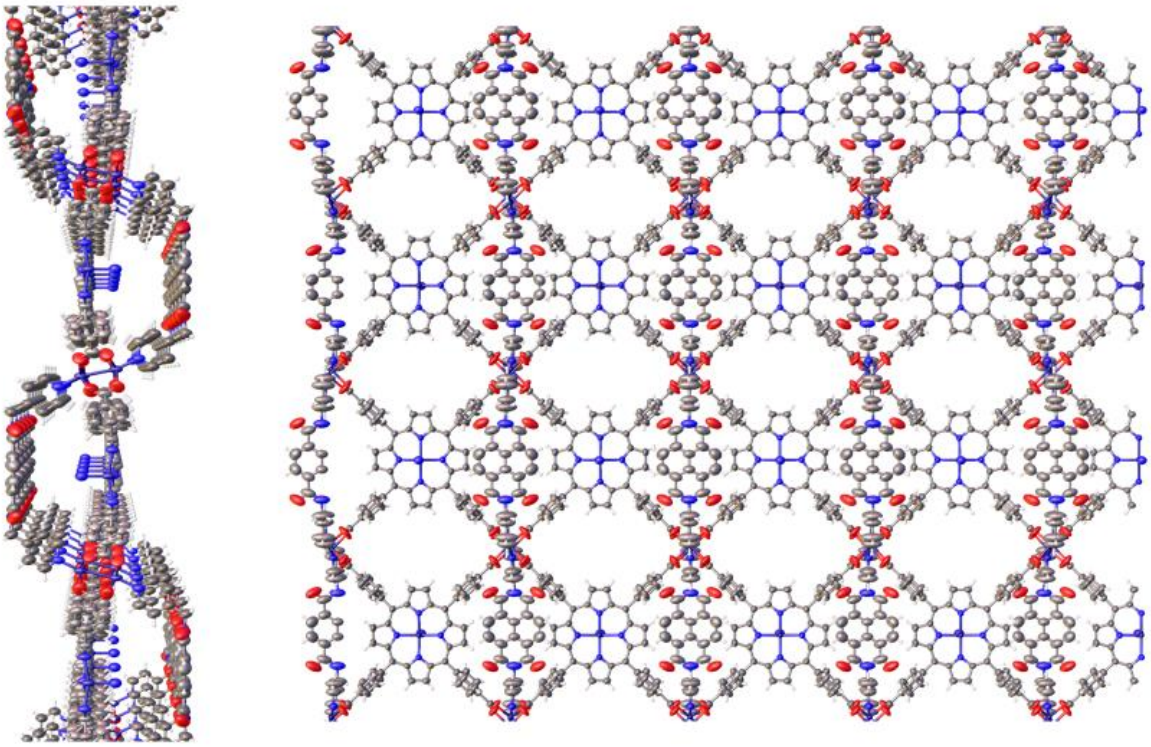

Figure 4.2. The previously synthesised Zn/NDI/porphyrin MOF. When viewed along the 100 axis (left) and the 010 axis (right) the staggered arrangement can be clearly seen. Adapted from unpublished work by C. Pfeiffer, Nottingham University.

4.2 Synthesis of NDI/Porphyrin [2]handcuff rotaxane

To synthesise the NDI/porphyrin [2]handcuff rotaxane, a toolbox approach, like that of a simpler rotaxane was employed. The three parts of that handcuff rotaxane were to be synthesised separately and combined to form the final handcuff (Figure 4.3). The dipillarene functionalised NDI and the stopper groups had been synthesised previously in the group[169] and were available for future reactions and therefore the synthesis of this will not be detailed here.

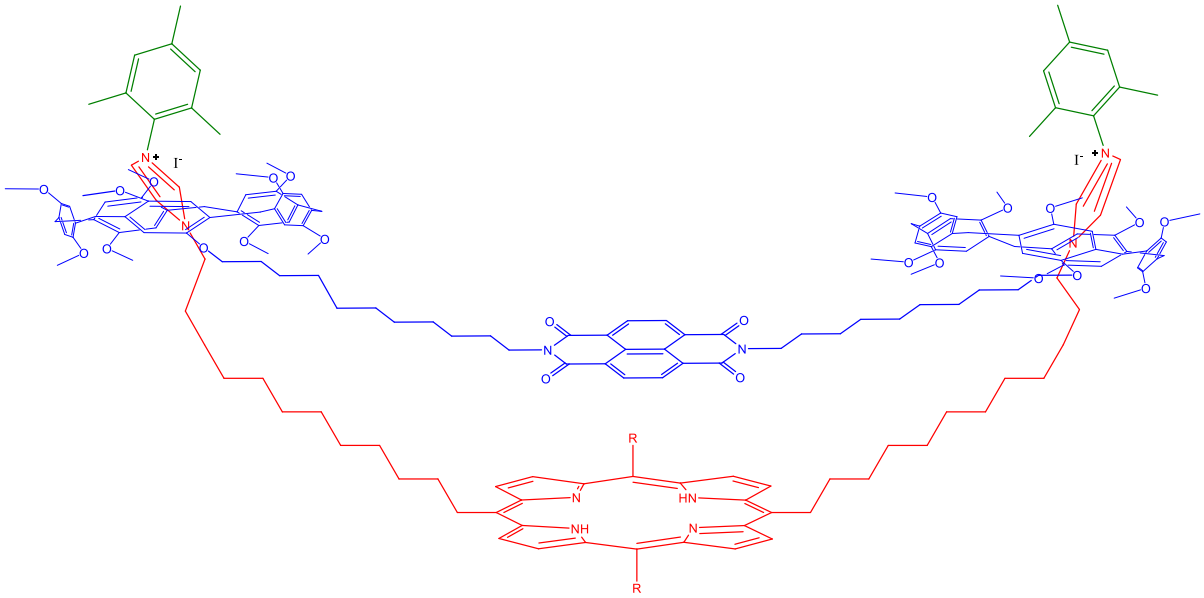

Figure 4.3. The initial target [2]handcuff molecule. Different colours represent different synthetic components.

4.3 Synthesis of an alkyl imidazole porphyrin rod

The most structurally simple porphyrin, porphine, was first synthesised by Paul Rothermund by a condensation reaction between formaldehyde and pyrrole with an acid catalyst.[170] By using different aldehydes, substitutions can be made in the *meso*-positions of the porphyrin,[171] and this is the initial approach used to synthesise the substituted porphyrin. A milder approach, the Alder-Longo method (Scheme 4.1),[172] can be used. The pyrrole and aldehyde are heated together in acetic acid for 24-48 hours. This reaction is generally low yielding, giving tar-like products that are hard to remove by purification.

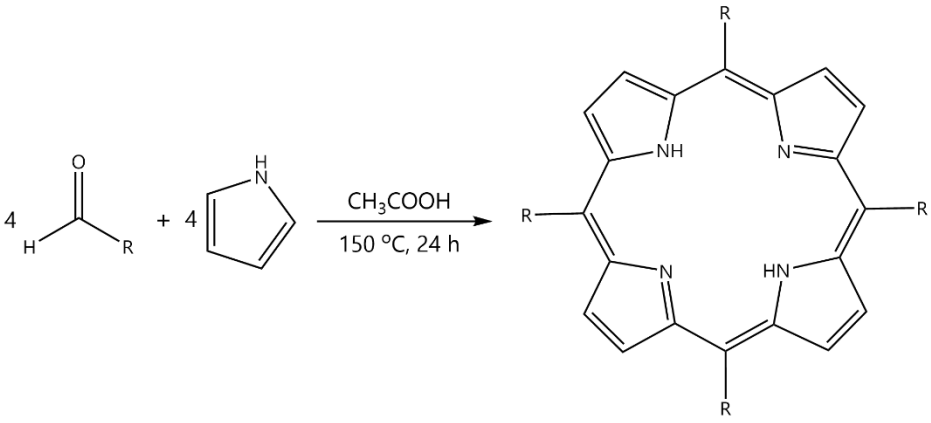

Scheme 4.1. Alder-Longo synthesis for porphyrins

The first step was to synthesise an appropriate aldehyde. The starting material chosen was 4-hydroxybenzaldehyde as an inexpensive and widely available starting point. A major concern with the final porphyrin was the solubility in chloroform. The final handcuff assembly gives the highest yields when in chloroform and for the reaction to work, all components must fully dissolve. For this reason, a long chain dibromoalkane was selected for the addition reaction with 4-hydroxybenxaldehyde.

4-Hydroxybenzaldehyde, (**23**) 1,12-dibromododecane and potassium carbonate were heated at 85 °C in dimethylformamide (DMF) for 24 h and purification the product was

attempted. Upon ^{1}H NMR spectroscopic analysis, it was found that the reaction had not been successful, and after even several repeats, the reaction consistently gave only starting materials.

It was suspected that the base used was not strong enough to adequately deprotonate the aldehyde and initiate the reaction. The reaction was repeated using the same method but with potassium *tert*-butoxide instead of potassium carbonate (Scheme 4.2). The product was analysed by ^{1}NMR spectroscopy and confirmed to be 4-((12-bromododecyl)oxy)benzaldehyde (**24**). MS-TOF spectroscopic measurements were taken, with the alkyl chain detaching to give a mass of 121.02, corresponding with the $C_7H_5O_2^-$ aryl fragment.

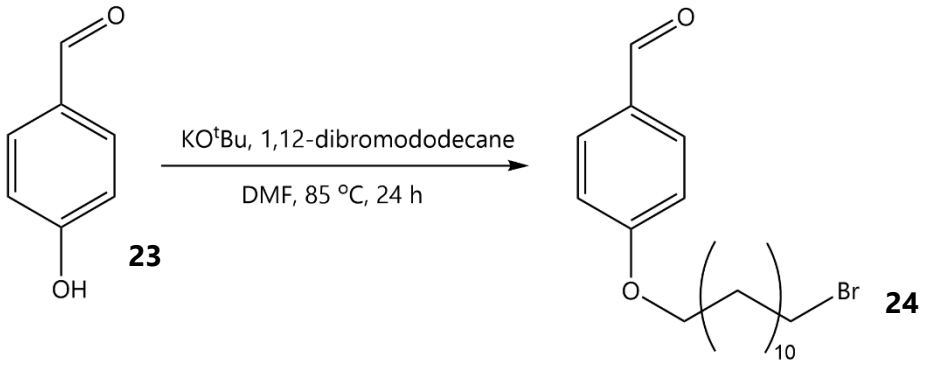

Scheme 4.2. The reaction to form 4-((12-bromododecyl)oxy)benzaldehyde, the precursor the imidazole porphyrin.

The alkylbromoaldehyde was then reacted with imidazole and potassium carbonate in DMF at 85 °C for 24 h. When examined using ^{1}H NMR spectroscopic measurements, it was shown that the reaction had not proceeded and the bromo starting material was still present. It was then decided that as the bromoalkyl aldehyde is suitable for porphyrin synthesis, it would be reacted with pyrrole in acidic conditions to test if the porphyrin formation reaction was feasible and, if successful, the imidazole groups could be added *via* S_N2 reaction, post synthesis.

4-((12-Bromododecyl)oxy)benzaldehyde (**24**) and pyrrole were heated at 150 °C in propanoic acid for 24 h. If the reaction was successful, dark porphyrin crystals should have precipitated out of solution, but this did not occur. This reaction was repeated, and the same result was observed. At this point, it was decided that a new approach was needed.

Macdonald employed a synthetic method that couples dipyrromethanes with aldehydes under acidic conditions at room temperature[173], a generalised version of which can be seen in Scheme 4.3. This method allows both symmetric and asymmetric porphyrins to be synthesised, if one or multiple dipyrromethanes are used. This [2+2] reaction not only allows for greater synthetic flexibility but also eliminates some of the problems associated with the Alder-Longo method.

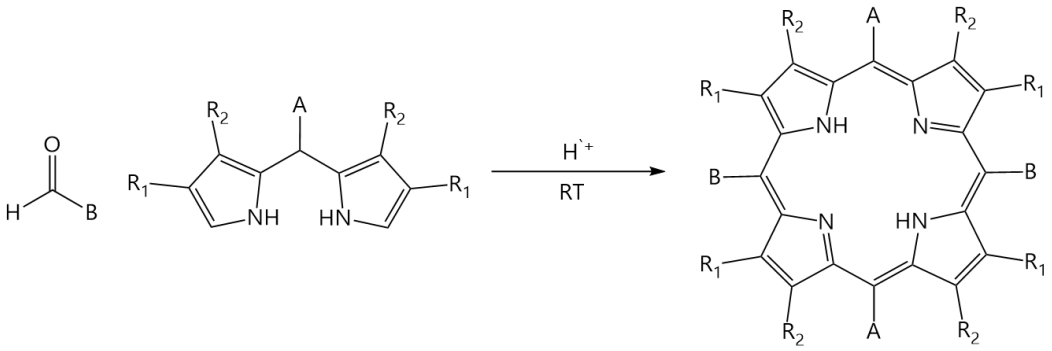

Scheme 4.3. Macdonald [2+2] coupling for porphyrin synthesis.

Methyl 2,2-dipyrroylacetate (**25**) was stirred with bromododecylbenzaldehyde (**23**), trifluoroacetic acid (TFA) and dichlorodicyanobenzoquinone (DDQ) (Scheme 4.4). A red side product was produced and discarded. Dark purple fractions were eluted and combined. The resulting solid was dissolved in a minimum amount of dichloromethane and excess hexane was added to crystalise the final product as a dark purple powder.

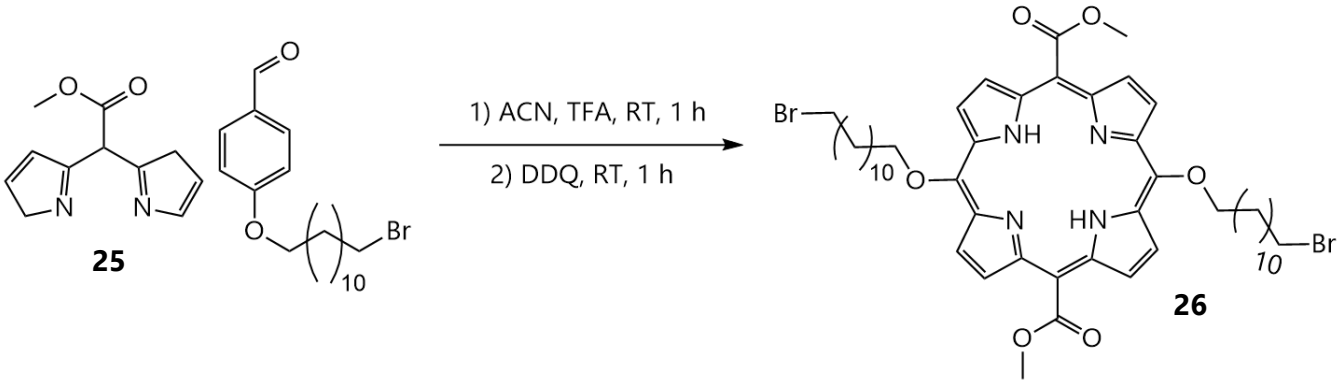

Scheme 4.4. The Macdonald synthesis reaction to form the target porphyrin (**26**).

Upon, ^{1}H NMR spectroscopic analysis, it was found that the porphyrin was most likely formed, but the sample was impure, possibly containing some side products of the reaction. Ideally, the reaction would produce only the desired porphyrin with the pyrrole and aldehyde reacting in a 1:1 ratio. Several side reactions can occur that give polymeric side products, that will have similar ^{1}H NMR spectra and overlap with the desired product.

Peaks at 8.18 (**a**) and 6.38 (**b**) ppm are observed can be assigned to the internal NH and external pyrrole protons, respectively. If the spectra of the aldehyde starting material and the product ^{1}H NMR are overlapped (Figure 4.4), it can be seen that these peaks are newly formed upon reaction. The integration of these peaks is lower than expected, however, confirming that the sample is impure and contains other side-products. The continued presence of the 9.90 ppm (**c**) resonance, consistent with the

aldehyde functionality, also shows that there has been only partial conversion of the aldehyde into the desired porphyrin.

Due to time restrictions, this is where the project was left. Going forward, if this reaction was repeated, a stronger base would be used for the imidazole addition step to ensure deprotonation occurs and the reaction proceeds. In addition, less polar column conditions would be used to ensure a greater product separation, giving just the desired diimidazole porphyrin product.

As pillararene-functionalised NDI has already been synthesised,[128] once a more refined synthesis for the imidazole-porphyrin component has been found, it is expected that the assembly of this structure would take place in a similar manner to that of the rotaxanes described in the previous chapter, self-assembling in cold chloroform and stoppered to give the desired handcuff molecule.

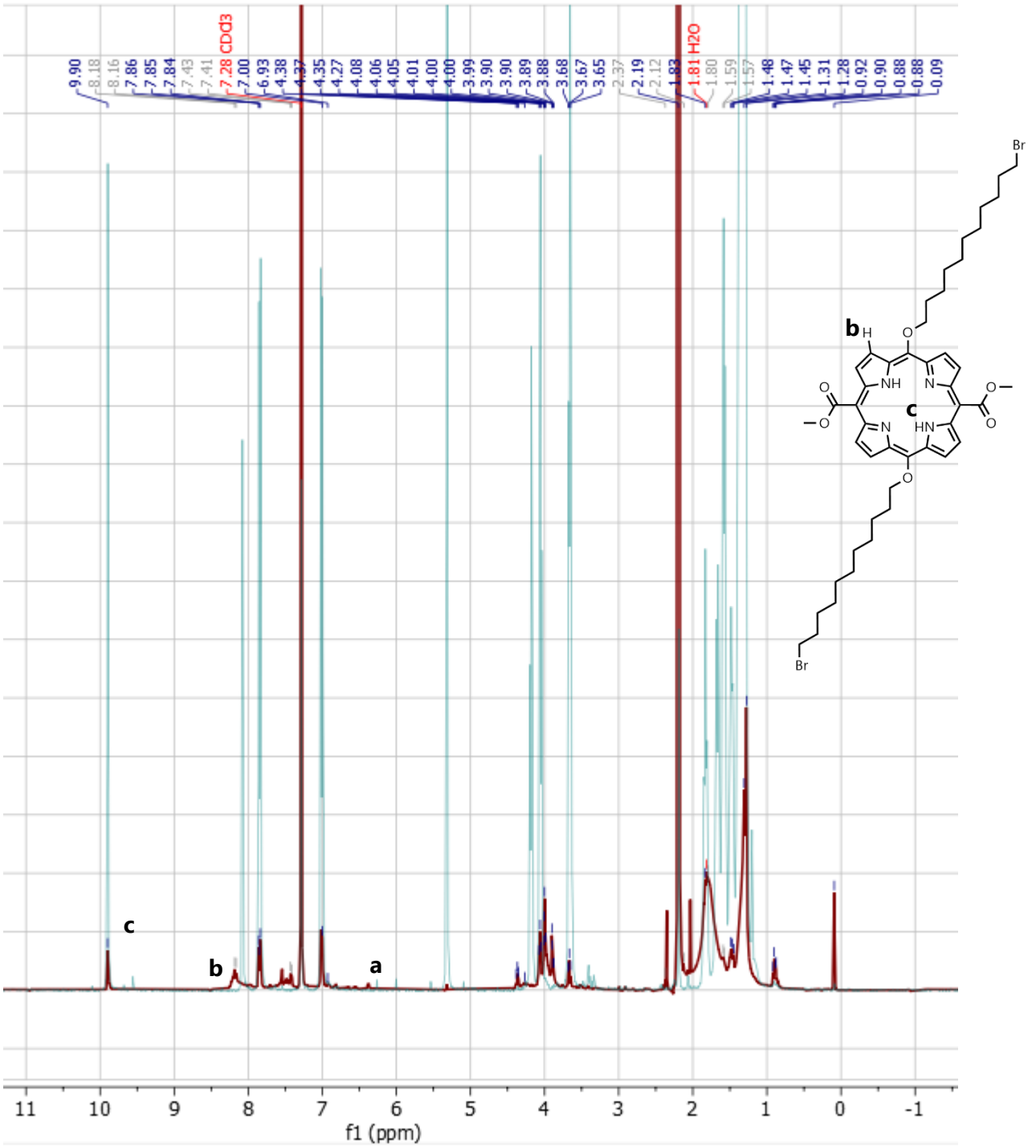

Figure 4.4. The stacked spectra of 4-((12-bromododecyl)oxy)benzaldehyde (**24**) (blue) and the porphyrin product (**26**) (red).

4.4 Conclusions

An impure porphyrinic compound was synthesised from a hydroxybenzaldehyde and a dipyrroylacetate in acidic conditions. This porphyrin was confirmed to have been synthesised using ^{1}H NMR spectroscopic measurements with characteristic peaks present, corresponding to the internal proton environments of the porphyrin.

4.5 Experimental

Synthesis of 4-((12-bromododecyl)oxy)benzaldehyde (**23**)

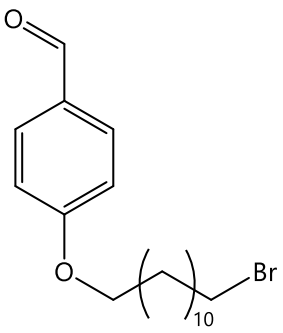

1,12-Dibromododecane (14.76 g, 0.045 mols), 4-hydroxybenzaldehyde (3.00 g, 0.025 mol) and potassium *tert*-butoxide (7.00 g, 0.062 mol) were stirred in dimethylformamide (120 mL) at 85 °C for 24 h. The reaction was cooled, filtered the solvent removed under reduced pressure. The residue was dissolved in dichloromethane, washed with water and brine, and dried with anhydrous magnesium sulfate. The crude product was purified *via* column chromatography (SiO_2, EtOAc/Hexane (1:9)) ^{1}H NMR (400 MHz, Chloroform-d) δ 9.90 (s, 1H), 7.84 (d, *J* = 8.4 Hz, 2H), 7.01 (d, *J* = 8.4 Hz, 2H), 4.18 (t, *J* = 6.7 Hz, 2H), 4.06 (t, *J* = 6.5 Hz, 2H), 1.83 (p, *J* = 6.8 Hz, 2H), 1.68 (dt, *J* = 14.0, 6.5 Hz, 2H), 1.63 – 1.53 (m, 4H), 1.48 (p, *J* = 7.1 Hz, 2H), 1.35 (d, *J* = 8.6 Hz, 10H). ^{13}C NMR (101 MHz, Chloroform-d) δ 190.85, 164.28, 161.24, 132.01, 129.75, 114.76, 68.44, 64.14, 63.09, 53.43, 32.81, 29.59, 29.55, 29.53, 29.47, 29.43, 29.33, 29.17, 29.05, 28.51, 25.96.

5. Conclusions and Future Work

5.1 Conclusions

The novel zinc/NDI nanotubes synthesised in this work were resynthesised reliably, giving identical nanotubular products each time. The UV/visible spectroscopic measurements, and the accompanying visible colour change in the bulk material, illustrated that the nanotubes were electronically active, although the extent and nature of radical formation will require further measurements, for example EPR studies, to be fully explored. The nanotubes were found to be mechanically flexible, which was not predicted initially, and the Raman measurements confirmed that chemical strain is present upon bending. These nanotubes are an exciting material, possessing both the porous nature of a MOF and the tubular structure making both post-synthetic modification and host-guest chemistry promising options for future work.

Although ultimately not having the intended outcome of a MORF framework, in the process, much was learnt about the processes and difficulties of MORF assembly. Although the solubility issues did hinder proceedings, it was ultimately the inability to find a solvent in which both the rotaxane and a metal complex could dissolve into that prevented MORF formation. This may be able to be counteracted with some kind of modification of the pillar[5]arene component. In spite of this, a crystal structure was obtained as a result of the MORF synthesis attempts that not only shows the complete solid-state structure of the rotaxane but also exhibited hydrogen bonding that effected the macrocycle position, something which is uncommon in rotaxane architectures. The work on alternative stopper groups, although also ultimately unsuccessful, did show that the rod formation reaction can still be performed using different constituents, showing the flexibility of the 'toolbox' approach.

The synthesis of the NDI/porphyrin handcuff molecule remains unfinished, in large part to time constraints; however, an impure porphyrin rod component was synthesised and confirmed by ^{1}H NMR spectroscopic measurement. As the NDI macrocyclic component for the handcuff molecule has already been previously

synthesised in the group, once the porphyrin has been synthesised and purified, it is reasonable to suggest that the handcuff would be relatively easy to obtain. Once this handcuff molecule is obtained, it can be compared to the NDI/porphyrin MOF previously synthesised.

5.2 Future Work

More work is needed to fully characterise the compounds synthesised in this work. Although the techniques used sufficiently identify the compounds discussed, elemental analysis, functional group analysis (IR, UV etc.), and more comprehensive NMR spectroscopic analysis is required for completeness of results.

NDI-MOF nanotubes, which can form an NDI radical once irradiated by UV light, allow for a 'switchable' structure with two modes and, due to the relaxation of the structure and the ability to repeat the irradiation and relaxation steps, and the visible colour change observed upon irradiation, the bulk material can be used as binary UV/visible radiation sensor.

The helical nature of the structure initially invites comparisons with DNA but, due to the lack of hydrogen bonding present in the MOF nanotubes, the nanotubes are more like CNTs. Due to the presence of a central cavity in the nanotubes, it may be possible to add a guest molecule to the nanotube cavity. This gives access to a multitude of host-guest chemistry or sterically controlled reactions such as catalysis, assuming suitable conditions and reagents can be found. The ~100 $Å^2$ two-dimensional area of the nanotube inner cavity, as well as the very long length of the tubes, allows small to medium molecules to fit into the channel and allow reactions to take place inside.

As previously stated, the NDI nanotubes are more like CNTs rather than organic helices. This introduces the idea of reactions taking place inside the cavity and on the outside surface the nanotube. CNTs have been previously used to facilitate polymerisation on their surface[174] and given the presence of the NDI radical and the long cavity present in the nanotubes, this in theory, has all the right conditions for size-selective chain polymerisation (Scheme 5.1). Small monomers will enter the nanotube with radical polymerisation initiated by the NDI radical present and then the long-chain polymer 'extruded' out the other end of the nanotube. This allows for straighter, regular chains to be produced due the steric hinderance of the polymer forming inside the nanotube.

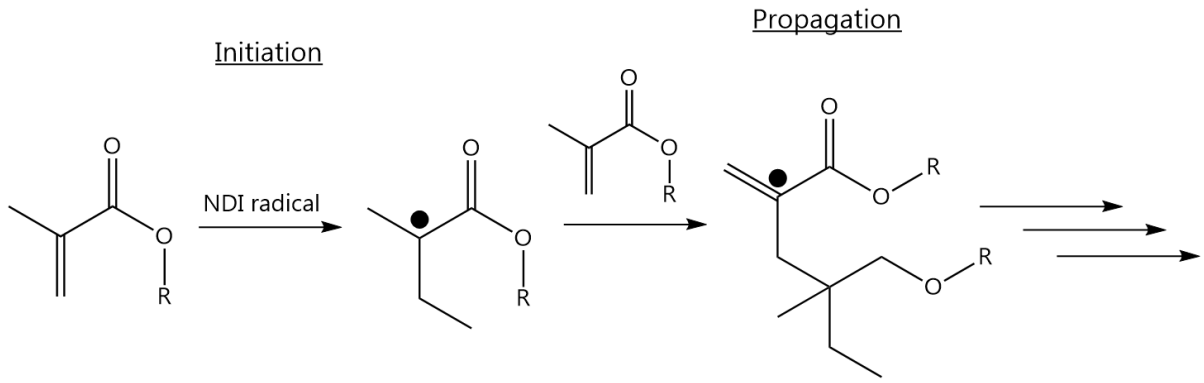

Scheme 5.1 A generalised proposed mechanism for radical polymerisation in the Zn/NDI MOF nanotubes

The tetracid rotaxanes had an issue of solubility, which greatly limited the viability is MORF synthesis. Post synthetic modifications could be performed, adding polar organic substituents such as hydroxyl groups or charged nitrogen functionalities to the pillararene macrocycle (Scheme 5.2).

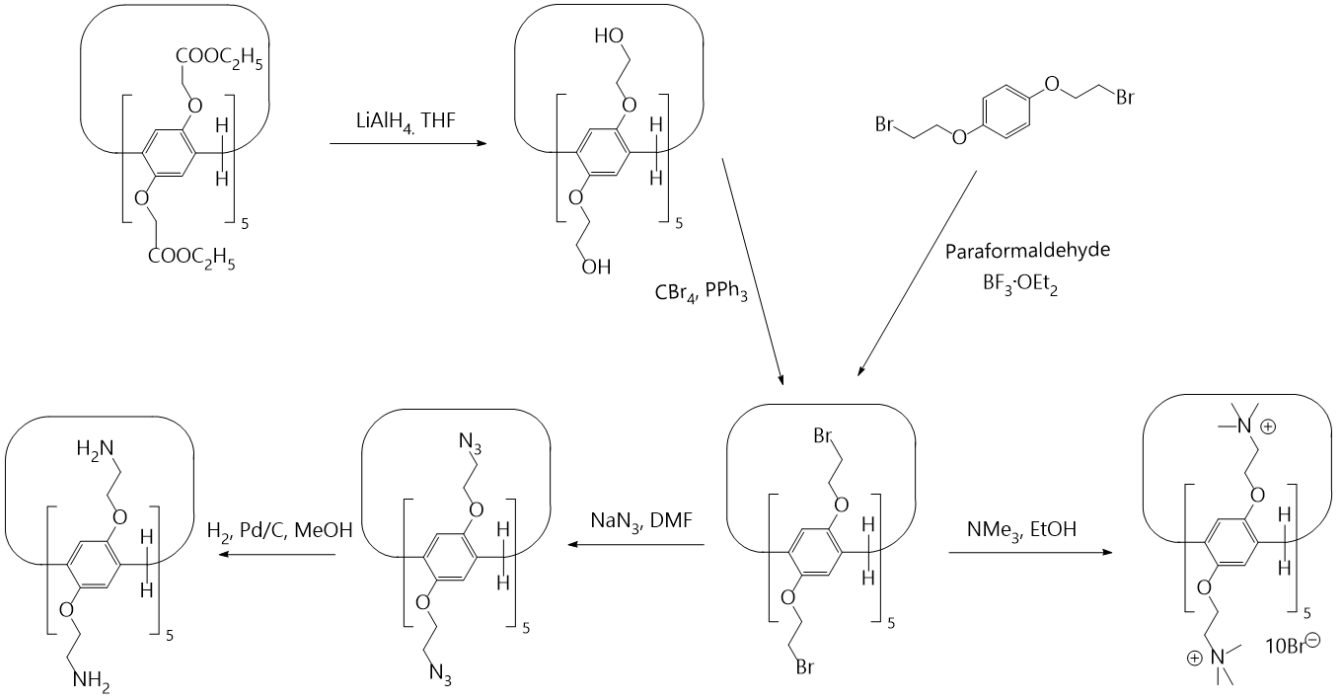

Scheme 5.2 A scheme showing possible post synthetic modifications that can be performed on the pillar[5]arene macrocycle.

Finally, the NDI/porphyrin [2]handcuff rotaxane, described in Chapter 4, requires more work to synthesise successfully. If successful, the Macdonald method of porphyrin synthesis would be used to assemble the final imidazole-functionalised porphyrin. Once the [2]handcuff rotaxane is obtained, the interactions between the NDI and porphyrin groups could be probed *via* cyclic voltammetry. This would allow the comparison between the MOF structure detailed in Chapter 4 and the handcuff molecules. The interactions between the NDI and porphyrin groups could be studied, probing the differences between the structures with one being in a rigid, uniform structure and the other 'free' structure held together by the intermolecular interactions. Catalytic NDI/porphyrin MOF systems have been reported in literature, with an example of an MOF in work by Xu *et al.*[175], in which the photosensitized oxidative coupling of benzylamine is catalysed inside the MOF with the porphyrin acting as an electron donor and the NDI an acceptor to generate superoxide radicals and singlet oxygen.

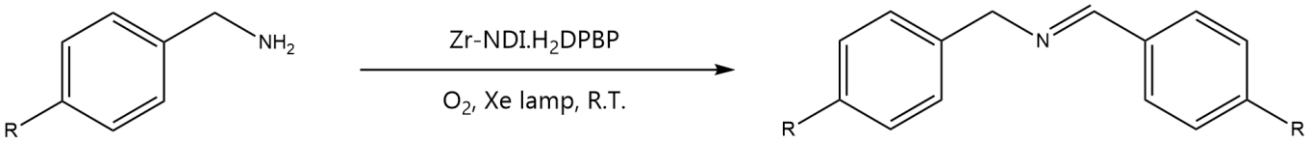

Scheme 5.3 The general oxidative coupling reaction in published work by Xu *et al.*[175]

The previous MOF architecture synthesised in the group is very similar in composition to that used in the literature and it would be reasonable to expect similar catalytic behaviour. The handcuff molecule, having the same NDI/porphyrin functionalities, could also be able to catalyse radical coupling reactions, and if both are successful, the contrast between a rigid MOF system and a flexible handcuff system would be interesting to study.

6. References

1 J. -M Lehn, *Angew. Chem. Int. Ed. Engl.*, 1988, **27**, 89–112.
2 C. J. Pedersen, *Org. Synth.*, 1972, **52**, 66.
3 C. J. Pedersen, *J. Am. Chem. Soc.*, 1970, **92**, 386–391.
4 D. E. Koshland, *Angew. Chem. Int. Ed. Engl.*, 1995, **33**, 2375–2378.
5 F. Yan, Z. Hao, *Nature*, 2017, **552**, 34–35.
6 P. A. Monnard, D. W. Deamer, *The Minimal Cell: The Biophysics of Cell Compartment, the Origin of Cell Functionality*, 2011, **207**, 123–151.
7 A. Pohorille, D. Deamer, *Res. Microbiol.*, 2009, **160**, 449–456.
8 G. Kim, C. Piao, J. Oh, M. Lee, *Nanoscale*, 2018, **10**, 8503–8514.
9 F. Wang, J. Tang, H. Liu, G. Yu, Y. Zou, *Mater. Chem. Front.*, 2019, **3**, 356–364.
10 L. F. Lindoy, K.-M. Park, S. Sung Lee, *Supramolecular Chemistry: From Molecules to Nanomaterials,* 2012.
11 D. J. Cram, K. Takahiro, R. C. Helgeson, G. M. Lein, *J. Am. Chem. Soc.*, 1979, **101**, 6752–6754.
12 K. E. Krakowiak, J. S. Bradshaw, *Isr. J. Chem.*, 1992, **32**, 3–13.
13 D. Landini, A. Maia, F. Montanari, P. Tundo, *J. Am. Chem. Soc.*, 1979, **101**, 2526–2530.
14 C. D. Gutsche, B. Dhawan, K. H. No, R. Muthukrishnan, *J. Am. Chem. Soc.*, 1981, **103**, 3782–3792.
15 J.-M. Lehn, A. Rigault, J. Siegel, J. Harrowfield, B. Chevriert, D. Morast, *Chemistry,* 1987, **84**, 2565–2569.
16 K. S. Chichak, S. J. Cantrill, A. R. Pease, S.-H. Chiu, G. W. V. Cave, J. L. Atwood, J. F. Stoddart, *Science,* 2004, **304**, 1308–1312.
17 Y. R. Lee, J. Kim, W. S. Ahn, *Kor. J. Chem. Eng.*, 2013, **30**, 1667–1680.
18 B. Zhang, Y. Luo, K. Kanyuck, N. Saenz, K. Reed, P. Zavalij, J. Mowery, G. Bauchan, *RSC Adv.*, 2018, **8**, 33059–33064.
19 P. Pachfule, R. Das, P. Poddar, R. Banerjee, *Cryst. Growth De.s*, 2011, **11**, 1215–1222.
20 J. Cravillon, S. Münzer, S. J. Lohmeier, A. Feldhoff, K. Huber, M. Wiebcke, *Chem. Mater.*, 2009, **21**, 1410–1412.
21 L. Huang, H. Wang, J. Chen, Z. Wang, J. Sun, D. Zhao, Y. Yan, *Micro. Meso. Mat.*, 2003, **58**, 2, 105-114.
22 N. Stock, S. Biswas, *Chem. Rev.*, 2012, **112**, 933–969.
23 Z. Ni, R. I. Masel, *J. Am. Chem. Soc.*, 2006, **128**, 12394–12395.
24 A. L. Garay, A. Pichon, S. L. James, *Chem. Soc. Rev.*, 2007, **36**, 846–855.
25 R. Zhang, W. Fei, *Nano. Superfiber Mat.,* 2014, 87-136.
26 A. Kolanowska, A. W. Kuziel, R. G. Jędrysiak, M. Krzywiecki, E. Korczeniewski, M. Wiśniewski, A. P. Terzyk, S. Boncel, *Nanomaterials,* 2019**, 9(11)**, 1619.
27 S. A. Miners, G. A. Rance, A. N. Khlobystov, *Chem. Soc. Rev.*, 2016, **45**, 4727–4746.
28 V. N. Khabashesku, M. X. Pulikkathara, *Mendeleev Commun.*, 2006, **16**, 61–66.
29 D. M. Sanders, A. Anders, *Surf. Coat. Tech.*, 2000, **133-134**, 78-90
30 S. Iijima, *Nature*, 1991, **354**, 56–58.

31 S. Iijima, T. Ichihashi, *Nature*, 1993, **363**, 603–605.
32 S. Itoh, S. Ihara, J.-I. Kitakami, *Phys. Rev. B,* 1993, **47**, 1703(R)
33 S. Amelinckx, X. B. Zhang, D. Bernaerts, X. F. Zhang, V. Ivanov, J. B. Nagy, *Proc. Natl. Acad. Sci. U.S.A*, 1994, **265**, 635–639.
34 N. Tang, J. Wen, Y. Zhang, F. Liu, K. Lin, Y. Du, *ACS Nano.*, 2010, **4**, 241–250.
35 M. D. Halls, H. B. Schlegel, *J. Phys. Chem. B*, 2002, **106**, 1921–1925.
36 M. Monthioux, *Carbon*, 2002, **40**, 10, 1809-1823.
37 L. Afchangi, M. Fazli, *Biointerface Res. Appl. Chem*, 2022, **12**, 6589–6607.
38 J. W. Jordan, A. I. Chernov, G. A. Rance, E. Stephen Davies, A. E. Lanterna, J. Alves Fernandes, A. Grüneis, Q. Ramasse, G. N. Newton, A. N. Khlobystov, *J. Am. Chem. Soc.*, 2023, **145**, 1206–1215.
39 B. Behnam, W. T. Shier, A. H. Nia, K. Abnous, M. Ramezani, *Int. J. Pharm.*, 2013, **454**, 204–215.
40 M. S. Ata, R. Poon, A. M. Syed, J. Milne, I. Zhitomirsky, *Carbon N Y*, 2018, **130**, 584–598.
41 F. G. Pacheco, A. A. C. Cotta, H. F. Gorgulho, A. P. Santos, W. A. A. Macedo, C. A. Furtado, *Appl. Surf. Sci.*, 2015, **357**, 1015–1023.
42 Y. Yang, Y. Chen, F. Leng, L. Huang, Z. Wang, W. Tian, *Appl. Sci.*, 2017, **7(12)**, 1215
43 V. Mittal, *Carbon Nanotubes Surface Modifications: An Overview*, Wiley-VCH, 2011.
44 C. Shamshoom, D. Fong, K. Li, V. Kardelis, A. Adronov, *ACS Omega*, 2018, **3**, 13935–13943.
45 R. Dubey, D. Dutta, A. Sarkar, P. Chattopadhyay, *Nanoscale Adv.*, 2021, **3**, 5722–5744.
46 S. Mallakpour, S. Soltanian, *RSC Adv.*, 2016, **6**, 109916–109935.
47 L. Afchangi, M. Fazli, *Biointerface Res. Appl. Chem.*, 2022, **12**, 6589–6607.
48 G. Biddeci, G. Spinelli, P. Colomba, F. Di Blasi, *Int. J. Mol. Sci.*, 2022, 23.
49 C. R. Murdock, D. M. Jenkins, *J. Am. Chem. Soc.*, 2014, **136**, 10983–10988.
50 L. Zou, C. C. Hou, Z. Liu, H. Pang, Q. Xu, *J. Am. Chem. Soc.*, 2018, **140**, 15393–15401.
51 H. L. Frisch, E. Wasserman, *J. Am. Chem. Soc.*, 1961, **83**, 3789–3795.
52 G. Schill, A. Lüttringhaus, *Angew. Chem. Int. Ed.*, 1964, **3**, 546–547.
53 H. L. Frisch, E. Wasserman, *J. Am. Chem. Soc.*, 1961, **20**, 3789–3795.
54 I. T. Harrison, S. Harrison, *J. Am. Chem. Soc.*, 1967, **89**, 5723–5724.
55 R. B. Merrifield., *J. Am. Chem. Soc.*, 1963, **85**, 2149–2154.
56 R. Jimenez, C. Martin, P. Lopez-Cornejo, *J. Phys. Chem. B*, 2008, **112**, 11610–11615.
57 A. H. G. David, P. García-Cerezo, A. G. Campaña, F. Santoyo-González, V. Blanco, *Chem. Eur. J.*, 2019, **25**, 6170–6179.
58 Y. Furusho, H. Sasabe, D. Natsui, K. Murakawa, T. Takata, T. Harada, *Bull. Chem. Soc. Jpn.*, 2004, **77**, 179–185.
59 T. Takata, N. Kihara, H. Kawasaki, *Bull. Chem. Soc. Japan.*, 1999, **28**, 1015–1016.
60 M. Asakawa, P. R. Ashton, R. Ballardini, V. Balzani, M. Bělohradský, M. T. Gandolfi, O. Kocian, L. Prodi, F. M. Raymo, J. F. Stoddart, M. Venturi, *J. Am. Chem. Soc.*, 1997, **119**, 302–310.
61 P. R. Ashton, R. Ballardini, V. Balzani, M. Bělohradskybělohradsky, M. T. Gandolfi, D. Philp, L. Prodi, F. M. Raymo, M. V Reddington, N. Spencer, J. F. Stoddart, M. Venturi, D. J. Williams, *J. Am. Chem. Soc.* 1996, **118,** 21, 4931–4951.

62 D. B. Amabilino, P. R. Ashton, M. Belohradsky, F. M . Raymo, J. F. Stoddart, *J. Chem. Soc., Chem. Commun.*, 1995, 751-753
63 P. R. Ashton, M. Belohradsky, D. Philp, J. F. Stoddart, *J. Chem. Soc., Chem. Commun.,* 1993, 1269-1274
64 P. R. Ashton, M. Belohradsky, D. Philp, N. Spencer, J. F. Stoddart, *J. Chem. Soc.,* Chem. Commun., 1993, 1274-1277
65 P. L. Anelli, N. Spencer, J. Fraser Stoddart, *J. Am. Chem. Soc.*, 1991, **113**, 5131–5133.
66 J. Yin, S. Dasgupta, J. Wu, *Org. Lett.*, 2010, **12**, 1712–1715.
67 Y. W. Wu, P. N. Chen, C. F. Chang, C. C. Lai, S. H. Chiu, *Org Lett*, 2015, **17**, 2158–2161.
68 J. Yin, S. Dasgupta, J. Wu, *Org. Lett.*, 2010, **12**, 1712–1715.
69 V. Aucagne, K. D. Hänni, D. A. Leigh, P. J. Lusby, D. B. Walker, *J. Am. Chem. Soc.*, 2006, **128**, 2186–2187.
70 J. D. Crowley, K. D. Hänni, A. L. Lee, D. A. Leigh, *J. Am. Chem. Soc.*, 2007, **129**, 12092–12093.
71 V. Aucagne, J. Berná, J. D. Crowley, S. M. Goldup, K. D. Hänni, D. A. Leigh, P. J. Lusby, V. E. Ronaldson, A. M. Z. Slawin, A. Viterisi, D. B. Walker, *J. Am. Chem. Soc.*, 2007, **129**, 11950–11963.
72 N. Song, Y. W. Yang, *Sci. China. Chem.*, 2014, **57**, 1185–1198.
73 T. Ogoshi, S. Kanai, S. Fujinami, T. A. Yamagishi, Y. Nakamoto, *J. Am. Chem. Soc.*, 2008, **130**, 5022–5023.
74 T. F. Al-Azemi, M. Vinodh, F. H. Alipour, A. A. Mohamod, *Org. Chem. Front.*, 2019, **6**, 603–610.
75 M.-X. Wu, Y.-W. Yang, *Polym. Chem.,* 2019, **10**, 2980-2985.
76 Z. Zhang, G. Yu, C. Han, J. Liu, X. Ding, Y. Yu, F. Huang, *Org Lett*, 2011, **13**, 4818–4821.
77 Z. Zhang, Y. Luo, J. Chen, S. Dong, Y. Yu, Z. Ma, F. Huang, *Angew. Chem. Int. Ed.*, 2011, **50**, 1397–1401.
78 Z. Zhang, B. Xia, C. Han, Y. Yu, F. Huang, *Org Lett*, 2010, **12**, 3285–3287.
79 X. B. Hu, L. Chen, W. Si, Y. Yu, J. L. Hou, *Chem. Comm.*, 2011, **47**, 4694–4696.
80 Y. Ma, X. Ji, F. Xiang, X. Chi, C. Han, J. He, Z. Abliz, W. Chen, F. Huang, *Chem. Comm.*, 2011, **47**, 12340–12342.
81 T. Ogoshi, M. Hashizume, T. A. Yamagishi, Y. Nakamoto, *Chem. Comm.*, 2010, **46**, 3708–3710.
82 T. Ogoshi, K. Umeda, T. A. Yamagishi, Y. Nakamoto, *Chem. Comm.*, 2009, 4874–4876.
83 S. Dong, J. Yuan, F. Huang, *Chem. Sci.*, 2014, **5**, 247–252.
84 N. Farahani, K. Zhu, C. A. O. Keefe, R. W. Schurko, S. J. Loeb, *Nat. Chem.*, 2016, 1–7.
85 P. Langer, L. Yang, C. R. Pfeiffer, W. Lewis, N. R. Champness, *Dalton Trans.*, 2019, **48**, 58–64.
86 M. Pan, M. Xue, *Chin. J. Chem.*, 2014, **32**, 128–132.
87 S. Dong, J. Yuan, F. Huang, *Chem. Sci*, 2014, **5**, 247–252.
88 V. Nesterov, D. Reiter, P. Bag, P. Frisch, R. Holzner, A. Porzelt, S. Inoue, *Chem. Rev.*, 2018, **118**, 9678–9842.
89 J. F. Stoddart, *Angew. Chem. Int. Ed.*, 2017, **56**, 11094–11125.
90 N. Zhu, K. Nakazono, T. Takata, *Chem. Lett.*, 2016, **45**, 445–447.

91 K. Zhu, C. A. O. Keefe, V. N. Vukotic, R. W. Schurko, S. J. Loeb, *Nature Chem.*, 2015, **7**, 514–519.
92 V. Balzani, A. Credi, F. M. Raymo, J. F. Stoddart, *Chem. Soc. Rev.*, 2009, **38**, 1542-1550.
93 L. Ceze, J. Nivala, K. Strauss, *Nat. Rev. Genet.*, 2019, **20**, 456–466.
94 H. H. Lee, R. Kalhor, N. Goela, J. Bolot, G. M. Church, *Nature Commun.,* 2019*,* **10**, 2383
95 F. Akram, I. ul Haq, H. Ali, A. T. Laghari, *Mol Biol Rep*, 2018, 45, 1479–1490.
96 D. B. Amabilino, P. R. Ashton, V. Balzani, C. L. Brown, A. Credi, J. M. J. Fréchet, J. W. Leon, F. M. Raymo, N. Spencer, J. F. Stoddart, M. Venturi, *J. Am. Chem. Soc.* 1996, **118**, 48, 12012–12020.
97 H.-C. Zhou, S. Kitagawa, *Chem. Soc. Rev.*, 2014, **43**, 5415–5418.
98 T. Gadzikwa, O. K. Farha, K. L. Mulfort, J. T. Hupp, S. T. Nguyen, *Chem. Comm.*, 2009, 3720–3722.
99 Z. Zhou, X. Xing, C. Tian, W. Wei, D. Li, F. Hu, S. Du, *Sci. Rep.,* 2018, **8**, 3117
100 M. J. Kalmutzki, N. Hanikel, O. M. Yaghi, *Science* Adv., 2018, **4**, 1-16.
101 A. Schoedel, M. Li, D. Li, M. O'Keeffe, O. M. Yaghi, *Chem. Rev.*, 2016, **116**, 12466–12535.
102 P. Z. Moghadam, A. Li, S. B. Wiggin, A. Tao, A. G. P. Maloney, P. A. Wood, S. C. Ward, D. Fairen-Jimenez, *Chem. Mat.*, 2017, **29**, 2618–2625.
103 V. N. Vukotic, S. J. Loeb, *Chem. Eur. J.*, 2010, **16**, 13630–13637.
104 V. N. Vukotic, K. J. Harris, K. Zhu, R. W. Schurko, S. J. Loeb, *Nat. Chem.*, 2012, **4**, 456–460.
105 A. Coskun, M. Hmadeh, G. Barin, F. Gándara, Q. Li, E. Choi, N. L. Strutt, D. B. Cordes, A. M. Z. Slawin, J. F. Stoddart, J.-P. Sauvage, O. M. Yaghi, *Angew. Chem.*, 2012, **124**, 2202–2205.
106 X. S. Wu, J. Liang, X. L. Hu, X. L. Wang, B. Q. Song, Y. Q. Jiao, Z. M. Su, *Cryst. Growth Des.*, 2015, **15**, 4311–4317.
107 H. J. Pang, J. Peng, C. J. Zhang, Y. G. Li, P. P. Zhang, H. Y. Ma, Z. M. Su, *Chem. Comm.*, 2010, **46**, 5097–5099.
108 L. K. Knight, V. N. Vukotic, E. Viljoen, C. B. Caputo, S. J. Loeb, *Chem. Comm.*, 2009, 5585–5587.
109 H. Y. Gong, B. M. Rambo, W. Cho, V. M. Lynch, M. Oh, J. L. Sessler, *Chem. Comm.*, 2011, **47**, 5973–5975.
110 T. Xia, Z. Y. Yu, H. Y. Gong, *Molecules,* 2021, **26**(14), 4241.
111 J. S. Geng, L. Mei, Y. Liang, L. Yuan, J. Yu, K. Hu, L. Yuan, W. Feng, Z. Chai, W. Shi, *Nat Comm.,* 2022, **13**, 2030.
112 S. J. Loeb, *Chem. Commun.*, 2005, 1511–1518.
113 H. Y. Gong, B. M. Rambo, E. Karnas, V. M. Lynch, J. L. Sessler, *Nature Chem*, 2010, **2**, 406–409.
114 Y. N. Gong, D. C. Zhong, T. B. Lu, *CrystEngComm*, 2016, **18**, 2596–2606.
115 G. Gholami, K. Zhu, J. S. Ward, P. E. Kruger, S. J. Loeb, *Eur. J. Inorg. Chem.*, 2016, **2016**, 4524–4529.
116 K. Zhu, V. N. Vukotic, C. A. Okeefe, R. W. Schurko, S. J. Loeb, *J. Am. Chem. Soc.*, 2014, **136**, 7403–7409.

117 N. Miyaura, K. Yamada, A. Suzuki, *Tetrahedron Letters*, 1979, **20**, 36, 3437-3440
118 R. Ciao, C. Talotta, C. Gaeta, L. Margarucci, A. Casapullo, P. Neri, *Org. Lett.*, 2013, **15**, 5694–5697.
119 A. Bogdan, Y. Rudzevich, M. O. Vysotsky, V. Böhmer, *Chem. Comm.*, 2006, 2941–2952.
120 C. Gaeta, M. O. Vysotsky, A. Bogdan, V. Böhmer, *J. Am. Chem. Soc.*, 2005, **127**, 13136–13137.
121 A. Goujon, T. Lang, G. Mariani, E. Moulin, G. Fuks, J. Raya, E. Buhler, N. Giuseppone, *J. Am. Chem. Soc.*, 2017, **139**, 14825–14828.
122 Z.-T. Li, P. C. Stein, J. Becher, D. Jensen, P. Mark, N. Svenstrup, *Chem. Eur. J*, 1996, **2**, 624–633.
123 T. Sato, T. Takata, *Tetrahedron Lett.*, 2007, **48**, 2797–2801.
124 H. Iwamoto, Y. Yawata, Y. Fukazawa, T. Haino, *Chem. Lett.*, 2010, **39**, 24–25.
125 Y. Yamada, R. Itoh, S. Ogino, T. Kato, K. Tanaka, *Angew. Chem. Int. Ed.*, 2017, **56**, 14124–14129.
126 Z. Meng, Y. Han, L. N. Wang, J. F. Xiang, S. G. He, C. F. Chen, *J. Am. Chem. Soc.*, 2015, **137**, 9739–9745.
127 V. Balzani, M. Clemente-León, A. Credi, J. N. Lowe, J. D. Badjić, J. F. Stoddart, D. J. Williams, *Chem. Eur. J.*, 2003, **9**, 5348–5360.
128 N. Pearce, M. Tarnowska, N. J. Andersen, A. Wahrhaftig-Lewis, B. S. Pilgrim, N. R. Champness, *Chem. Sci.,* 2022, **13**, 3915-3941.
129 L. Yang, P. Langer, E. S. Davies, M. Baldoni, K. Wickham, N. A. Besley, E. Besley, N. R. Champness, *Chem. Sci.*, 2019, **10**, 3723–3732.
130 S. V Bhosale, H. Jani, S. J. Langford, *Chem. Soc. Rev.*, 2008, **37**, 331–342.
131 M. Al Kobaisi, S. V. Bhosale, K. Latham, A. M. Raynor, S. V. Bhosale, *Chem. Rev.*, 2016, **116**, 11685–11796.
132 S. Lee, F. Miao, H. Phan, S. Herng, J. Ding, J. Wu, *ChemPhysChem*, 2017, 591–595.
133 S. Kumar, P. Mukhopadhyay, *Green Chem.*, 2018, **20**, 4620–4628.
134 H. E. Katz, J. Johnson, C. Kloc, T. Siegrist, W. Li, Y.-Y. Lin, *Nature*, 2000, **404**, 478–480.
135 H. Tanaka, R. Arima, M. Fukumori, D. Tanaka, R. Negishi, Y. Kobayashi, S. Kasai, T. K. Yamada, T. Ogawa, *Sci. Rep.,* 2015, **5**, 12341.
136 J. Wen, C. Xiao, A. Lu, H. Hayashi, L. Zhang, *Chem. Commun.*, 2018, 5542–5545.
137 B. A. Jones, A. Facchetti, M. R. Wasielewski, T. J. Marks, *J. Am. Chem. Soc*, 2007, **56**, 15259–15278.
138 F. N. Castellano, *Dalton*, 2012, **41**, 8493–8501.
139 Z. Liu, G. Zhang, Z. Cai, X. Chen, H. Luo, Y. Li, J. Wang, D. Zhang, *Adv. Mater.*, 2014, **26**, 6965–6977.
140 S. Tang, X. Lv, D. Liu, Z. Li, S. Li, G. Chen, L. Kang, D. Liang, R. Jin, *J. Taiwan Inst. Chem. Eng.*, 2017, **76**, 35–43.
141 J. R. Mulder, C. F. Guerra, J. C. Slootweg, K. Lammertsma, F. M. Bickelhaupt, *J. Comp. Chem.*, 2016, **37**, 304–313.
142 R. Bhosale, R. S. K. Kishore, V. Ravikumar, O. Kel, E. Vauthey, N. Sakai, S. Matile, *Chem. Sci.*, 2010, **1**, 357–368.

143 N. Sakai, R. Bhosale, D. Emery, J. Mareda, S. Matile, *J. Am. Chem. Soc.*, 2010, **132**, 69236925.
144 G. Sforazzini, R. Turdean, N. Sakai, S. Matile, *Chem. Sci.*, 2013, **4**, 1847–1851.
145 Q. Song, F. Li, Z. Wang, X. Zhang, *Chem. Sci.*, 2015, **6**, 3342–3346.
146 C. Bergquist, G. Parkin, N. York, N. York, R. V April, E. I. Chem, 1999, **577**, 6322–6323.
147 N. L. Marana, S. Casassa, E. Longo, J. R. Sambrano, *J. Phys. Chem. C*, 2016, **120**, 12, 6814–6823.
148 F. Yang, M. Wang, D. Zhang, J. Yang, M. Zheng, Y. Li, *Chem. Rev.*, 2020, **120**, 2693–2758.
149 V. I. Artyukhov, E. S. Penev, B. I. Yakobson, *Nat. Commun.*, 2014, **5**, 4892
150 D. Winogradoff, P. Y. Li, H. Joshi, L. Quednau, C. Maffeo, A. Aksimentiev, *Adv. Sci.*, 2021, **8**, 1-15.
151 O. V Dolomanov, L. J. Bourhis, R. J. Gildea, J. A. K. Howard, H. Puschmann, *J. Appl. Cryst.* 2009, **42**, 2009.
152 A. L. Spek, *J. Appl. Cryst.*, 2003, **36**, 7–13.
153 L. Zou, C.-C. Hou, Z. Liu, H. Pang, Q. Xu, *J. Am. Chem. Soc.*, 2018, **140**, 15393–15401.
154 B. Xu, N. Mao, Y. Zhao, L. Tong, J. Zhang, *J. Phys. Chem. Lett.*, 2021, **12**, 7442–7452.
155 N. Kumari, S. Naqvi, M. Ahuja, K. Bhardwaj, R. Kumar, *J. Mat. Sci*, 2020, **31**, 4310–4322.
156 B. Q. Ma, K. L. Mulfort, J. T. Hupp, *Inorg. Chem.*, 2005, **44**, 4912–4914.
157 S. Yuan, J. S. Qin, L. Zou, Y. P. Chen, X. Wang, Q. Zhang, H. C. Zhou, *J. Am. Chem. Soc.*, 2016, **138**, 6636–6642.
158 N. Sikdar, K. Jayaramulu, V. Kiran, K. V. Rao, S. Sampath, S. J. George, T. K. Maji, *Chem. Eur. J.*, 2015, **21**, 11701–11706.
159 B. Y. W. Fuller, *J. Phys. Chem.*, 1959, **63**, 1705–1717.
160 E. Haak, H. Hopf, U. Jahn*, Angew. Chem. Intl.*, 2006, **45**, 6, 855-857
161 K. Bowden, M. Heilbron, E. R. H. Jones, D. C. L. Weedon, *J. Chem. Soc.*, 1946, 39–45.
162 M. Di Antonio, F. Doria, M. Mella, D. Merli, A. Profumo, M. Freccero, *J. Org. Chem.*, 2007, **72**, 8354–8360.
163 S. V. Bhosale, C. H. Jani, S. J. Langford, *Chem. Soc. Rev.*, 2008, **37**, 331–342.
164 G. Andric, J. F. Boas, A. M. Bond, G. D. Fallon, K. P. Ghiggino, C. F. Hogan, J. A. Hutchison, M. A. P. Lee, S. J. Langford, J. R. Pilbrow, G. J. Troup, C. P. Woodward, *Aus. J. Chem.,* 2004, **57**, 1011–1019.
165 N. Pearce, K. E. A. Reynolds, S. Kayal, X. Z. Sun, E. S. Davies, F. Malagreca, C. J. Schürmann, S. Ito, A. Yamano, S. P. Argent, M. W. George, N. R. Champness, *Nat. Comm.*., 2022, **13**, 415.
166 B. Lü, Y. Chen, P. Li, B. Wang, K. Müllen, M. Yin, Nat Commun., 2019, **10**, 767.
167 Y. Zhou, L. Han, *Coord Chem. Rev.*, 2021, **430**, 213665.
168 J. Shukla, P. Mukhopadhyay, *Eur. J. Org. Chem.*, 2019, **2019**, 7770–7786.
169 R. S. K. Kishore, V. Ravikumar, G. Bernardinelli, N. Sakai, S. Matile, *Journal of Organic Chemistry*, 2008, **73**, 738–740.
170 J. S. Lindsay, *Acc. Chem. Res.* 2010, **43**, 2, 300–311.
171 P. Rothemund, A. R. Menotti, *J. Am. Chem. Soc*. 1941, **63**, 1, 267–270
172 B. D. Alan Adler, F. R. Longo, W. Shergalis, *J. Am. Chem. Soc.* 1964, **86**, 15, 3145–3149.

173 J. S. Lindsey, I. C. Schreiman, H. C. Hsu, P. C. Kearney, A. M. Marguerettaz, *J. Org. Chem.* 1987, **52**, 5, 827–836.

174 Z. Yao, N. Braidy, G. A. Botton, and A. Adronov, *J. Am. Chem. Soc.*, 2003, **125(51)**, 16015-16024.

175 W. J. Xu, B. Huang, G. Li, F. Yang, W. Lin, J. Gu, H. Deng, Z. Gu, and H. Jin, *ACS Cat.*, 2023, **13(8)**, 5723-5732.